Nanoscale Horizons

ROYAL SOCIETY OF CHEMISTRY

REVIEW

View Article Online
View Journal

Cite this: DOI: 10.1039/d5nh00710k

Emerging two-dimensional supported atomic and cluster catalysts for CO_2 electroreduction

Yimeng Sun,[a] Lin Tao,*[a] Yaqiong Su,*[b] Davoud Dastan,[c] Han Zhang,[a] Hongwei Zhao,[a] Lixiang Li[a] and Baigang An*[a]

In recent years, the electrocatalytic carbon dioxide reduction reaction (CO_2RR), driven by renewable energy and operated under mild conditions with controllable reaction pathways, has emerged as a promising route for carbon-neutral energy conversion. Two-dimensional supported catalysts have attracted particular interest owing to their tunable electronic structures and well-defined active sites. However, how the number and spatial configuration of active centers govern CO_2RR activity and selectivity remains insufficiently understood, limiting the rational design of efficient catalysts. This review provides a comprehensive overview of recent experimental and theoretical advances in two-dimensional supported catalysts for the CO_2RR, including single-atom (SACs), double-atom (DACs), and three-atom (TACs) catalysts, and metal clusters, with an emphasis on insights obtained from density functional theory (DFT). The fundamental reaction pathways of the CO_2RR are first summarized, highlighting structure–activity relationships between active-site characteristics and catalytic performance. Subsequently, the advantages and limitations of different catalyst architectures are critically compared, and the mechanisms of CO_2 reduction to C_1 products such as CO, HCOOH, and CH_4 are systematically analyzed. Particular attention is given to the role of DFT in elucidating reaction pathways, charge transfer, and adsorption energetics, thereby revealing key descriptors governing activity and selectivity. By integrating experimental observations with theoretical insights, this review aims to provide a mechanistic framework and design principles for the development of advanced two-dimensional supported catalysts for efficient CO_2RRs.

Received 23rd October 2025,
Accepted 21st January 2026

DOI: 10.1039/d5nh00710k

rsc.li/nanoscale-horizons

[a] School of Chemical Engineering, University of Science and Technology Liaoning, Anshan 114051, China. E-mail: taolin@ustl.edu.cn, bgan@ustl.edu.cn
[b] School of Chemistry, Engineering Research Center of Energy Storage Materials and Devices of Ministry of Education, National Innovation Platform (Center) for Industry-Education Integration of Energy Storage Technology, Xi'an Jiaotong University, Xi'an, 710049, China. E-mail: yqsu1989@xjtu.edu.cn
[c] Department of Materials Science and Engineering, Cornell University, Ithaca, NY 14850, USA

1. Introduction

Against the backdrop of global climate change, CO_2 emissions have become a core focus.[1] Since the Industrial Revolution, humanity's extensive reliance on fossil fuels and significant changes in land use patterns have led to a sharp increase in the concentration of CO_2 in the atmosphere, jumping from

Yimeng Sun

Yimeng Sun received her BE degree in Energy Storage Science and Engineering from the University of Science and Technology Liaoning in 2025. She is currently a master's student in Chemical Engineering and Technology at the same institution, under the supervision of Associate Professor Lin Tao. Her research focuses on the electroreduction of carbon dioxide.

Lin Tao

Lin Tao is currently an Associate Professor at the University of Science and Technology Liaoning. He received his PhD in Metallurgical Engineering from the same institution in 2021. His research interests focus on electrochemical materials, computational chemistry, and metal oxide semiconductor gas sensors.

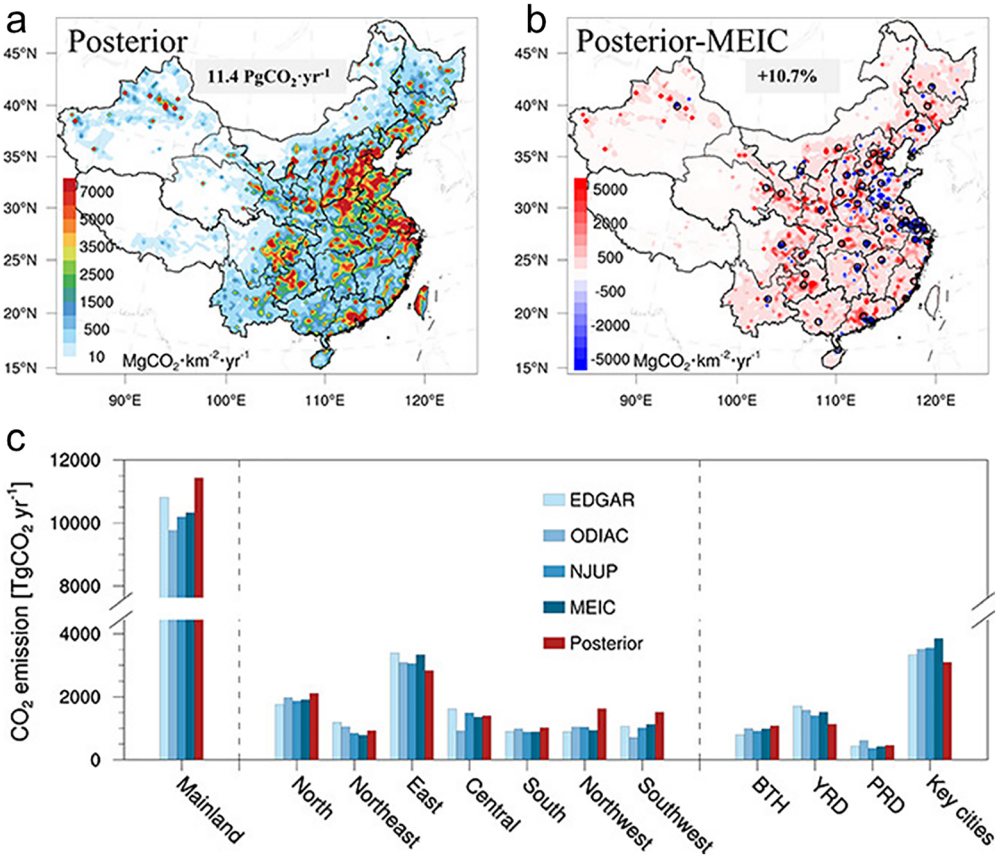

Fig. 1 The spatial distribution of (a) the *posteriori* emissions, (b) the absolute discrepancies between the *a posteriori* and MEIC inventories (Mg km^{-2} year^{-1}) for total annual CO_2 emissions across China, and (c) a provincial-level comparison ($TgCO_2$ per year) of the two emission datasets. Reproduced with permission from ref. 3, Copyright 2024 by American Chemical Society.

approximately 285 ppm before industrialization to 417 ppm in 2022.[2] As shown in Fig. 1, the total CO_2 emissions from fossil fuels in China reached as high as 11.4 ± 1.5 $PgCO_2$ per year. This continuous and large-scale emission is triggering a series of severe environmental problems.[3–5] Therefore, accurately grasping the spatio-temporal characteristics of CO_2 emissions and analyzing their underlying causes have become key to formulating effective emission reduction strategies and mitigating the impacts of climate change.

The utilization of CO_2 serves as a fundamental prerequisite for establishing a sustainable artificial carbon cycle. As a key feedstock in C_1 chemistry, CO_2 can currently be converted through three primary pathways. The first involves reforming CO_2 with CH_4 to produce syngas.[6] The second entails transforming CO_2 into fuels *via* electrochemical, photochemical, or thermochemical reactions.[7] The third pathway focuses on the production of high-value chemicals through catalytic hydrogenation.[8] CO_2 transformation not only reduces fossil

Yaqiong Su

Yaqiong Su is currently a full Professor in School of Chemistry, Xi'an Jiaotong University, China. He received his PhD degree in Catalysis at Eindhoven University of Technology in 2019. His main research interests are computational energy catalysis, electrochemistry of materials, and interfaces/surface-enhanced Raman Theory of Surface Enhanced Raman Spectroscopy.

Baigang An

Baigang An is currently a Professor at the University of Science and Technology Liaoning. He received his PhD in Applied Chemistry from Tianjin University in 2003. His research interests focus on energy materials and electrochemical energy storage technologies.

fuel consumption but also effectively alleviates the environmental impact of CO_2 generated from human production and daily life,[9] making it one of the important approaches to tackle excessive CO_2 emissions. However, the CO_2 molecule is linearly symmetrical in shape with the carbon atom in the highest oxidation state. The C–O bond length is only 0.116 nm and exhibits certain triple bond characteristics, and has a bond energy as high as 750 kJ mol^{-1}, which indicates that breaking the C═O double bond requires great energy.[10] In general, CO_2 molecules exhibit chemical stability, thermodynamic stability, and kinetic inertness, making their activation and transformation highly challenging.[11,12] Additionally, the CO_2RR involves complex processes entailing multiple electron transfer steps, hydrogenation, and C–C bond coupling, which result in CO_2 conversion with high energy consumption and low efficiency.

Light, electric, and thermal energy act as the requisite energy sources in the photocatalytic, electrocatalytic, and thermal catalytic reductions of CO_2, respectively.[13] Among these approaches, the thermal catalytic CO_2RR is capable of generating a wide range of products, including various liquid fuels. However, it typically requires elevated temperatures and pressures and often depends on fossil fuel-derived energy sources.[14] In contrast, photocatalysis and electrocatalysis can harness solar energy and electrical energy to drive the transformation of CO_2 into C_1 or C_{2+} products.[15,16] Consequently, photocatalytic and electrocatalytic CO_2RRs represent key pathways for achieving the sustainable utilization of new energy and are important strategies for attaining carbon neutrality. Notably, the CO_2RR stands out as a pivotal technology for transforming CO_2 into valuable energy products such as CO, HCOOH, and other C_1 compounds, owing to its efficiency and controllability.[17–22]

The core function of an electrocatalyst lies in reducing the activation overpotential of the reaction. In addition, the active sites of catalysts can optimize the reaction process and decrease the activation energy by opening up an alternative reaction pathway. That is, catalysts can adsorb CO_2 molecules and generate new intermediates. By controlling the adsorption behavior of the above new intermediates and weakening the interaction force between them, a more favorable condition for the reaction is obtained. Nevertheless, the diverse range of CO_2RR products (including CO, CH_4, CH_3OH, C_2H_4, C_2H_5OH, *etc.*) and their similar reaction potentials[23] tend to result in the formation of mixed products. Furthermore, the hydrogen evolution reaction (HER) is a major competitive side reaction in the CO_2RR, leading to extra energy consumption and reduction of reaction efficiency. Therefore, exploring novel, high-performance CO_2RR electrocatalysts with low overpotential and the ability to inhibit the HER is of great significance.

The unique quantum confinement effects of two-dimensional (2D) materials have positioned them as a rapidly emerging and highly regarded platform in catalytic research, adjustable electronic structures, abundant active sites, large specific surface areas, and cost-effectiveness.[24–31] In the selection of carriers for atomic dispersion catalysts, apart from two-dimensional materials, porous crystal materials such as metal–organic frameworks (MOFs) and zeolites have also attracted extensive attention due to their regular and ordered pore structures, extremely high specific surface areas, and precisely modifiable coordination sites. For instance, MOFs provide an ideal space for anchoring and confining metal precursors, which is conducive to the preparation of SACs with high loading capacity.[32–34] The rigid framework and ion-exchange sites of zeolites can effectively stabilize metal cations and prevent their migration and agglomeration.[35,36] These carrier systems have demonstrated unique potential in the CO_2RR. Graphene, with its two-dimensional layered architecture[37–39] and remarkable properties, has sustained global focus. This material exhibits a high visible-light transmittance of 97.7%, a heat conduction capability up to 3×10^3 W m^{-1} K^{-1} at 298 K, an electrical conduction of approximately 10^4 Ω^{-1} cm^{-1}, along with a specific surface area of 2630 m^2 g^{-1} as well as a Young's modulus of 1.1 TPa.[40,41] Owing to these properties, it demonstrates significant potential for applications spanning energy (*e.g.*, storage, solar cells), electronics (*e.g.*, transparent electrodes), aerospace, and advanced materials (*e.g.*, composites, biomedicine, catalysis, HER),[42–45] holding the potential to replace numerous traditional materials. However, its zero-bandgap nature restricts its application in the field of logic electronic devices.[46,47] Beyond graphene, a multitude of two-dimensional materials have achieved successful prediction and laboratory-based synthesis in recent years. Of the hundreds of existing 2D materials, there are single-atom[48–52] and double-atom[53–57] catalysts where metal atoms serve as active centers embedded in a 2D substrate, as well as three-atom[58–62] and metal cluster catalysts,[63–67] transition metal-supported two-dimensional carbon nitrides,[68–72] and so on. The combination of high charge carrier mobility, efficient heat dissipation, and mechanical stability in these standalone materials makes them promising for high-performance CO_2RR electrocatalysis.

Since the 20th century, as research into material structures has deepened, traditional research methods have struggled to meet specific investigative demands. However, the rapid advancements in computing technologies and quantum physical theories have enabled the computer-based simulation of material characteristics. Researchers have successively created a variety of computational methods and theoretical frameworks, including quantum mechanical first-principles, molecular dynamics, and machine learning.[73,74] Among these, quantum mechanical first-principles simulate material properties based on the atomic spatial arrangement and electronic structures.[75] The scale of the systems it can handle typically ranges from several to hundreds of atoms, and it exhibits remarkable strengths in calculating electronic structures and optomagnetic properties. Quantum chemistry addresses chemical problems by applying the classical theories of quantum mechanics, allowing the acquisition of data including molecular orbital energies and the total energy of chemical systems.[76] Density functional theory (DFT), a major breakthrough during the evolution of electronic structure theory, establishes a correspondence between the ground-state wave function and the ground-state electron density.[77,78] This approach significantly reduces computational complexity while

maintaining accuracy, proving capable of conducting in-depth studies on material reaction mechanisms thus enabling the rational design of materials and screening.

However, the reduction reaction of CO_2 still faces several fundamental challenges at the mechanism level in theoretical calculation research. Firstly, the initial activation path of the reaction remains controversial, and the adsorption strength of the intermediate has a significant impact on the selectivity of the main product. The identification of key intermediates (such as COOH and OCHO) and their formation sequence are difficult to define clearly. The reason why different metal and non-metal catalysts can generate a variety of CO_2RR products is mainly because they have unique adsorption capacity and reactivity for intermediates. Secondly, the carbon–carbon coupling mechanism for generating C_{2+} products has not been fully elucidated. Multiple pathways such as CO dimerization and Co–*CHO coupling are relatively close on the reaction energy barrier, leading to disputes over the rate-determining steps of the reaction and the sources of product selectivity.[79,80] The essence of these problems lies in the fact that the current theoretical models have limitations in accurately describing the real electrochemical interface environment, including the synergistic effects of multiple factors such as solvation and interface electric fields, which have not been fully quantified. Furthermore, the dynamic structural evolution of the catalyst surface at the working potential leads to significant differences between the calculation results based on the ideal static model and the structure and properties of the actual active sites, thereby severely restricting the ability to precisely predict reaction pathways and product selectivity at the atomic scale. To effectively overcome the energy barrier in the electron-transfer-proton coupling process, accelerate the catalytic reaction rate and suppress the occurrence of unwanted side reaction pathways, it is crucial to develop and design ideal catalysts with high selectivity and low energy consumption.

This review summarizes the recent research progress in CO_2RR catalysts for converting CO_2 into one-carbon products. The catalysts include two-dimensional materials such as single-atom, diatomic, and triatomic catalysts, and metal cluster catalysts embedded in two-dimensional substrates with metal active sites, and two-dimensional carbon nitrides supported by transition metals. It reveals the structure–activity relationship between the material properties and performance. In addition, it not only elaborates on the advantages and disadvantages of different catalysts and details the mechanism of CO_2 reduction to one-carbon products but also reviews the relevant content of density functional theory (DFT) calculations and electrocatalysis. This review aims to provide a basis for more suitable catalysts and accurate mechanisms for the CO_2RR.

2. CO_2RR on 2D materials

2.1. Single-atom catalysts

SACs have become highly promising material systems in the field of CO_2RR due to their nearly 100% atomic utilization rate, unique electronic structure, and precisely controllable coordination environment. Their design principles and performance optimization strategies have been systematically expounded in many recent reviews.[81–85] These works systematically summarize the latest research progress of carbon-based SACs in the field of CO_2 electroreduction, elaborating in detail their synthesis methods, characterization techniques, electrocatalytic performance and reaction mechanisms, and highlighting the improvement effect on catalytic activity and selectivity through optimization strategies such as regulating the coordination environment and constructing carrier defects.[86–90] At the same time, the challenges and prospects in this field in terms of controllable synthesis, performance enhancement and practical application were prospected, providing a comprehensive and in-depth reference for the research and development of efficient CO_2 conversion electrocatalysts.[91,92] Based on this, this paper particularly focuses on the SAC systems with two-dimensional materials as carriers, exploring how they can achieve more precise and diverse regulation of metal active sites through the introduction of carrier characteristics.[93]

Compared with traditional three-dimensional porous carbon or oxide carriers, two-dimensional carriers (such as graphene, carbon nitride, MXene, *etc.*) have clear surface geometric structures and tunable electronic properties, providing an ideal platform for constructing and stabilizing specific coordination structures of SACs.[94–97] A large number of studies have shown that by precisely regulating the coordination number, types of coordination atoms (such as N, O, S, and Cl), and coordination configurations of the metal center on the two-dimensional carrier, the physical and chemical state can be effectively optimized, thereby directing the improvements in CO_2RR performance.

Specifically, coordination number regulation is a key means to adjust the d-band center of the catalyst and change the adsorption strength of key intermediates (such as COOH). For example, compared with the common $M–N_4$ configuration, low coordination number $Co–N_2$ sites have been proven to effectively reduce the formation energy barrier of COOH, achieving up to 94% CO selectivity under appropriate overpotential.[98] Coordination atom engineering involves introducing different electronegative heteroatoms to adjust the charge distribution of the metal center. For example, pyrrole N species can stabilize the Fe^{3+} valence state and optimize the reaction pathway;[99] while axial coordination of Cl (such as $Fe–N_4Cl$) can significantly change the adsorption behavior of intermediates.[100] Moreover, the defects and pore engineering of the two-dimensional carrier (such as constructing nitrogen vacancy $Ni–N_3–V$ structure) not only provide abundant anchoring sites for metal atoms but also enhance the mass transfer of CO_2 and electrolyte, raising the current density to industrial relevant levels (such as >100 mA cm^{-2}).[101]

Further strategies include constructing double-atom sites (such as Ni–Fe and Co–Cu) to achieve dual-center cooperative catalysis, and using tandem catalytic design (coupling SACs with Cu-based catalysts) to expand the product range from C_1 (CO, HCOOH) to high-value C_{2+} products (ethylene,

ethanol).[102–104] It is worth noting that advanced *in situ* characterization techniques have revealed that SACs may undergo dynamic structural evolution under reaction conditions (such as Fe^{3+}/Fe^{2+} valence state changes), which is closely related to their final activity and selectivity.[105] More cutting-edge research even utilizes atomic-level-resolved *in situ* electrochemical STM to directly observe the dynamic migration and reorganization process of Cu single-atom sites at the reaction interface and correlate it with the selectivity switch of products.[106] In summary, SAC systems based on two-dimensional carriers achieve precise control of the CO_2RR pathway through multi-dimensional and cross-scale structural design, demonstrating great potential from fundamental understanding to practical applications. Since Zhang's research group published their pioneering work in 2011,[107] SACs have developed in a crucial direction for overcoming bottlenecks within the realm of heterogeneous catalysis. Their research demonstrated that the activity of the Pt_1/FeO_x SACs in the CO oxidation reaction exceeds that of nano-platinum catalysts by three times.[108,109] With an atomic architecture where metal centers are coordinated by non-metal atoms, this type of catalyst offers unique advantages by maximizing the exposure of active sites. Its distinctive coordination structure and electronic properties can significantly accelerate the kinetic process of the CO_2RR, thus exhibiting great potential in this field.[110–113] Notably, the agglomeration of single atoms on the substrate continues to be a challenging issue in the preparation of SACs, as it can diminish the catalyst's performance. Therefore, a suitable support is required to form strong bonds with single atoms, preventing metal aggregation. Typical supports include chalcogenides, oxides, and carbon materials.[114] While metal oxide supports can enhance CO_2RR activity through strong interactions with single atoms,[115–117] the oxygen species on their surfaces may cause the oxidation of metal single atoms, thereby reducing catalytic efficiency. In contrast, two-dimensional carbon-centric materials possess considerable application prospects, owing to their outstanding stability in reaction environments.[118–122]

With its unique structure, two-dimensional graphitic carbon nitride (g-C_3N_4) has proven effective for anchoring Cu, Pd, and Pt single atoms, serving as an excellent SAC support. This prominence stems from its cost-effectiveness, robust physicochemical stability, and facile synthesis protocols.[123–126] Sun and colleagues[69] elucidated a general mechanistic principle governing g-C_3N_4-catalyzed CO_2 conversion (Fig. 2a), non-spontaneous processes are characterized by positive reaction energies, and such processes arise when CO_2 is adsorbed on the surface or undergoes transformation *via* an odd count of H^+/e^- pairs to form free radicals. Conversely, spontaneous processes with negative reaction energies are associated with the release of products involving even H^+/e^- pairs, including CO, H_2CO, and CH_3OH. Transition metal dichalcogenides (TMDs) have also garnered growing interest, with their asymmetric layered structures[127–129] conferring unique physical properties that theoretically and experimentally enhance CO_2RR efficiency.[130–134]

The Janus WSSe (J-WSSe) monolayer, a novel two-dimensional TMD, is synthesized *via* selective epitaxial atomic replacement (SEAR), where one Se layer in WSe_2 is substituted with S.[135] This architecture—with W bonded to S on one side and Se on the other—breaks inversion symmetry. Transition metal J-WSSe SACs with anchored (TM) show outstanding electrocatalytic activity, yet the potential of J-WSSe with TM anchoring and Se incorporation vacancies as high-performance CO_2RR catalysts warrants systematic investigation. Chen *et al.*[136] explored 2d 3d, 4d, and 5d transition metals anchored on J-WSSe *via* anchoring, designing and screening a library of SACs (Fig. 2b). Their findings identified Os@J-WSSe, Cu@J-WSSe, Mn@J-WSSe, and Cr@J-WSSe as optimal catalysts for CO, HCOOH, CH_3OH, and CH_4 production, respectively. Notably, Cr@J-WSSe displayed unique dynamic stability, maintaining consistent active sites pre- and post-reaction. Tan and coworkers[137] reported CO_2RR performance of p-block metal SACs supported on N-doped graphene (M–N_4G, where M = In, Tl, Ge, Sn, Pb, Sb, Bi. Fig. 2c). Experimental results showed most M–N_4G catalysts exhibit superior CO_2RR selectivity over the competing HER. As a key intermediate species, *HCOO's adsorption energy has stood out as a trustworthy indicator to evaluate activity. Among these, Ge/Pb–N_4G demonstrated exceptional electrocatalytic efficacy for HCOOH synthesis, offering insights for rational SAC design.

Anna and colleagues[68] studied the stability of first-row transition metal atoms anchored on g-C_3N_4 monolayers in the CO_2RR. As displayed in Fig. 2(d), Sc, Ti, V, and Zn have large proton affinity ($\Delta G(H^*) < -0.3$ eV), which will result in active site blockage and possibly inhibit CO_2 conversion. In contrast, Cr, Mn, Fe, Co, and Ni have moderately positive energies of proton binding ($\Delta G(H^*)$ = 0.1–0.4 eV), enabling suppression of the competing HER. Among systems with relatively strong binding energies showing repulsion (Ni, Mn, Co) Ni_1/C_3N_4 stands out, as its moderate *CO adsorption energy (−0.52 eV), optimized d-band center position (−2.3 eV *vs.* Fermi level), and charge modulation of the metal by coordinated nitrogen sites (Δq = 0.53 e^-) achieve an optimal balance between overpotential (η_{CO_2RR} = 0.38 V) and selectivity (78% CO Faraday efficiency). Liu *et al.*[70] systematically investigated CO_2RR over metal-modified C_3N_4 nanotubes (Mn/CNNTs) in Fig. 2e for CO and formic acid production. Detailed analysis of geometric and electronic structures revealed that CNNTs' unique adsorption sites efficiently activate CO_2 and preferentially direct the CO_2RR toward the CO pathway, enhancing selectivity. Single-atom-modified armchair CNNTs (M/aN-6) exhibit the highest CO selectivity in the CO_2RR.

Furthermore, extensive research confirms that the local coordination environment dictates the electrocatalytic activity and selectivity of SACs, serving as a cornerstone for efficient electrocatalysis. Typically, SACs' active centers adopt coordination frameworks, with catalytic efficiency hinging on the central metal, coordination atom types/numbers, support properties, and functional group modifications.[71,72] Even subtle structural perturbations can markedly alter SACs' performance.[138] In M–N–C systems, for instance, modifying the carbon support

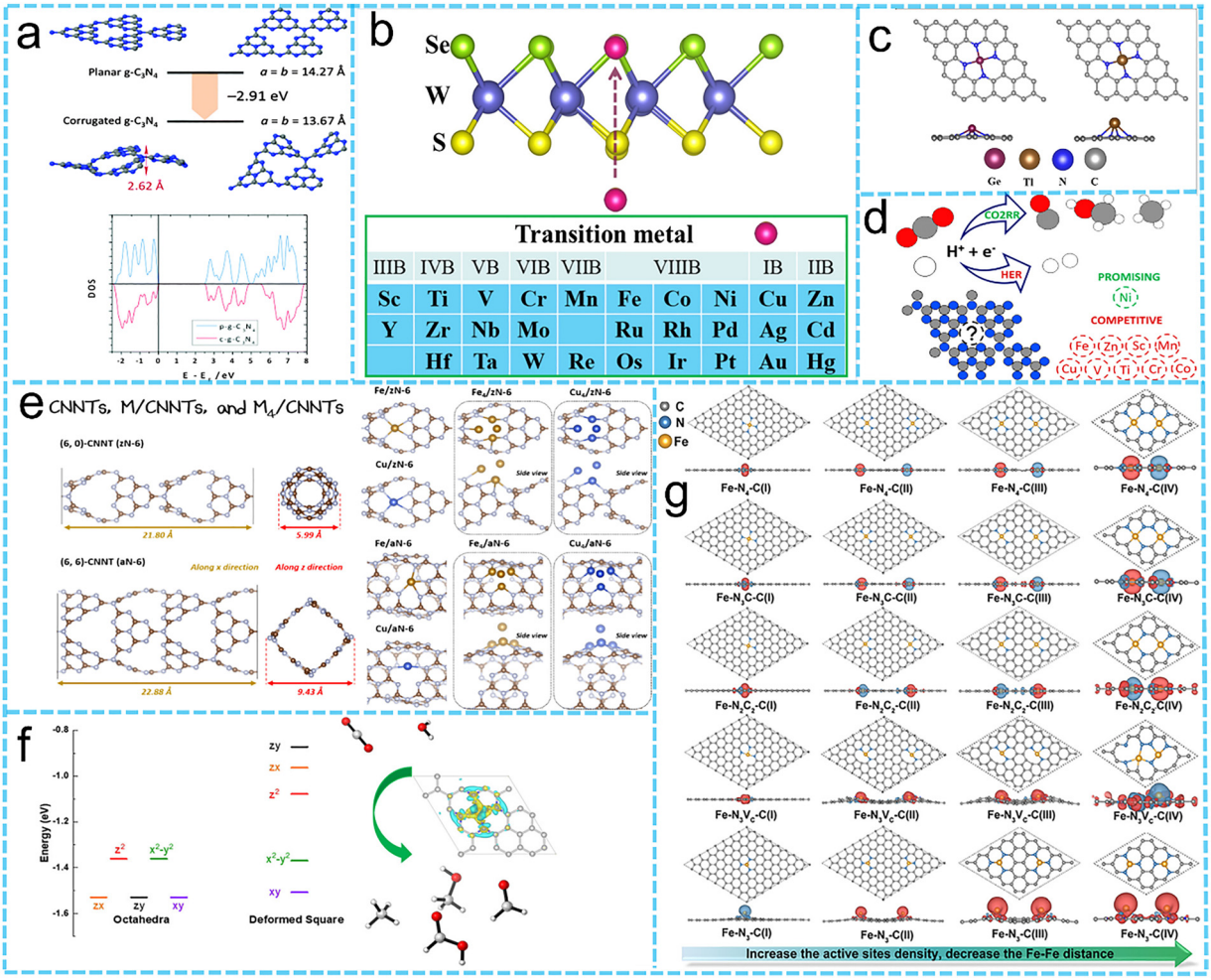

Fig. 2 (a) Optimized configurations of planar and corrugated 2 × 2 g-C_3N_4 sheets, showing their resulting electronic DOS. Reproduced with permission from ref. 69, Copyright 2016 by the Royal Society of Chemistry. (b) Schematic of the TM@J-WSSe structure with 28 transition metal (TM) atoms anchored onto the substrate. Reproduced with permission from ref. 136, Copyright 2025 by Elsevier. (c) Stable structures of Ge-N_4G and T_l-N_4G. Reproduced with permission from ref. 137, Copyright 2025 by American Chemical Society. (d) Schematic of first-row transition metal single atoms anchored on a g-C_3N_4 monolayer for the CO_2RR. Reproduced with permission from ref. 68, Copyright 2025 by American Chemical Society. (e) Optimized atomic structures of the investigated catalyst series. Reproduced with permission from ref. 70, Copyright 2024 by American Chemical Society. (f) Schematic diagram of the structure of M–N_4@Gr (M = Fe/Co/Ni). Reproduced with permission from ref. 110, Copyright 2022 by American Chemical Society. (g) Top and side views of the optimized geometric structures for the Fe–N_x–C catalyst series (models I–IV). Reproduced with permission from ref. 140, Copyright 2023 by American Chemical Society.

morphology and generating nearby defects serves to both expose active sites and regulate the metal's electronic states, leading to enhanced catalytic efficacy.[139] Yang *et al.*[110] confirmed that the coordination environment modulates d-orbital electron occupancy in M–N_4@Gr (M = Fe/Co/Ni) SACs (Fig. 2f), inducing distinct electron spin polarization that influences catalytic selectivity and performance. Fe–N_4@Gr exhibits significant spin polarization, with decreasing polarization following the sequence of Fe > Co > Ni.

In the deformable coordination field, metal–ligand bond distortion alters d-orbital splitting, regulating intermediate adsorption strength. Ni's $d_{x^2-y^2}$ and d_{xy} orbitals bond with N 2p orbitals, leaving few empty orbitals to accept electrons and resulting in weak CO_2 adsorption. In contrast, Fe's d_{z^2}/d_{zx} orbitals and Co's d orbitals remain partially occupied, endowing Fe/Co single atoms with both electron-donor and acceptor capabilities. This work demonstrates optimized catalytic performance *via* precise regulation of the coordination environment around non-precious metals, underscoring its significance for SACs. Wang *et al.*[140] elucidated the structure–activity relationship of Fe–N_xC_y–C (x = 2–4, y = 0–2) catalysts in the CO_2RR in Fig. 2g, that spin characteristics of Fe sites can induce modulation of the nearby coordination environment and density of active sites. The Fe–N_3P–C structure can sustain high CO yields over a wide potential range. This study demonstrates the intrinsic structure–performance relationship revealed by the reaction itself, and suggests that the synergism between coordination environment and the density of active sites is the key to understanding and enhancing the performance of SACs.

Although SACs have great potential, the homogeneity of their active sites still requires in-depth research, and achieving their controllable synthesis under different coordination environments remains challenging. Importantly, current SAC-derived CO_2RR products are predominantly CO, with limited reports of CH_4, HCOOH, *etc.* There is a paucity of research on generating high-value C_{2+} hydrocarbon fuels by tuning single-atom-support interactions, emphasizing the need to develop new SAC materials for highly selective hydrocarbon synthesis.

2.2. Dual atom catalysts

The efficacy of metal catalysts stems from interactions at unsaturated centers, which facilitate the binding of key species and subsequently enhance catalytic turnover.[89,141] Enhancing metal atom utilization by rationally lowering metal loading has emerged as an effective strategy to control overall costs while preserving intrinsic catalytic activity.[141–143] Consequently, a growing body of research is focused on reducing the size of nanocatalysts, thereby increasing the number of low-coordinated metal centers. Atomic-scale catalyst design, which maximizes the utilization of every atom in supported catalysts, represents the most efficient approach. Additionally, to more flexibly enhance the optimized adsorption of active centers and intermediates, DACs with proximate diatomic sites have emerged as a novel class of catalysts. Compared with SACs and nanoparticle systems, they exhibit multiple advantages such as high metal atom loading, highly adjustable active sites, easily modifiable electronic structures, and the synergistic effect of adjacent metal centers.[144–151] Leveraging these features, DACs aim to surpass the inherent reactivity of single metals by synergistically regulating intermediate adsorption/desorption and activation processes, thereby exhibiting unprecedented catalytic performance.

As illustrated in Fig. 3(a), Liu *et al.*[152] investigated CeO_2(110)-supported diatomic catalysts (M_α–M_β/CeO_2, where M_α–M_β are 3d/4d/5d transition metals). Analysis of binding and aggregation energies revealed that metals with lower electronegativity and higher d-orbital occupancy stabilize supported DACs. High-throughput descriptor calculations identified a series of potential DACs with both high activity (turnover frequency, TOF $> 0.1\ s^{-1}$) and selectivity ($>50\%$). Among these, heterogeneous Au-based DACs (*e.g.*, Au–Fe) exhibited good performance. The introduction of Au further activated adsorbed oxygen and weakened CO binding. This theoretical study establishes a foundational framework for the rational design of dual-site catalysts. Current DAC research remains in its infancy. DACs are classified as homonuclear or heteronuclear based on the identity of the two atoms in the active center.

As shown in Fig. 3(b), Huang's group[153] demonstrated that modulation *via* diatomic catalysts or heteroatomic ligands is a promising strategy to optimize SACs for more efficient CO_2 conversion to high-value chemicals. Their study focused on electrocatalytic CO_2 reduction to CO using an N/S-coordinated Fe–Ni diatomic pair embedded in a carbon matrix (FeNi–NSC). Gibbs free energy analysis of CO_2RR steps revealed that S coordination weakens Fe site activity and collaborates with adjacent Ni sites to regulate bidentate adsorption of the COO* intermediate, significantly reducing the CO desorption barrier and altering the rate-determining step. Wei *et al.*[57] proposed that the catalytic property of bimetallic atomic sites may be enhanced by regulating the binding mode of crucial intermediates supported by bonding interaction and electronic structure analyses. As shown in Fig. 3(c), their study screened four typical transition metals (TM = Fe, Co, Ni, Cu) and then constructed ten TM_1/TM_2-N@Gra to systematically assess homonuclear and heteronuclear DACs for CO_2 to C_1 products. Among them, Fe/Co and CO_2 displayed optimal limiting potentials (U_L) for HCOOH formation (-0.37 V and -0.34 V, correspondingly), indicating the best catalytic performance. The enhanced activity for CO_2 reduction was attributed to the optimal adsorption energy of the HCOOH intermediate on Fe/Co sites, as revealed by electronic structure analysis.

Bui's team[154] proposed a new strategy to boost CO_2RR performance by integrating well-defined structural clusters. As shown in Fig. 3(d), they designed g-CN molecular skeletons hosting various transition metal (TM) dimers for the CO_2RR, ultimately identifying five atomic pairs (Cr_2, CrFe, Mn_2, MnFe, Fe_2) with excellent active performance. The performance of Fe_2@g-CN in the CO_2RR was further optimized by regulating the integration of iron atomic clusters. It is worth noting that the introduction of Fe_{13} atomic clusters enhanced the CO_2 adsorption capacity while effectively inhibiting hydrogen activation. In addition, it also breaks the scale relationship between the intermediates (CO and CHO), thereby significantly enhancing the performance of CO_2RR and reducing the limiting potential of the C_1 path to -0.45V. This work broadens understanding of DAC mechanisms in the CO_2RR and offers insights for rational design and integration of heterogeneous DACs with specific atomic clusters for other applications. Chen *et al.*[155] screened bimetallic dimers supported on nitrogen-doped graphene (including homonuclear and heteronuclear transition metals). As shown in Fig. 3(e), C–C coupling analysis revealed that six catalysts (Cr–Cu, Mn–Cu, Co–Co, Co–Ni, Co–Cu, and Ni–Cu) showed coupling energy barriers under the threshold (0.75 eV), with the top five showing notably lower barriers. All six DACs demonstrated superior C_2 pathway selectivity in competitive HER and CO_2RR.

Despite atomic vibrations, the bimetallic atoms and their six coordinated nitrogen atoms maintained strong bonding without obvious structural distortion, indicating excellent heat stability at 500 K. This suggests these DACs are able to stably retain their configuration under both mild and high-temperature conditions. As displayed in Fig. 3(f), Zhu *et al.*[56] studied CO_2 activation based on the Ni–Cu catalyst. As shown, the secondary Cu could tune the energy level of the Ni 3d orbital into the Fermi level and then enhance the emergence of the rate-determining *COOH intermediate. Remarkably, a CO TOF of 20 695 h^{-1} was obtained at -0.6 V (vs RHE) with the maximum CO Faraday efficiency of 97.7%. *In situ* XAFS monitoring of dynamic structural evolution further clarified interactions between Ni centers and CO_2 molecules, along with the Ni–Cu synergistic mechanism enhancing CO_2RR activity.

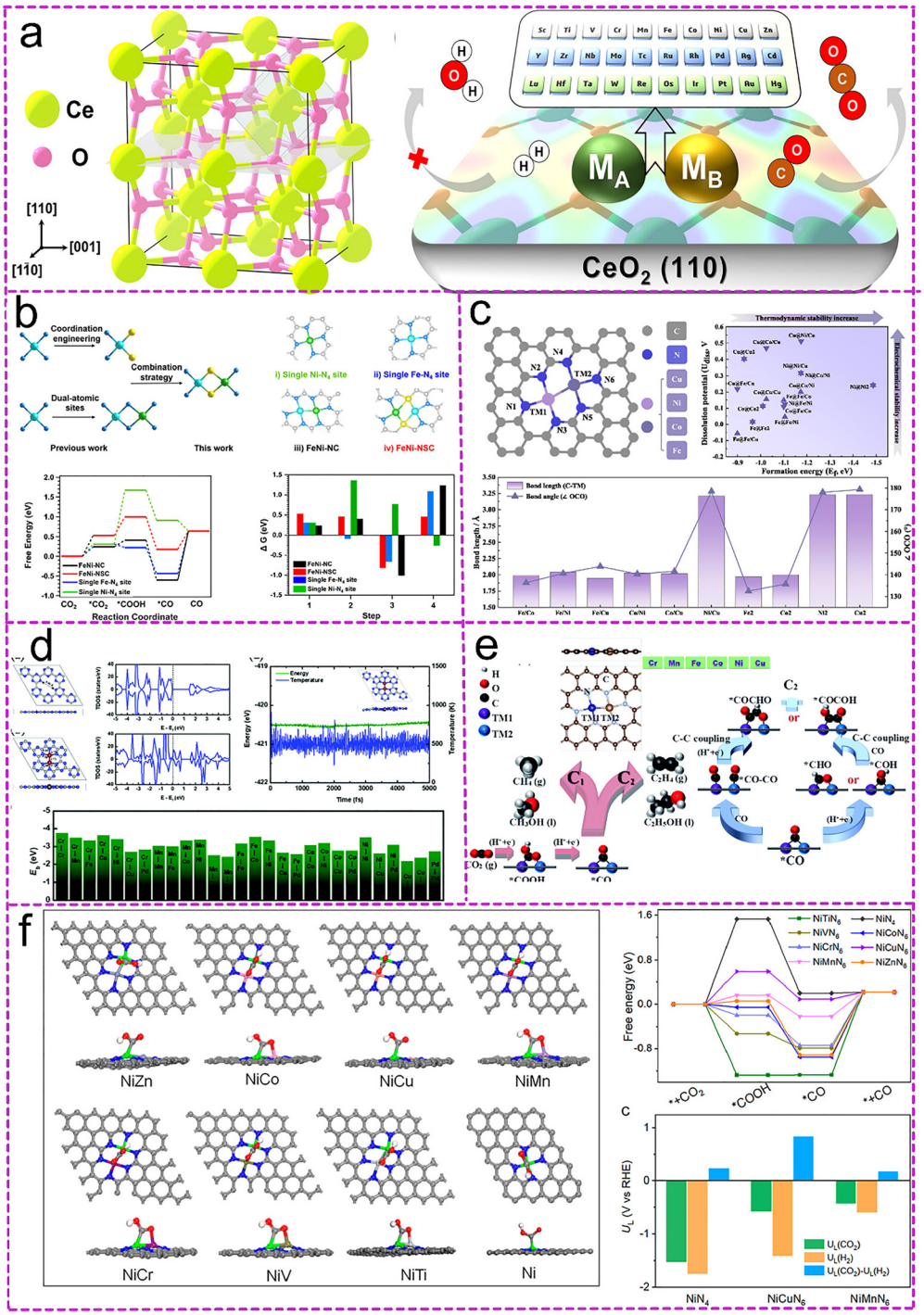

Fig. 3 (a) Atomic structure of CeO_2 (1 × 1 × 1) with Ce (green) and O (pink) atoms, and schematic search diagram of DACs/CeO_2(110) for CO PROX. Reproduced with permission from ref. 152, Copyright 2025 by American Chemical Society. (b) DFT study of bimetallic Ni–Fe–N–C catalysts, structural configurations (Ni–N_4, Fe–N_4, FeNi–NC, FeNi–NSC with C-gray, N-blue, S-yellow, Ni-green, Fe-cyan) and their catalytic reaction energetics, including free energy profiles and stepwise energy comparisons. Reproduced with permission from ref. 153, Copyright 2024 by American Chemical Society. (c) Computational characterization of bimetallic TM_1/TM_2-N@Gra systems showing geometric configurations, thermodynamic stability, and CO_2 adsorption geometry. Reproduced with permission from ref. 57, Copyright 2022 by Elsevier. (d) Structural and electronic properties of pristine g-CN and Fe_2-doped g-CN systems. Illustrated are the optimized geometries (top and side views), TDOS, and comparative binding energy analysis. Reproduced with permission from ref. 154, Copyright 2021 by the Royal Society of Chemistry. (e) Proposed reaction pathway for CO_2 to C_2H_5OH, C_2H_4 on N-graphene based dual-atom catalysts, geometric configurations and overall reaction network encompassing both C_1 (CH_3OH, CH_4) and C_2 products, and two distinct reaction pathways from the *CO intermediate to C_2-coupled species. Reproduced with permission from ref. 155, Copyright 2020 by the Royal Society of Chemistry. (f) DFT study of Ni-based SACs for the CO_2RR, showing COOH* adsorption configurations on $NiMN_6$ and NiN_4 sites. Reproduced with permission from ref. 56, Copyright 2022 by American Chemical Society.

Constructing structures where one metal atom binds exclusively to another (especially in dimer form) remains a major challenge. Inhomogeneity in support pores and defects hinders precise fabrication of diatomic sites. In contrast, nano synthetic catalysts or SACs outperform DACs in terms of controllability and performance.[156] Excessive metal precursor usage can form metal nanoparticles, while reducing dosage may promote single-atom dispersion and isolation. However, DACs exist in an intermediate state, making precise control of precursor dosage difficult and often leading to uneven metal distribution in catalytic centers. Due to imprecise metal loading control, coexistence of single atoms, atomic clusters, and even larger aggregates is inevitable, triggering active site aggregation. When catalysts contain ill-defined clusters or particles, clarifying the structure–performance relationship of dual-site metal catalysts becomes challenging. Most current DACs use carbon-based supports, with relatively few studies concerning other substrates. Thus, the feasibility and performance of DACs on non-carbon supports require further exploration.

2.3. Three-atom catalysts

TACs offer expanded possibilities for complex electrochemical reactions, due to their enhanced metal atom loading, increased contact area, and unique structural features. First, their higher metal atom loading capacity brings active sites in closer proximity.[157] In contrast, the formation of metal–metal or metal–bridge bonds offers a strategic approach to modulate the co-adsorption energetics of various reactants and intermediates.[158,159] TACs have many types of asymmetric adsorption sites, which may destruct the linear scaling relationship and present different catalytic behaviors. The asymmetric active site is more applicable for complex catalytic reaction with more than one step and intermediate. In addition, the cooperation among three atoms can tune the d-band electronic structure to enhance the catalytic activity.[160,161] Through such active center synergies, TACs transcend the performance's simple additive relationship improvement, demonstrating robust efficacy within multi-molecular reaction systems.[162] The variety in atomic species and valence states further expands the research space for triatomic sites.

Jia *et al.*[163] reported that TACs behave as high current electrocatalysts for the CO_2RR because the large number of active sites in TACs benefit from both the high electrochemical surface area offered by the nanocubes and fast charge migration. The electronic properties and stability of TACs are also related to their carrier materials. By anchoring the three atoms on appropriate carriers and taking advantage of their interfacial interactions, the agglomeration of clusters can be effectively avoided,[164] and an optimized triatomic coordination environment can effectively enhance catalytic performance.[165] For example, when three metal atoms are atomically dispersed on supports such as nitrogen-doped graphene or g-C_3N_4, TACs with either random[166–168] or triangular[169,170] structures can form. Such catalysts actively participate in electrochemical reactions—including N–N bond/O–O bond cleavage or C–C coupling—*via* orbital coupling or non-bonding interactions between metal atoms.[171]

Zhou's group[60] explored the utility of graphdiyne-supported 3TM-GY (TM = Cu, Fe, Co) applied in the CO_2RR to generate C_1 products, as shown in Fig. 4(a). The singular triangular TM trimer anchored on graphdiyne, characterized by strong adsorption energy and a distinct curved configuration, creates a beneficial setting for CO_2 adsorption and initial activation. 3Cu-GY preferentially reduces CO_2 to CH_4, exhibiting higher selectivity than other C_1 products and surpassing most atomically dispersed electrocatalysts. At increased applied potentials, the CO_2RR on 3Cu-GY favors high-throughput production of HCOOH and CH_4, while 3Fe-GY/3Co-GY favor deeply reduced products. Hydrogen evolution is strongly inhibited, rendering CO_2RR dominant. This performance enhancement is attributed to synergies among multiple metal centers, which promote adsorption of critical species, notably HCOO* and CH* and facilitate pathways conducive to CO_2 reduction.[172] Sun *et al.*[173] compared SACs and TACs (Fig. 4(b)), and showed that SACs maximize atomic utilization and provide uniform active sites, while TACs precisely regulate intermediate adsorption *via* interatomic synergies, overcoming traditional catalytic limitations. Among their findings, 3Mo-C_2N_1 and 3Ti-C_2N_1 exhibited exceptional catalytic activity for CO and HCOOH production, respectively. Swapnil *et al.*[174] investigated CO_2 adsorption *via* TM_n-doped C_2N monolayers, revealing that TM_3-C_2N achieves a maximum adsorption capacity of 6 CO_2 molecules per trimer—significantly outperforming TM_1-C_2N and TM_2-C_2N systems.

Copper demonstrates unique efficacy in catalyzing the CO_2 reduction reaction toward hydrocarbon products, owing to its unique ability to adsorb *CO intermediates. However, traditional Cu catalysts suffer from deficiencies in CH_4 selectivity and activity. As shown in Fig. 4(c), Pan's team[59] addressed this atomic-level engineering of Cu sites and mesoscale control of support porosity, enabling dynamic transformation of single-atom Cu–N_3 into N- and OH^--anchored Cu_3 clusters under reaction conditions. The N, OH-Cu_3 site stabilizes *CO at −0.76 eV. The kinetic barrier for its hydrogenation to *CHO is 0.85 eV, markedly lower than the C–C coupling barrier (2.03 eV), suggesting that formate formation is kinetically preferential, selectively promoting CH_4 formation. Its moderate adsorption of CO capacity and low barriers for CO hydrogenation are key to high selectivity. Additionally, dual continuous mesoporous channels create a water-deficient local microenvironment, inhibiting hydrogen evolution and prolonging *CO intermediate retention, thereby promoting deep CO_2 reduction.

Similarly, as presented in Fig. 4(d), Li *et al.*[58] developed a series of high-performance non-noble triatomic catalysts ($TM_1TM_2TM_3$@GY, where TM = Mn, Fe, Co, Ni, Cu, Mo) supported on the 2D material graphdiyne, investigating their CO_2RR selectivity. MnMoFe@GY and MnMoCu@GY displayed optimal CO_2RR performance, achieving the highest activity and selectivity among all tested catalysts, with effective hydrogen evolution inhibition. They demonstrated good experimental feasibility, stable catalytic performance, and excellent CO_2RR

selectivity—confirming TACs' potential in CO_2RR catalysis. Liu *et al.*[175] designed a series of trimetallic TM-NiFe catalysts as presented in Fig. 4(e), finding that Zn–NiFe performs exceptionally in the CO_2RR-to-CO pathway. Cr–NiFe prefers the

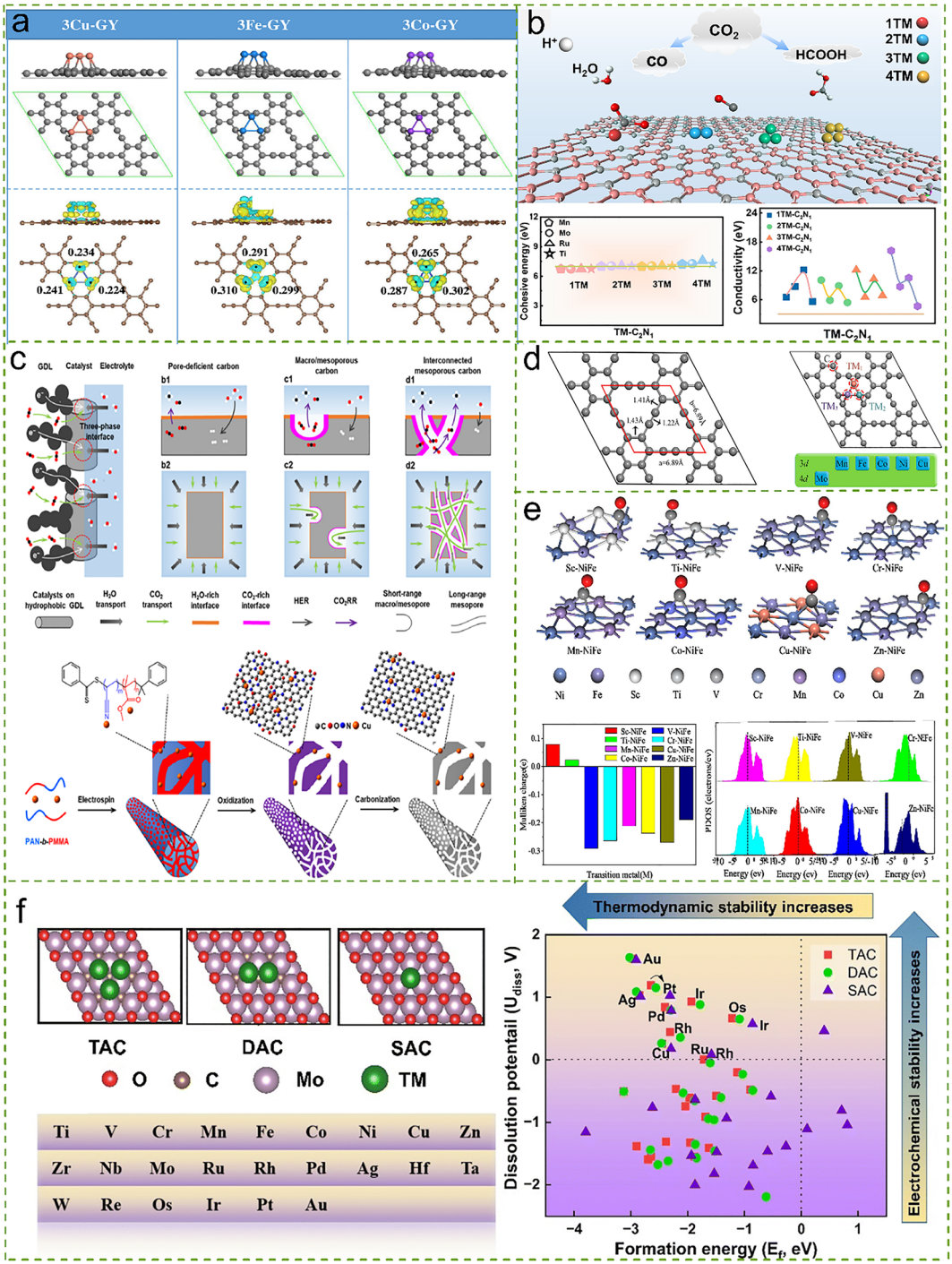

Fig. 4 (a) Optimized atomic structures and charge density difference distributions of the 3TM-GY catalysts. Reproduced with permission from ref. 60, Copyright 2021 by Elsevier. (b) A schematic diagram showing the stability and conductivity of TM-C_2N_1. Reproduced with permission from ref. 173, Copyright 2024 by the Royal Society of Chemistry. (c) Design strategy and synthesis implementation. Reproduced with permission from ref. 176, Copyright 2024 by American Chemical Society. (d) Top-view structure of the trimetallic $TM_1TM_2TM_3$@GY catalyst. Reproduced with permission from ref. 58, Copyright 2024 by Elsevier. (e) Optimized CO* adsorption configurations on TM-NiFe catalysts, with corresponding Mulliken charges and projected density of states (PDOS) of the transition metal (TM) atoms. Reproduced with permission from ref. 175, Copyright 2023 by Elsevier. (f) Structural models of SACs, DACs, and TACs on Mo_2CO_2 MXene, with their corresponding transition metal constituents, formation energies, and dissolution potentials. Reproduced with permission from ref. 172, Copyright 2023 by the Royal Society of Chemistry.

COOH* pathway over HCOO* for HCOOH production, enabling efficient HCOOH synthesis while significantly inhibiting competing reactions (hydrogen evolution and CO_2RR-to-CO). These results highlight the abundance of CO_2RR active sites in TACs. Xiao *et al.*[172] observed that homonuclear diatomic and triatomic catalysts supported on 2D Mo_2CO_2 materials exhibit superior CO_2RR performance compared to single-atom systems. As shown in Fig. 4(f), multinuclear reaction sites in multi-atom catalysts significantly enhance adsorption of crucial intermediates (*e.g.*, HCOO* and CH*), which facilitates the selective reduction to CH_4 at ultra-low overpotentials. Additionally, multinuclear sites effectively promote C–C coupling, creating conditions for efficient C_2H_5OH production.

Benefiting from multi-metal synergy, high selectivity, and cost-effectiveness, TACs have attracted significant research interest in CO_2 electroreduction. However, rational TAC design faces fundamental challenges. Future efforts must address precise synthesis, stability enhancement, and industrial adaptation. Integrating advanced characterization and computational simulation will be critical to advancing TACs from laboratory research to large-scale applications, contributing to global carbon neutrality goals.

2.4. Cluster

Atomic clusters, ranging from a few to hundreds of atoms, typically exhibit a particle size measuring 1 nm, with a maximum value of 3 nm, placing them in the category of ultrafine particulate materials (Fig. 5a).[177] Relative to traditional nanoparticles (with sizes of 5–500 nm), their atypically small size confers unique properties absent in larger nanoparticles, arising from pronounced quantum size effects. For conventional nanoparticles, functional performance is governed by surface structure and geometry.[178–180] The electronic structure of atomic clusters demonstrates a hybrid nature, lying between molecular-like states and the band structure of bulk materials, endowing them with distinctive characteristics.[181–184] Additionally, clusters possess diverse structural features unobserved in other chemical species, including constituent atom count, element types, elemental proportions, atomic arrangement, and geometric symmetry. These features thus allow for the creation of numerous active sites tailored to adsorb and convert specific reactants and intermediates in the CO_2RR.[64,65] This ability to maintain high utilization efficiency with polymetallic atoms provides substantial flexibility in material design. Furthermore, their molecular-scale spatial configurations and electronic structures have great potential for achieving novel properties and functions, effectively promoting reactant activation and modulating the adsorption of key species (*e.g.*, *COOH, *OCOH) to facilitate the CO_2RR.[185]

As illustrated in Fig. 5(b), Wu *et al.*[186] demonstrated that iron cluster sites anchored on mesoporous carbon materials exhibit enhanced electrocatalytic performance in the CO_2RR. Similarly, a study on CuAg bimetallic clusters[187] utilized DFT to analyze relationships between catalyst structure, composition, and activity, revealing that specific cluster configurations favor the formation of target products such as CH_3OH. These findings underscore the critical role of atomic arrangement within clusters in optimizing CO_2RR efficiency. Tamtaji's group[188] reported five configurations comprising five metals Fe, Co, Ni, Cu, and Rh. In Fig. 5(c), CoNiCuRh@FeN_4, FeN_4 serves as the active center, while the CoNiCuRh high-entropy cluster serves as a regulatory unit, achieving a low overpotential for CO production in the CO_2RR. In FeNiCuRh@CoN_4, CoN_4 synergizes with the FeNiCuRh high-entropy cluster as the active site, enabling selective reduction of CO_2 to methanol at an overpotential—outperforming traditional SACs. Fig. 5(d) highlights that binuclear Cu(I) complexes serve as efficient catalysts for CO_2-to-C_3 product conversion *via* C–C coupling, indicating that multinuclear arrangements can promote C_{2+} formation by offering a favorable microenvironment for CO_2 activation and subsequent coupling steps.[189]

DFT-based explorations of alloy and bimetallic clusters are also prominent. Mechanistic analyses indicate that C–C coupling is influenced by the catalyst's ability to manage competing reactions (*e.g.*, hydrogen evolution). Multinuclear catalysts can regulate these kinetics to favor CO_2 reduction pathways. For example, a study on AuCu clusters[190] employed first-principles calculations to simulate catalytic behavior, emphasizing how alloying modulates adsorption energies and reaction pathways. Similarly, investigations of Cu@CNT catalysts[191] established that certain Ni-based clusters preferentially convert CO_2 to CO, demonstrating the utility of computational methods in predicting catalytic performance from cluster composition. Studies on defects and near-surface atomic structures have further elucidated their impact on catalytic activity. Zhang *et al.*[192] used DFT to analyze defective Cu_4X_n clusters, finding that defects alter adsorption sites and lower activation barriers, thereby enhancing the CO_2RR. Jo *et al.*[193] explored surface FCC dependence, using DFT to clarify how different Cu surface facets influence HCOOH formation pathways. They found that electronic properties related to surface coordination and roughness significantly affect catalytic efficiency, emphasizing the critical role of surface engineering for nanoparticle catalysts. Xu *et al.*[194] synthesized CuO nanosheets with controllable nanostructures as effective CO_2RR catalysts, noting that surface oxygen and Cu^+ species are not essential for C_{2+} product formation, suggesting catalytic activity is primarily determined by metal surface structure and morphology. Deng *et al.*[195] further supported size-dependent activity, combining theoretical and experimental methods to identify an optimal silver nanoparticle size (8–10 nm) balancing activity and selectivity—emphasizing the need for precise size control in CO_2RR nanoparticle catalysts.

Fig. 5e demonstrates the outstanding CO_2RR performance of the FT-Cu_3@MoSX (X = Se, Te) catalyst. CO_2 is stably adsorbed on the catalyst surface, and the charge transfer (0.59–0.97*e*) and orbital hybridization are significant, converting linear CO_2 into V-shaped $CO_2^{\delta-}$ active species (OCO bond angle 121.7°–136.8°, C═O bond length increasing to 1.30 Å). Moreover, the electron transfer efficiency at the S-terminated surface is better, with an adsorption energy (−0.51 to −0.55 eV) superior to that of the non-polar MoS_2 system. This effectively

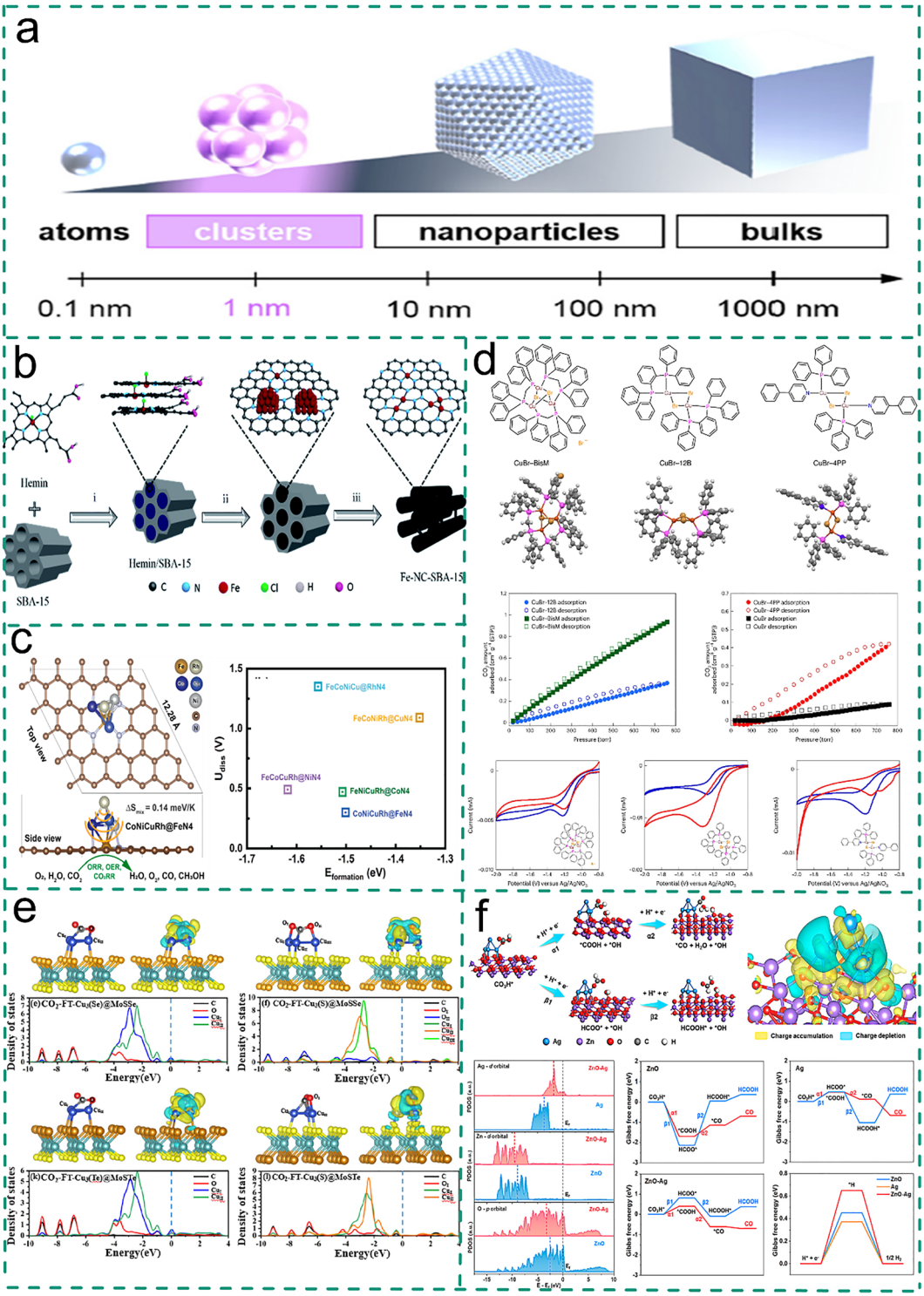

Fig. 5 (a) Material classification by size scale. Reproduced with permission from ref. 176, Copyright 2024 by the Royal Society of Chemistry. (b) Schematic of the synthesis of Fe–NC–SBA-15. Reproduced with permission from ref. 185, Copyright 2020 by the Royal Society of Chemistry. (c) Structural model of the CoNiCuRh@FeN_4 high-entropy catalyst (ΔS_{mix} = 0.14 meV K^{-1}), and the correlation between its dissolution potential (U_{diss}) and formation energy ($E_{formation}$). Reproduced with permission from ref. 187, Copyright 2025 by Elsevier. (d) Molecular structures of three copper-bromide-phosphine complexes: [$Cu_3(\mu\text{-}Br)_2$(bis-methyl-bisphenylphosphine)$_3$] Br-(CuBr–BisM), $Cu_2(\mu\text{-}Br)_2$(1,2-phenyl-bisphenylphosphine)$_2$ (CuBr–12B) and $Cu_2(\mu\text{-}Br)_2$(triphenylphosphine)$_2$(4-phenylpyridine)$_2$ (CuBr–4PP). Reproduced with permission from ref. 188, Copyright 2024 by Nature. (e) Most stable CO_2 adsorption configurations, charge density difference isosurfaces, and projected density of states (PDOS) for CO_2 on the FT Cu_3(Se)@MoSSe, FT Cu_3(S)@MoSSe, FT Cu_3(Te)@MoSTe, and FT Cu_3(S)@MoSTe catalysts. Reproduced with permission from ref. 196, Copyright 2024 by American Chemical Society. (f) Theoretical simulations of the CO/HCOOH formation pathways, electronic structure analysis (charge density and PDOS of d-/p-bands) of the ZnO, Ag, and ZnO–Ag systems, and the corresponding HER processes. Reproduced with permission from ref. 200, Copyright 2021 by American Chemical Society.

activates CO_2 and lowers the reaction energy barrier, demonstrating its high catalytic potential.[196] Structural engineering of atomic catalysts—including multinuclear arrangements—has been shown to provide multiple reaction pathways and synergistic effects, enhancing overall electrocatalytic activity.[188] Innovative catalyst design strategies include Zhang *et al.*'s[197] Zn–Ag–O catalytic materials in Fig. 5f, featuring nanoscale nanoparticles within nanopores to achieve high performance and durability, illustrating how nanoscale structural design boosts CO_2RR efficiency. Gang *et al.*[198] explored the scalability and practicality of nanoparticle catalysts, developing a one-step pyrolysis method to prepare M–N–C catalysts synthesized from carbon nanotubes and nitrogen precursors—an economical, effective approach enabling scalable CO_2RR catalysts and expanding practical application potential.

It is worth noting that, based on multi-metal cluster catalysts, high-entropy alloy clusters (HEA Clusters) are emerging as an emerging frontier. HEA clusters are typically composed of five or more principal metal elements in a nearly equimolar ratio, and their extremely high configurational entropy is expected to confer them unique electronic structures and outstanding structural stability. For instance, as mentioned earlier in this review, the CoNiCuRh@FeN_4 system[188,199] already possesses characteristics of being multi-component and having high entropy, demonstrating its unique control ability over different product pathways in the CO_2RR. Theoretically, the vast component space of HEA clusters contains infinite possibilities for electronic structures, providing an unprecedented platform for 'tailoring' CO_2RR catalysts with high activity, high selectivity, and ultra-high stability. However, the controllable synthesis, precise characterization, and elucidation of the relationship between structure and function remain significant challenges. In the future, by leveraging high-throughput computing and machine learning, the optimal combinations from the vast 'high-entropy chemical space' will be selected, and *in situ* characterization techniques for sub-nanometer-scale high-entropy systems will be developed, which will be the key to achieving breakthroughs in this field.

Theoretical and spectroscopic techniques, such as multinuclear magnetic resonance, have been used to study hyperpolarized nuclear spin behavior in multinuclear systems, informing the design of more effective catalysts. Additionally, integrating multinuclear complexes into molecular junctions to enhance thermoelectric performance highlights the broader applicability of multinuclear structures in energy-related catalysis. In summary, these studies collectively emphasize the significance of multinuclear metal complexes in advancing CO_2RR technology. Incorporating multinuclear structures into catalyst design provides a universal strategy to overcome current CO_2RR limitations, enabling more efficient, selective, and stable catalytic systems. Sustained mechanistic research and structural innovation are critical to fully harnessing the viability of multinuclear catalysts for sustainable energy CO_2 conversion technologies.

3. Catalytic performance of the main C_1 products

3.1. CO_2 reduction to CO

The CO_2RR has evolved into a pivotal approach to producing high-value chemicals and fuels, showing substantial promise for advancing global carbon neutrality objectives and tackling energy scarcity challenges.[201] Among the diverse electrochemical CO_2 conversion pathways, CO generation stands out due to its near-100% selectivity, rendering it industrially viable.[202] Notably, strategic modulation of electronic effects, steric hindrance, stabilization of metal-CO_2 intermediates, and rational ligand design to facilitate C–O bond cleavage have yielded significant progress in product selectivity control.[203] However, kinetic barriers in electrocatalytic processes necessitate substantial overpotentials, which inadvertently promote the HER as a competing side reaction, thereby compromising CO selectivity.

The mechanism for CO_2-to-CO conversion involves a process of transferring 2 electrons ($2e^-$) and 2 protons ($2H^+$). The CO_2 reduction process commences with the efficient adsorption of CO_2 molecules on the surface (Fig. 6a). The adsorbed CO_2 is reduced to the *COOH intermediate. Subsequent attack by an additional H^+ and e^- converts *COOH to H_2O and *CO, with the final step involving *CO desorption from the electrode surface to release CO.[202] Current research has confirmed that the two key bottlenecks restricting the production efficiency of carbon monoxide lie in the fact that too weak COO^- adsorption energy hinders the formation of COOH intermediates, while too strong *CO adsorption inhibits the desorption of the products.[204,205] Multiple studies corroborate that the *CO binding energy on Cu surfaces acts as a key activity descriptor to characterize CO_2RR products beyond $2e^-$ pathways, aligning with the Sabatier principle. Overly strong *CO binding results in catalyst poisoning, whereas weak binding causes premature CO desorption, preventing further reduction. Optimal *CO adsorption balances high CO uptake with HER suppression, thereby maintaining high CO_2RR Faraday efficiency.

3.1.1. Performance and mechanisms on SACs. To address these challenges, innovative catalyst designs have been developed. Cheng *et al.*[206] employed DFT to investigate single-atom bimetallic alloys, highlighting their potential as electrocatalysts enabling CO_2 reduction to C_1 hydrocarbons, with particular emphasis on Au or Ag-mediated initial CO formation. This work underscores single-atom alloys as cascade catalysts where CO generation constitutes a pivotal step. Zhang *et al.*[99] developed an FeN_5 single-atom supported on graphene catalyst that achieves 97% faradaic efficiency for CO production at low overpotentials, demonstrating the efficacy of atomically dispersed Fe active sites. Recent studies emphasize the critical role of atomic configuration and electronic structure tuning. Han *et al.*[207] demonstrated through Fig. 6b that the fluorine-modified Ni–N_4 SACs, supported by ultrathin carbon nanosheets, maintained a CO Faradaic efficiency of over 90% (up to nearly 95%) and a hydrogen evolution efficiency of less than 10% in the range of −0.8 to −1.1 V *vs.* RHE after fluorine

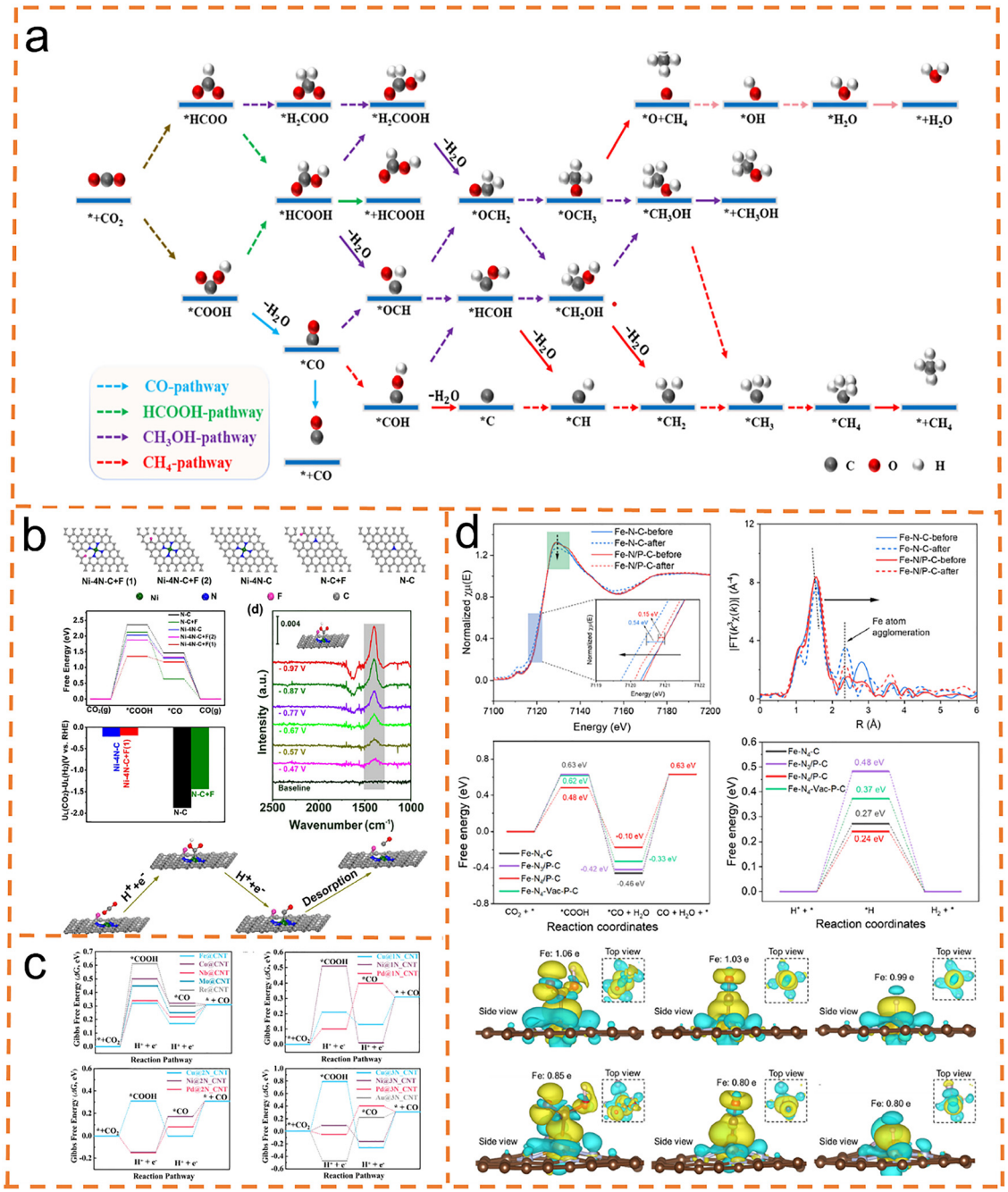

Fig. 6 (a) Proposed reaction pathways and key intermediates for the CO_2RR to CO products. Reproduced with permission from ref. 201, Copyright 2025 by Elsevier. (b) Depicted are multiple aspects of the catalytic system, including the model structures, computed Gibbs free energy profiles for CO_2-to-CO conversion, the disparity between CO_2RR and HER limiting potentials, potential-dependent *in situ* ATR-IR spectra in CO_2-saturated 0.5 M $KHCO_3$, and the proposed CO_2RR mechanism on Ni-SAs@FNC. Reproduced with permission from ref. 99, Copyright 2021 by Elsevier. (c) Gibbs free energy diagram for the electrochemical CO_2RR process. Reproduced with permission from ref. 207, Copyright 2022 by American Chemical Society. (d) XAS characterization and theoretical computation of the single-atom Fe catalyst. Reproduced with permission from ref. 208, Copyright 2022 by American Chemical Society.

modification. Moreover, the linear scanning voltammetry reduction current was significantly higher than that of the unmodified sample, directly demonstrating that fluorine regulation greatly enhanced the activity and selectivity of CO_2 reduction. The Tafel slope dropped to 68 mV dec^{-1} (82 mV dec^{-1} for the unmodified sample), indicating that fluorine modification reduced the energy barrier formed by the *COOH intermediate to accelerate the reaction kinetics. After 12 hours of potentiostatic testing, the current remained above 92% of the initial value, confirming its high stability. The result of a 40% reduction in charge transfer resistance, combined with the ultrathin morphology feature, confirmed that the fluorine

modification and structural design synergistically enhanced the interface charge transfer. Moreover, the optimal fluorine doping amount (3.2–4.5 at%) corresponds to the performance peak and the phenomenon that excessive doping will damage the Ni–N_4 structure, further indicating that fluorine regulation needs to be precisely quantified. The CO_2 electroreduction performance of the Ni–N_4 single-atom catalyst has been effectively optimized. Cao *et al.*[208] conducted a systematic analysis using density functional theory to investigate the regulatory mechanism of the metal atom's electron loss behavior on CO_2 adsorption in N-doped carbon nanotubes loaded with transition metal monatomic catalysts (M@CNT, M@1N_CNT, M@2N_CNT, M@3N_CNT). The free energy of the CO_2 reaction pathway is shown in Fig. 6c. Ni@2N_CNT and Pd@2N_CNT exhibit an energy descent feature of 0.15 eV during the first step of hydrogenation to form the *COOH intermediate, while the free energy of this step for other coordination environment catalysts such as Cu@1N_CNT and Ni@1N_CNT is positive. The free energy curve of the M@2N_CNT system in Fig. 4 further clarifies that the formation of *COOH is spontaneous and the energy barrier for the second step of hydrogenation to generate *CO is only 0.23–0.32 eV. These data indicate that the coordination number of metal atoms and N atoms will affect the activation energy barrier of CO_2 through regulating the electron transfer efficiency. The double-N coordination (M@2N_CNT) can enhance the ability of metal atoms to lose electrons and strengthen CO_2 adsorption and activation, ultimately making Pd@2N_CNT and Ni@2N_CNT the preferred catalytic systems for CO_2 reduction to CO, providing a clear thermodynamic basis for the optimization of the coordination environment of SACs. Li *et al.*[209] by doping with P, showed that the electronic structure of the active center and the coordination environment of the Fe–N–C monometallic catalyst can be regulated and optimized. The data in Fig. 6d of the study show that the Fe–N_3P coordination configuration formed by P doping reduces the free energy barrier for the formation of the *COOH intermediate from 0.63 eV in the Fe–N_4 configuration to 0.48 eV, and the desorption energy barrier of *CO decreases from 1.09 eV to 0.81 eV. Meanwhile, the free energy barrier of the HER remains at 0.24 eV (close to 0.27 eV in the Fe–N_4 configuration). The charge density distribution analysis in Fig. 6d further indicates that the introduction of P causes the local aggregation of the electron cloud at the Fe center and a reduction in the oxidation state. This not only confirms that P doping can enhance CO_2 activation and *CO desorption, inhibit competitive HER, and thereby improve the catalytic performance, but also enable the Fe–N/P–C catalyst to achieve a 98% CO faradaic efficiency at a low overpotential of 0.34 V. After a 24-hour stability test, there is no Fe atomic aggregation (no characteristic Fe–Fe bond peaks in the EXAFS spectrum), proving that P doping is an effective strategy for regulating the activity, selectivity, and stability of Fe–N–C monometallic catalysts. It provides key experimental and theoretical support for the synergistic optimization of single-atom catalytic systems with heteroatoms. The introduction of S into Co–N–C SACs was found to boost the CO_2-to-CO conversion by optimizing the electronic structure of the active centers.[210] Additionally, Wang *et al.*[211] revealed that asymmetric coordination brings about electronic localization at Ca sites, facilitating efficient CO_2-to-CO reduction. These findings collectively demonstrate that precise atomic-level control over electronic structures is paramount for optimizing catalyst activity.

The coordinative environment and electronic structure are pivotal in determining the catalytic efficacy. Wang's group[212] developed a catalyst featuring bismuth atomic sites co-coordinated by nitrogen and sulfur. Synthesized *via* a cation–anion diffusion strategy, this catalyst exhibits enhanced electrocatalytic activity.[213] Li *et al.*[214] explored low-valent $Zn^{\delta+}$ single-atom sites, which demonstrated high current density and promising industrial application potential. Moreover, Song *et al.*[215] introduced a boron-doped Ni–N_4 SAC, where boron atoms collaborate with nickel to lower the energy barrier of *COOH generation, thereby realizing excellent performance in CO_2 reduction. Guo *et al.*[216] revealed a correlation between the tailored atomic environment of SnN_3O_1 sites and enhanced transformation of CO_2 into CO *via* regulating the intermediates' binding energy, while simultaneously inhibiting competitive pathways such as HCOOH generation. In a related vein, Chaipraditgul *et al.*[217] investigated transition metal modifications on alumina supports to modulate surface interactions, though their research extended to CO_2 hydrogenation for alkene production.

3.1.2. Performance and mechanisms on dual-/tri-atom catalysts. The role of multi-atomic configurations and electronic interactions in DACs has also garnered significant attention. Jiao *et al.*[218] documented a diatomic catalyst featuring two adjacent Cu atoms. This configuration promotes the bimolecular step of CO_2 reduction by lowering the activation barrier, thereby exhibiting superior selectivity and stability. Hu *et al.*[219] validated that atomic sites can function both as active centers and electronic regulators. Similarly, Zhang *et al.*[220] documented a Ni–Cu diatomic catalyst dispersed on N-doped carbon, demonstrating that the electronic Ni–Cu atomic interaction acts as a key driver for the pH-universal electroreduction of CO_2 to CO. These studies underscore the importance of multi-atomic configurations in tuning electronic properties and improving catalytic efficiency. Efforts have also been made to construct dual-site catalysts with tailored atomic interactions to optimize catalytic performance.

Sun *et al.*[221] showed that regulating the microenvironment of Ni–Fe binary SACs using ionic liquids can further enhance CO_2 electroreduction, indicating that microenvironment engineering is pivotal for the performance of diatomic catalysts. The synergistic effects observed in these diatomic systems are supported by *in situ* spectroscopic and theoretical studies, which confirm that such configurations can reduce activation energy and promote the selective generation of CO. Additionally, Sun's team[173] conducted a comparative study between single-atom and multi-atom catalysts. By designing transition metal catalysts (TM-C_2N_1) supported on single-layer nitrogen-doped graphene, they achieved CO_2 reduction to CO using both single-atom and multi-atom catalyst systems. Gibbs free energy

and electronic structure studies on 3TM-C_2N_1 indicated their superior catalytic performance for CO during the CO_2RR, with relatively low limiting potentials, which offer a novel approach to promoting sustainable CO_2 conversion.

The Huang team[222] reported the Fe–Se bimetallic single-atom catalyst FeSe–NC, prepared by a selenic acid etching-assisted method, achieves efficient CO_2-to-CO conversion through the synergistic effect of Fe–N_4 and Se–C_2 sites. The core mechanism was characterized and verified by Fig. 7a and theoretical calculations. *In situ* ATR-FTIR showed that the introduction of Se atoms significantly weakened the adsorption strength of *CO at the Fe sites and accelerated the desorption of

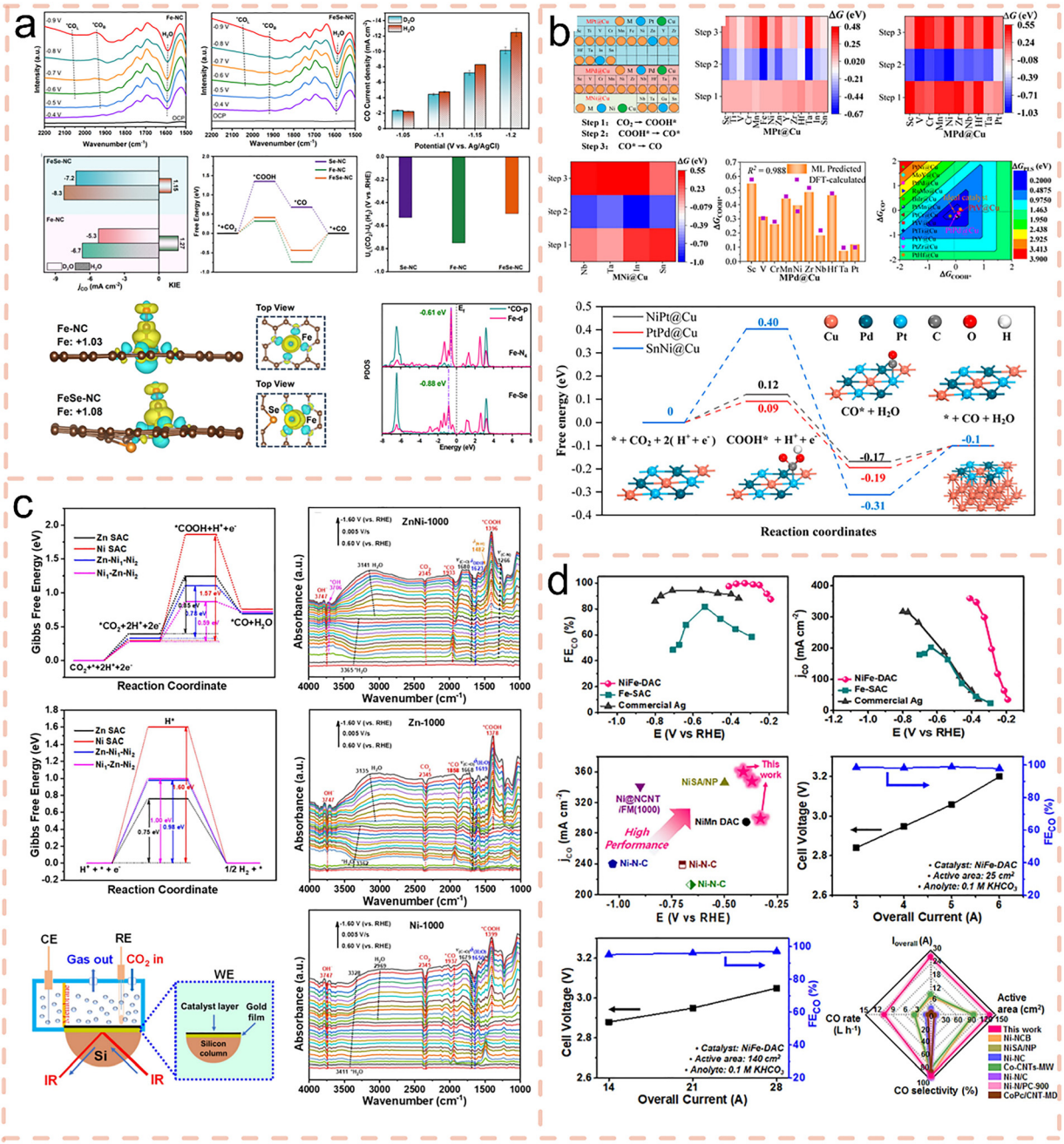

Fig. 7 (a) *In situ* ATR-FTIR spectra, CO partial current densities in H_2O/D_2O, kinetic isotope effects, and theoretical calculations comparing the CO_2 reduction reaction performance and electronic structure of Fe–NC and FeSe–NC catalysts. Reproduced with permission from ref. 222, Copyright 2024 by American Chemical Society. (b) Performance evaluation of the three ML algorithms. Reproduced with permission from ref. 224, Copyright 2023 by American Chemical Society. (c) Gibbs free energy profiles for CO_2-to-CO and the HER on various structural models, a schematic of the *in situ* ATR-SEIRAS setup, and the corresponding spectra for the ZnNi-1000, Zn-SAC, and Ni-SAC catalysts. Reproduced with permission from ref. 225, Copyright 2024 by Elsevier. (d) Electrochemical CO_2 reduction performance in a GDE flow cell and a zero-gap MEA electrolyzer using a NiFe-DAC catalyst. Metrics include CO faradaic efficiency (FE_{CO}), partial current density, and comparative performance analysis against state-of-the-art catalysts across multiple scales. Reproduced with permission from ref. 223. Copyright 2024 by Elsevier.

*CO. KIE analysis indicated an improvement in proton transfer kinetics. DFT calculations confirmed that the Fe-Se synergy not only lowered the formation energy barrier of *COOH but also optimized the thermodynamics of *CO desorption. Moreover, the negative shift of the d-band center of Fe (−0.61 to −0.88 eV) and the increase in the difference in the limit potential between the CO_2RR/HER enhanced the inhibition of the HER side reaction. Combined with the mass transfer advantage of the hierarchical porous structure, the catalyst was stably generated as CO at high FE_{CO} (up to 97.7%) and industrial-grade j_{CO} (228 mA cm^{-2}).

Similarly, Han *et al.*[223] investigated that the high CO selectivity of NiFe-DAC is attributed to the cooperative electronic regulation of Fe–$N_5$and Ni–N_4Ni–N_4 sites. As shown in Fig. 7d, the Fe–N_5 site preferentially adsorbs activated CO_2 to form the *COOH intermediate (with a binding energy similar to that of Fe-SAC), and the adjacent Ni–N_4 site weakens the Fe's adsorption of *CO through electron coupling (the desorption free energy decreases from 1.1 eV to 0.1 eV), avoiding site poisoning and accelerating the desorption of *CO, moreover, the Ni site has a stronger adsorption of H_2O, inhibiting its own adsorption of CO_2, thus enabling the CO_2 to selectively accumulate at the Fe site.

Xiong *et al.*[224] utilized machine learning (support vector regression algorithm) to predict that the overpotential of this catalyst is 0.11 V. As shown in Fig. 7b, the decisive step for the reduction of CO_2 to CO is $CO_2 \rightarrow COOH^*$, and its overpotential is only 0.09 V. The results of the two are highly consistent, confirming the reliability of the catalytic activity. Electrochemical tests showed that at an electrode potential of −0.8 V vs RHE, the CO faradaic efficiency of this catalyst is as high as 82.12%, significantly higher than that of pure Cu (57.04%), Pd@Cu (79.25%), and Pt@Cu (71.24%). Meanwhile, the faradaic efficiency of H_2 is lower than those of the above control catalysts. This effectively inhibits the HER. In the stability experiment, after continuous electrolysis in the H-cell for 12 hours, the current density and CO faradaic efficiency did not show significant decline, and XRD characterization confirmed that its crystal structure remained stable with no significant changes. This verified the core value of PdPt@Cu as an efficient catalyst for CO_2 reduction to CO.

Furthermore, studies have shown that the performance of the ZnNi-TACs catalyst in converting CO_2 to CO is superior to that of SACs.[225] As confirmed by Fig. 7c, the free energy curve of the CO_2RR for its core triatomic structure (Zn–Ni_1–Ni_2, Ni_1–Zn–Ni_2) is significantly lower than that of SACs, significantly reducing the activation energy barrier for the formation of COOH, which is more favorable for subsequent CO hydrogenation and desorption thermodynamics, and effectively inhibiting the HER. The *in situ* ATR-SEIRAS spectroscopy further captured the evolution of key intermediates. The peaks at 3365 cm^{-1} and 1623 cm^{-1} confirmed the adsorption and dissociation of H_2O on the Zn atoms, the peak at 3706 cm^{-1} and the peak at 1482 cm^{-1} indicated that *H was stabilized by the N atom; the intensity of the characteristic peaks at 1396 cm^{-1} (*COOH) and 1933 cm^{-1} (*CO) increased with the negative shift of the potential, and the peak positions and intensities were higher than those of Zn-SAC and Ni-SAC, confirming that the triatomic structure accelerates the formation and transformation of intermediates. This enables efficient and highly selective CO generation.

3.1.3. Performance and mechanisms on metal clusters. As illustrated in Fig. 8(a), Cai's team[226] verified *via in situ* ATR-IR that local electric fields enhance *COOH adsorption, promoting CO formation during the CO_2RR. Wang *et al.*[229] showed that atomically dispersed Pt on CeO_2 nanoparticles efficiently catalyze CO_2 reduction, with *in situ* DRIFTS unraveling the interplay mechanism between isolated atoms and nanoclusters. Galvita *et al.*[230] prepared bifunctional 5% Ni/CeO_2–Fe_2O_3 (1 : 1) samples, which enable CO_2-to-CO conversion *via* the CH_4 + CO_2/CO_2 redox cycle. The incorporation of Ni enhances the material's activity in the temperature range of 873–973 K. During the reductive step CH_4 reacts with CO_2 on Ni sites to diminish the oxygen storage component, while in the oxidation step, the oxygen storage component is further oxidized by CO_2 to form CO. Similarly, Zhanaidarova *et al.*[231] investigated the anchoring of Re(*t*Bu-bpy)$(CO)_3$Cl on MWCNTs, which increases the current density, lowers the overpotential, and maintains CO selectivity under aqueous conditions. This highlights that polyatomic catalysts supported on conductive substrates can boost CO_2 electroreduction efficiency.

The role of metal/oxide interactions in regulating catalytic activity was further exemplified by Huo *et al.*,[232] who studied Cu/SnO_x heterostructure CNT-supported nanoparticles. Their systematic analysis revealed that component-dependent metal-oxide interplay significantly affects CO_2 electroreduction, suggesting that multi-atomic configurations can optimize the selectivity toward target products. Nanostructured Au catalysts are also employed in electrochemical CO_2 reduction. Pan *et al.*[59] obtained dynamic reconfiguration of N,OH–Cu_3 clusters originated from atomically single-metal sites. Fig. 8b shows Cu–N_3 sites by regulating the atomic-level structure of Cu active sites and designing the engineered macro-morphology of the carbon support. Benefiting from the moderate CO adsorption ability and low CO hydrogenation energy barrier, the N,OH–Cu_3 site attains an unprecedented Faraday efficiency of 74.2% for the CO_2-to-CH_4 conversion at an industrial-grade current density of 300 mA cm^{-2}. Nursanto *et al.*[233] found that the CO selectivity exhibited a positive dependence on Au loading, plateauing at 78% as the morphology evolved from clustered to layered structures. The superior mass activity of 4 nm nanoparticles definitively confirmed that the nanoscale architecture dictates the CO production reactivity and selectivity.

Alfonso *et al.*[234] further analyzed ligand-protected Au_{25} clusters, noting that fully ligand-protected clusters lack efficiency for CO_2 reduction due to the high electrocatalytic potential required to form the key carboxyl intermediate, emphasizing the importance of surface and ligand engineering in cluster catalysts. Au_{25} nanoclusters reported by Wu's team[235] are equipped with thiol ligands, one hand to maintain the $Au_{25}(SR)_{18}$ structure, but cover all Au sites to CO adsorption and make the intact catalyst dead, while the other to detach from

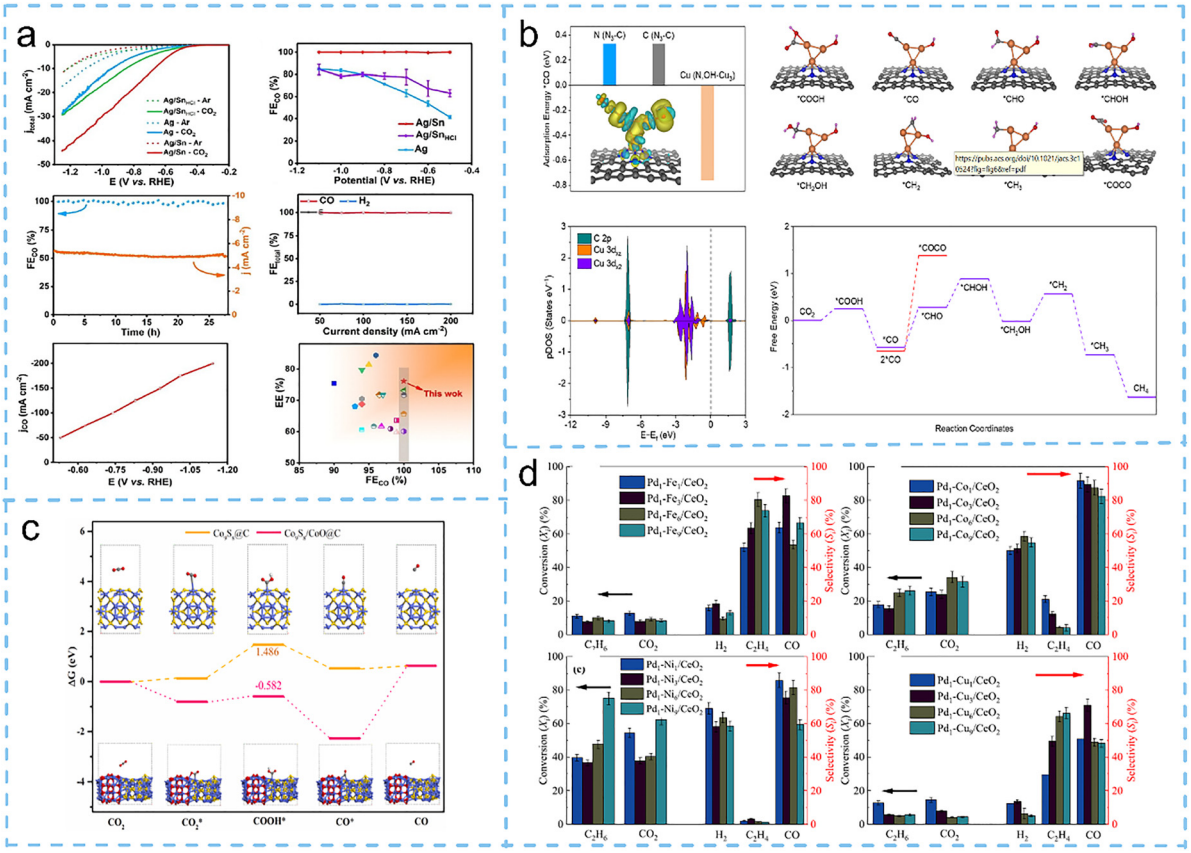

Fig. 8 (a) Electrochemical performance of the CO_2RR on the catalyst structure. Reproduced with permission from ref. 226, Copyright 2022 by Wiley. (b) Depicted are the predicted *CO adsorption energies and DOS at different sites, the optimized adsorption geometries of key intermediates on N, OH-Cu_3, and the free energy profiles (at 0 V *vs.* RHE) for CO_2 reduction to CH_4 and for *COCO coupling on the same active site. Reproduced with permission from ref. 59, Copyright 2024 by American Chemical Society. (c) Energy profiles along the pathway for photochemical CO_2-to-CO conversion. Reproduced with permission from ref. 227, Copyright 2021 by Elsevier. (d) The catalyst library of Pd–Fe/Co/Ni/Cu bimetallic systems with different doping ratios, applied in the ethane/CO_2 reaction. Reproduced with permission from ref. 228, Copyright 2021 by Elsevier.

the $Au_{25}(SR)_{18}/CeO_2$ interface at $\geq$423 K to activate CO and induce low-temperature CO oxidation on the $Au_{25}(SR)_{18}/CeO_2$ rod-shaped catalyst. Xiao *et al.*[236] highlighted the significance of metal–ligand cooperation in dinickel complexes, showing that bimetallic synergy significantly enhances catalytic reactivity—their $Ni^{II}Ni^{II}$(bphpp)$(AcO)_2$ complex exhibits 5-fold higher reactivity than mononuclear analogs.

As indicated in Fig. 8(c), Xu *et al.*[227] found epitaxially grown Co_9S_8 embedded with CoO, which strengthens CO_2 adsorption affinity and activates the molecule *via* bond length extension, facilitating reduction to CO. This underscores the value of engineering multi-atomic structures to promote CO_2 activation. Additionally, doping the catalyst matrix can regulate activity and selectivity. Han's team[237] reported a high-performance atomic Fe–In–NC catalyst for CO_2 reduction, which achieved a 95% CO faradaic efficiency and surpassed Fe–NC across a broad potential range. This performance was attributed to the Fe–In d–p orbital hybridization, which concurrently promotes *CO desorption and reduces the *COOH formation barrier. Li *et al.*[228] explored Pd doping in Fe/Ni/CeO_2 catalysts (Fig. 8(d)), where Ni_6/CeO_2 achieved 96.5% CO selectivity in ethane-CO_2 dry reforming, demonstrating excellent performance. However, Pd doping in Ni-based catalysts reduces syngas selectivity due to enhanced cleavage of C–C bonds and increased activation of CO_2 energy barriers, which is unfavorable for CO generation. Fe-based and Pd-doped Fe-based catalysts preferentially produce ethylene, with minimal impact on CO.

In summary, the production of *COOH is considered to be the rate-determining step in the conversion of CO_2-to-CO.[238] Therefore, the final selectivity and energy yield of this reaction are greatly limited by the *COOH intermediate adsorption on the effective sites of the surface. Furthermore, it is reasonable to construct a strong atomic local electric field by heteroatom doping to improve the *COOH adsorption.

3.2. CO_2 reduction to HCOOH

The electrocatalytic transformation of CO_2 to liquid fuels utilizing renewable energy offers a compelling strategy to mitigate carbon footprints while addressing energy storage challenges.[238] Among the diverse products of the CO_2RR, HCOOH stands out due to its high molar electron uptake and inherent energy density and chemical fuel.[239] Achieving efficient HCOOH production requires innovative synthetic approaches to precisely engineer atomically dispersed active

sites *via* atomic-level compositional tuning,[240] alongside a deep understanding of structure–performance–activity relationships across metal species to enable knowledge-driven catalyst design.

To date, extensive efforts have focused on developing catalysts for HCOOH/$HCOO^-$ production in the CO_2RR, primarily involving p-block metals.[241] This 2-electron transfer process has a complex reaction mechanism. After decades of research, the potential pathways have been identified. CO_2 is adsorbed at the active sites of the catalyst, undergoes activation and reduction processes to form intermediates such as *HCOO, *COOH or *OCHO, and eventually generates HCOOH/$HCOO^-$.

3.2.1. Performance and mechanisms on SACs. In the research on the reduction of HCOOH by CO_2, SACs precisely directed the HCOO or OCHO reaction pathways through active site regulation, heteroatomic coordination modification and carrier structure optimization, effectively inhibiting side reactions and the HER, demonstrating excellent catalytic performance and selectivity. Zheng *et al.*[242] recently combined *in situ* spectroscopic analysis complemented by theoretical modeling calculations to reveal that Cu active sites in Pb_1Cu catalysts regulate the initial protonation step of the CO_2RR, steering the reaction toward *HCOO (rather than *COOH) formation. This pathway avoids by-product generation, achieving a Faradaic efficiency of 96% toward formate. Zhang *et al.*[243] proposed transition metal-embedded 2D C_3N materials as stable, conductive platforms for the CO_2RR, shedding light on how stability and metallic conductance enhance electron transfer in the course of reduction. They evaluated CO_2RR performance of M-CC catalysts—formed by embedding transition metal single (TM) atoms in C=C double bond vacancies of C_3N monolayers—alongside TM-N-C (TM-N co-doped carbon) materials. M-CC catalysts facilitate electron transport in electrocatalysis, with all M-CCs showing superior selectivity for the CO_2RR over the HER. Notably, Cu-CC exhibits a low U_L of 0.68 V toward HCOOH production. Song *et al.*[244] explored SACs embedded in antimonene monolayers for the CO_2RR, finding that 3d non-precious TMs anchored on antimonene exhibit superior CO_2RR selectivity over the HER. Among these, Zn-based SACs uniquely produce HCOOH, while others primarily generate CH_4. Co@antimonene exhibits a low overpotential (0.50 V), which rivals that of state-of-the-art electrocatalysts. The interaction between TMs and antimonene modulates SACs intrinsic activity, while TM binding to potential-determining step (PDS) intermediates dictates CO_2RR overpotential and product selectivity.

The He team[245] investigated the single-atom Cu adsorbed Janus MoSSe monolayer catalyst (MoSSe-Cu). Fig. 9a clearly presents the complete reaction pathway of $CO_2 \rightarrow$ HCOOH. The rate-determining step is *OCHO $\rightarrow$ *HCOOH, and the corresponding free energy is only 0.49 eV, which is significantly lower than that of g-C_3N_4 and C_2N monolayer-loaded transition metal trimer catalysts (0.86 eV, 0.57 eV). The thermodynamic feasibility is better. From the free energy change in Fig. 9a, it can be seen that the step of $*CO_2$ combining with the proton-electron pair to form *OCHO has a free energy reduction of 0.78 eV, which is a spontaneous reaction, while the free energy for generating the competing intermediate *COOH is only reduced by 0.10 eV. Thermodynamically, the *OCHO path is dominant, ensuring the high selectivity of HCOOH. Chen *et al.*[246] found that introducing sulfur atoms into the NiN_4 coordination structure specifically formed NiN_2S_2 (Fig. 9(b)). Their work highlights the critical role of heteroatom coordination in modulating the performance of Ni SACs, as the sulfur dopants regulate the electronic properties environment of Ni active centers to favor *OCHO adsorption and subsequent formic acid formation.

Similarly, Zeng's team[247] explored MOF-derived 2D SACs based on transition metal-tetra hydroxybenzoquinone frameworks. These materials offer abundant accessible active sites and versatile functionalization capabilities, enabling precise tuning for specific reaction pathways—including selective reduction of CO_2. The MOF-based platform offers a flexible avenue for optimizing catalytic selectivity through structural design. Qian *et al.*[248] demonstrated that doping iron into a boron cage ($B_{10}H_{14}$) yields an innovative catalyst ($Fe@B_{10}H_{14}$) capable of catalyzing CO_2 hydrogenation by means of a two-step reduction pathway. As presented in Fig. 9(c), their quantum mechanical studies revealed that this catalyst can sequentially reduce two CO_2 molecules to produce HCOOH, highlighting the potential of metal-doped boron-based frameworks in CO_2 reduction. Further research into nickel-based SACs has also been conducted to explore their catalytic performance in formic acid generation, expanding the portfolio of promising catalyst systems for this reaction. As shown in Fig. 9d, Li *et al.*[249] reported the further protonation behavior of the HCOOH intermediate on the surface of $Mn@NbS_2$ indicates that the energy barriers required for its conversion to HOCHOH and *OCH intermediates are as high as 2.05 eV and 1.91 eV respectively, significantly higher than the energy barrier of 0.53 eV required for direct desorption to form HCOOH. Thermodynamically, this effectively inhibits the formation of by-products such as CH_4 and CH_3OH, ensuring the high selectivity of the HCOOH product. In terms of catalytic activity, Fig. 9d compares the limiting potential of $Mn@NbS_2$ with those of previously reported single-atom transition metal anchored two-dimensional transition metal chalcogenide (TMD) catalysts such as $Ti@WTe_2$, $Fe@MoTe_2$, and $Ni@MoTe_2$. This shows that the limiting potential of $Mn@NbS_2$ is as low as -0.53 V, which is within the optimal potential range for efficient catalytic reactions (absolute value <0.6 V), and only requires a lower applied driving voltage to achieve efficient reaction.

3.2.2. Performance and mechanisms on DACs/TACs. Liu's group[251] performed *in situ* DFT calculations at constant potential and microkinetic simulation analyses on 16 transition metal-main group metal combinations, as shown in Fig. 10(a). Operatively, dynamic reconstruction of CO_2 (from chemisorbed to physiosorbed states) drives the reaction to *OCHO (rather than *COOH) intermediates as a result of asymmetric charge buildup at bimetallic centers, and correlates this charge buildup with a proposed charge aggregation intensity (CAI) reactivity descriptor. Screening catalysts according to the CAI

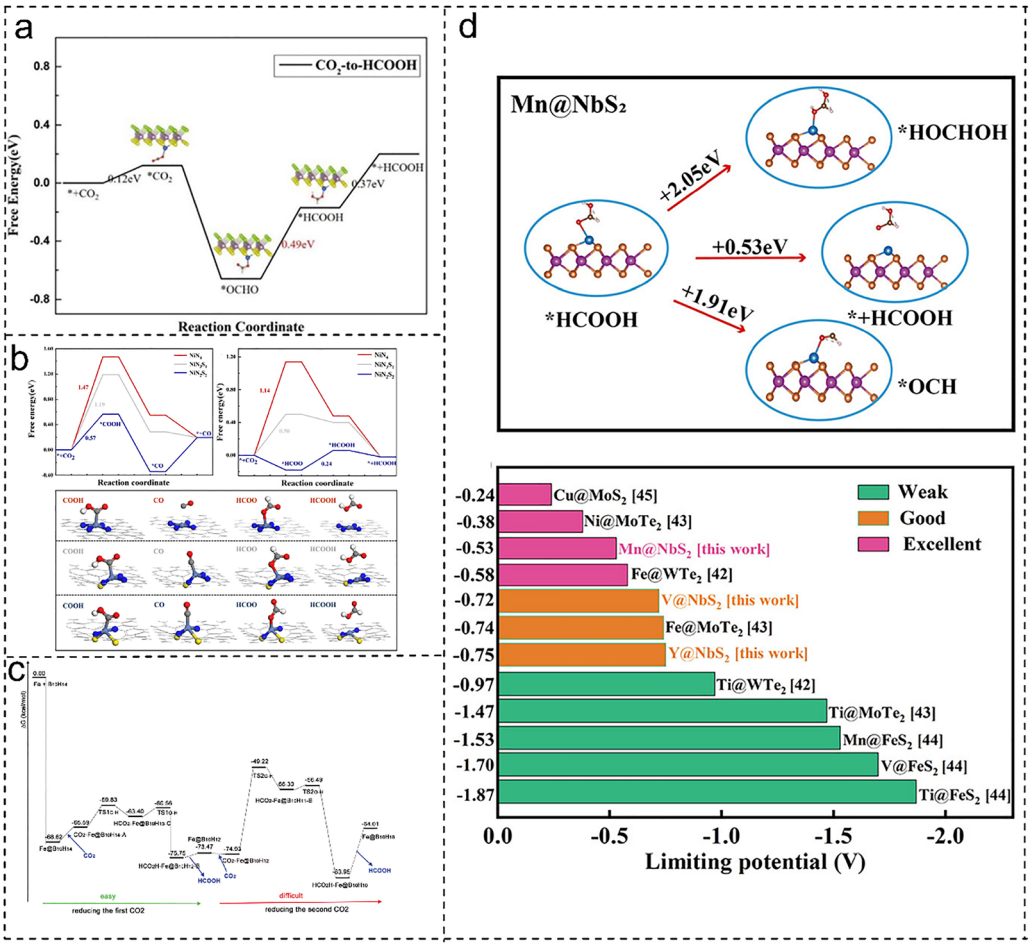

Fig. 9 (a) The reaction pathways and Gibbs free energy of CO_2 reduction to HCOOH on MoSSe-Cu. Reproduced with permission from ref. 245, Copyright 2023 by Elsevier. (b) Gibbs free energy profiles for the CO_2RR pathways to CO and HCOOH, along with the adsorption configurations of key intermediates on NiN_4, NiN_3S_1, and NiN_2S_2. Reproduced with permission from ref. 246, Copyright 2023 by the Royal Society of Chemistry. (c) The full catalytic cycle depicting the reduction of two CO_2 molecules by one equivalent of $Fe@B_{10}H_{14}$, computed at the B_3LYP-D_3 level. Reproduced with permission from ref. 250, Copyright 2017 by the Royal Society of Chemistry. (d) Potential reaction pathways from *HCOOH and comparative limiting potentials for CO_2-to-HCOOH conversion on single-atom transition metal catalysts supported on TMDs. Reproduced with permission from ref. 249, Copyright 2025 by American Chemical Society.

descriptor identifies the NiSb diatomic catalyst as very promising for HCOOH conversion. During formic acid synthesis, as shown in Fig. 10(b), the Cr-NiFe catalyst exhibits a preference for the COOH* pathway rather than the HCOO* pathway, with surface Cr atoms' negative charge and low d-band center enabling efficient formic acid production at an exceptional overpotential as low as 0.080 V while markedly inhibiting competing reactions.

Similarly, Fig. 10(c) shows Yang *et al.*[252] used DFT to screen M@2D-FeS_2 catalysts, revealing Co@2D-FeS_2 exhibits excellent activity and selectivity for HCOOH while strongly inhibiting the HER. Sun's team[173] compared SACs and multi-atom catalysts (MACs), developing TM-C_2N_1 for the CO_2RR. Gibbs free energy and electronic structure analyses on 3TM-C_2N_1 show favorable CO_2RR catalytic performance with low limiting potentials. Notably, 3Ti-C_2N_1 achieves optimal HCOOH production corresponding to a U_L of −0.42 V, positioned at the volcano plot vertex (Fig. 10(d)), offering a new route for sustainable CO_2 conversion. Liu *et al.*[175] designed trimetallic TM-NiFe catalysts, constructing 2D activity volcano curves to evaluate their performance in CO_2-to-CO and HCOOH conversion. Additionally, Sun *et al.*[253] engineered PtS_2-based SACs with 3d TMs as candidate CO_2RR electrocatalysts, systematically investigating pathways to C_1 products. All TM-PtS_2 SACs show higher selectivity for C_1 products over the HER. For Sc, Ti, V, Cr, Mn, Fe, and Cu supported on PtS_2-SV (sulfur-vacancy PtS_2), HCOOH is the dominant product, while Co^-, Ni^-, and Zn-PtS_2 generate diverse C_1 products.

3.2.3. Performance and mechanisms on metal clusters. In catalyst design, targeted structural engineering and interface regulation have emerged as effective strategies to enhance formic acid production in CO_2 electroreduction. Wu *et al.*[254] developed a 3D porous-structured bimetallic Bi–Sn aerogel and well-defined Bi–Sn interfaces. Compared to monometallic Bi or Sn catalysts, this aerogel exposes an increased number of active sites and demonstrates superior mass transfer capabilities,

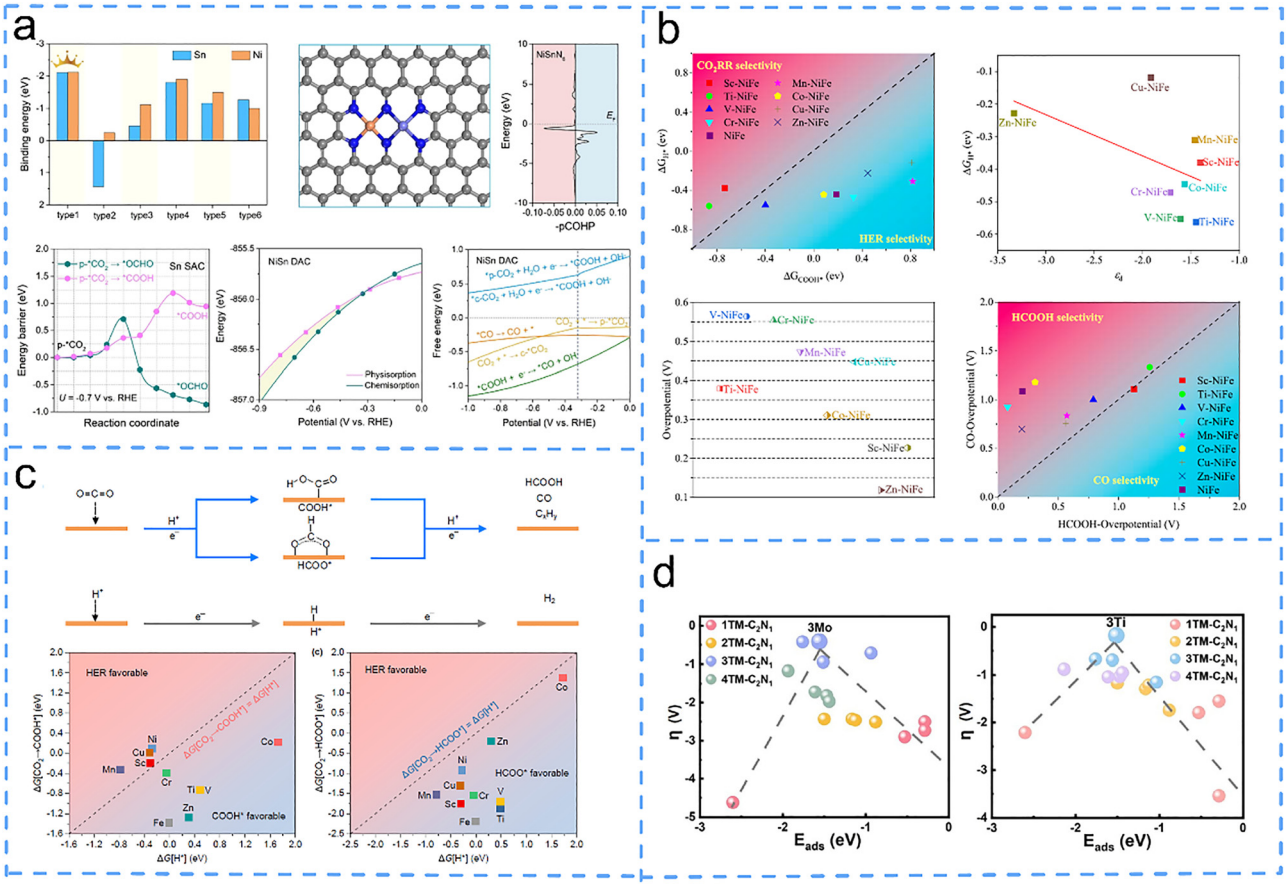

Fig. 10 (a) Calculated binding energies of NiSn DACs in various configurations, pCOHP between Ni and Sn atoms, reaction pathways for *CO_2 protonation to COOH/OCHO, potential-dependent total energies of adsorption configurations, and free energy profiles for the CO_2-to-CO reduction process. Reproduced with permission from ref. 226, Copyright 2025 by American Chemical Society. (b) Gibbs free energy comparisons for the CO_2RR and HER, the correlation between ΔG_h* and ε_d, the HER overpotential on TM-NiFe catalysts, and mechanistic analysis of CO/HCOOH selectivity *via* the *COOH intermediate. Reproduced with permission from ref. 175, Copyright 2023 by Elsevier. (c) Reaction pathways and corresponding Gibbs free energy diagrams for the HER and the conversion of CO_2 to COOH/HCOO intermediates. Reproduced with permission from ref. 252, Copyright 2021 by Elsevier. (d) Correlation between the adsorption energy of products and their corresponding overpotential. Reproduced with permission from ref. 173, Copyright 2024 by the Royal Society of Chemistry.

enabling a HCOOH faradaic efficiency (FE_{COOH}) of up to 93.9% and achieving superior selectivity for CO_2-to-HCOOH conversion. Wei *et al.*[255] further highlighted the critical role of bimetallic interfaces by investigating surface-defined In–Cu nanoparticles (Fig. 11(a)). Their indium-based catalyst achieved a breakthrough in formic acid faradaic efficiency of 90%—significantly outperforming traditional indium-based materials. DFT calculations revealed the underlying mechanism. The In (101) crystal planes in $In_\gamma Cu_\gamma$ nanoparticles effectively enhance the stability of the *OCHO species, thereby decreasing the reaction energy barrier associated with CO_2-to-HCOOH conversion while also accelerating the overall reaction kinetics.

At the atomic scale, Jiang *et al.*[256] observed that in CO_2-saturated 0.1 M $KHCO_3$ solution, Pd-B/C catalysts achieve a format Faraday efficiency (η_{HCOO^-}) of 70% following 2 hours of electrolysis. Even at potentials more negative than the −0.5 V mark—where CO formation (η_{CO}) increases—the η_{HCOO^-}/η_{CO} selectivity ratio remains significantly higher for Pd–B/C than Pd/C, indicating that subsurface B doping on Pd preferentially promotes adsorption and formation of the format-pathway intermediate *HCOO over the CO^- pathway intermediate *COOH. Catalyst structural features, such as grain boundaries and nanostructures, also modulate CO_2 reduction performance. Kumar *et al.*[250] then demonstrated that SnO_2 porous nanowires with diminished SnO_2 grain boundaries, and thus increased active-site density, exhibit enhanced CO_2-to-HCOOH conversion. This catalyst can initiate formic acid synthesis at a low overpotential (350 mV) and sustain a faradaic efficiency of 80% at −0.8 V *vs.* RHE, with higher energy conversion efficiency than similar systems.

Advances in catalyst design extend to ultrathin 2D nanostructures. Zhang *et al.*[259] obtained ultrathin Bi nanosheets synthesized by liquid-phase exfoliation (Fig. 11(b)), where *OCHO intermediate formation preferentially occurs at edge sites (confirmed by lower Gibbs free energy) rather than basal planes. These nanosheets achieve an 86.0% formate Faraday efficiency at −1.1 V *vs.* RHE, where the current density reaches

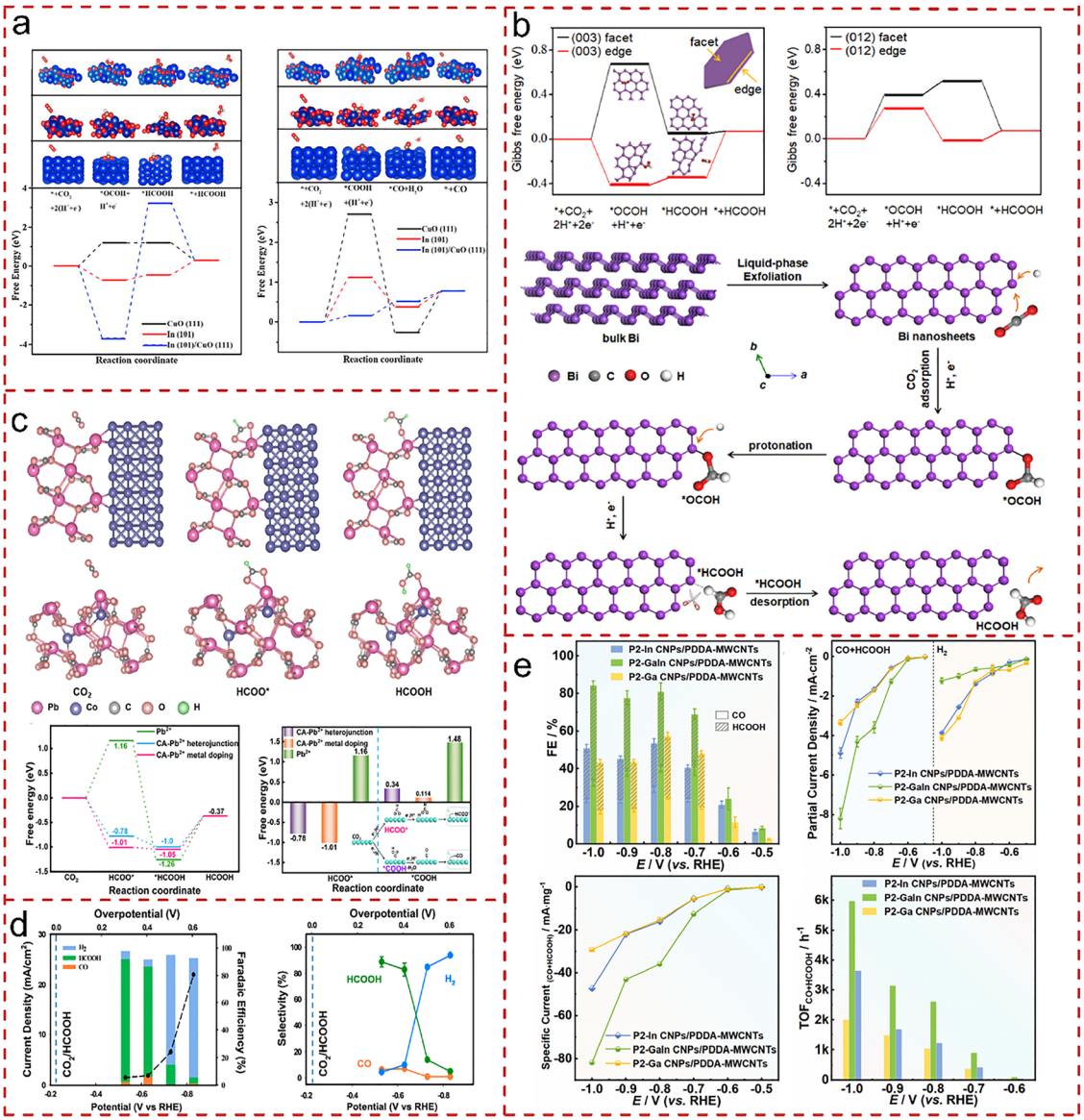

Fig. 11 (a) Comparative free energy diagrams for CO_2 reduction to HCOOH and CO on the In (101) (red) *versus* CuO (111) (black) facets. Reproduced with permission from ref. 255, Copyright 2021 by Elsevier. (b) Displayed are the DFT-calculated ΔG for the CO_2-to-formate pathways on both facet and edge sites of Bi (003) and (012) planes. A schematic diagram illustrates the mechanism for selective formate formation on Bi nanosheets. Reproduced with permission from ref. 256, Copyright 2018 by Elsevier. (c) The adsorption configurations of CO_2, HCOO* and HCOOH in the Co–$PbCO_3$ heterojunction and uniform metal doping, as well as the free energy diagram of the CO_2RR on the surface. Reproduced with permission from ref. 238, Copyright 2023 by Elsevier. (d) The average current density obtained at different overpotentials, faradaic efficiencies, and the product selectivities of H_2, HCOOH and CO generated at different overpotentials. Reproduced with permission from ref. 257, Copyright 2017 by American Chemical Society. (e) The faradaic efficiency, bias current density, specific current and conversion frequency of CO + HCOOH and H_2 are presented. Reproduced with permission from ref. 258, Copyright 2021 by Elsevier.

16.5 mA cm^{-2}, outperforming bulk Bi due to superior conductivity and plentiful edge sites. Atomically precise clusters offer tunable selectivity. Liu *et al.*[260] found that double tetrahedral Cu_8 clusters exhibit a formic acid Faraday efficiency of 92% at −1.0 V *vs.* RHE, surpassing cubic Cu_8 clusters. Theoretical studies reveal weaker competition with hydrogen evolution and lower *HCOO adsorption free energy on the double tetrahedral structure, clarifying how intermediate interactions govern activity and selectivity. Zhang's group[239] reported Co-modified $PbCO_3$ electrocatalysts achieving a formate faradaic efficiency of 98.15% at −0.70 V *vs.* RHE (Fig. 11(c)), and this performance stems from reduced *HCOO formation barriers and enhanced adsorption at Co–Pb^{2+} sites, where Pb^{2+} charge enrichment boosts formate selectivity. Tang *et al.*[257] highlighted the role of negatively charged hydrides in copper hydride nanoclusters (*e.g.*, $Cu_{32}H_{20}L_{12}$. Fig. 11(d)), which direct selectivity toward formic acid over CO at low overpotentials. DFT calculations further predict weaker hydrogen evolution

competitiveness under these conditions. Wang *et al.*[261] developed heterostructures of ultrasmall polymetallic sulfide clusters on MWCNTs (Fig. 11(e)), achieving >80% faradaic efficiency for CO_2-to-C_1 conversion (including formic acid) with a high turnover frequency (5974.62 h^{-1}) and 12-hour stability.

Thus, designing efficient electrocatalysts remains central to advancing CO_2RR for HCOOH production. Component engineering, defect engineering, and controlled morphology engineering are established strategies, but critical gaps persist including precise pore structure tuning for enhanced active surface area properties and mass transport capabilities. Future work still needs to address the issue of separating electrolytes from formic acid. The form of the product is closely related to the pH value of the system. Formic acid is formed under acidic conditions, while formate is formed under weakly alkaline conditions. Therefore, the separation process needs to be designed specifically based on this.[258] Notably, suppressing the thermodynamically favored HER still stands as a key challenge, requiring synergistic optimization of catalyst and reactor design.

3.3. CO_2 Reduction to CH_4

3.3.1. Performance and mechanisms on SACs. SACs demonstrate unique advantages in regulating active centers during the CO_2 reduction to CH_4 reaction. Different research teams have precisely designed the coordination environment and active sites to reveal multiple efficient conversion pathways. Zhang *et al.* discovered[262] that the generation of CH_4 in Ru_1/CeO_2 originates from the hydride species (H^-) induced by the formate (HCOO*) pathway. As shown in Fig. 12a, the Ru monomer is anchored in the vicinity of the oxygen vacancy on the (110) surface of CeO_2 in a tetrahedral coordination form. The difference in spin charge density indicates that Ru has +3 valence, and the formation energy of the oxygen vacancy is 0.37 eV (endothermic), which is consistent with the EPR and EXAFS characterization results. H_2 undergoes dissociative decomposition at the O–O_v site on the surface of Ru_1/CeO_2, generating H^- and H^+ species (*in situ* DRIFTS detected the H^- characteristic peak at 2130 cm^{-1}). This process releases 0.47 eV of heat, which is thermodynamically favorable, as shown in Fig. 12a. The H^- species preferentially attacks the $C^{\delta+}$ site of the adsorbed CO_2 to form an intermediate HCOO, and this step only requires overcoming an energy barrier of 1.00 eV and releases 0.44 eV of heat. The energy barrier for H^+ attacking the $O^{\delta-}$ site of CO_2 to form COOH can be as high as 2.34 eV, making this step kinetically unfavorable, thereby enabling Ru_1/CeO_2 to exhibit high CH_4 selectivity.

Similarly, the Han team[263] reported the SA-Zn/MNC single-atom catalyst, which achieves selective regulation of intermediates by the Zn-N_4 active site (Zn is +2 valence), successfully

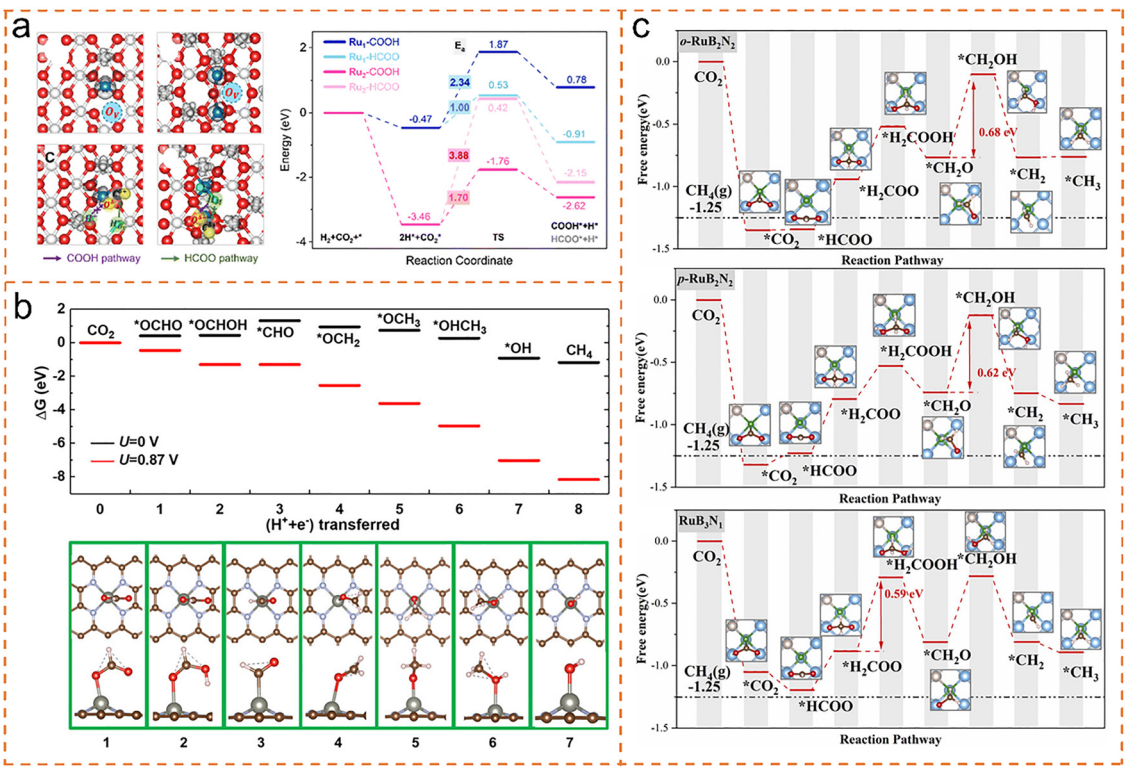

Fig. 12 (a) Structure and spin charge density analysis of Ru_1/CeO_2 and Ru_2/CeO_2 catalysts for selective CO_2 hydrogenation, including adsorption configurations, reaction pathways, and calculated energy profiles. Reproduced with permission from ref. 262, Copyright 2025 by the Royal Society of Chemistry. (b) Free energy diagrams and corresponding stable intermediate structures for the electrocatalytic reduction of CO_2 to CH_4 on a Zn–N_4-graphene catalyst. Reproduced with permission from ref. 263, Copyright 2020 by American Chemical Society. (c) Free energy for converting CO_2 to CH_4 *via* an 8-electron process on *o*-RuB_2N_2@TiN, *p*-RuB_2N_2@TiN and RuB_3N_1@TiN. Reproduced with permission from ref. 264, Copyright 2024 by Elsevier.

completing the CO_2 electroreduction to CH_4. Fig. 12b clearly shows its 8-electron transfer free energy pathway. CO_2 preferentially forms the OCHO intermediate at the Zn site (energy barrier 0.46 eV), rather than the key COOH (energy barrier 1.2 eV), blocking the competing pathways at the source. Fig. 12b also shows that OCHO forms bonds with the O atom through the O atom and carbon terminal protonation to form a stable configuration, with the rate-determining step being OCHOH → CHO (energy barrier 0.87 V). Each intermediate maintains stable coordination with Zn in Fig. 12b, and the $OHCH_3$ protonation releases CH_4, and the residual OH combines with H^+ to form H_2O, completing the cycle. *In situ* ATRSEIRAS further confirmed the existence of OCH_2 and *O CH_3 and no CO signal. Combined with the catalyst's microporous structure (525 m^2 g^{-1}, 1.04 nm) and the charge transport advantage of nitrogen-doped carbon support, SA-Zn/MNC achieved 85% CH_4 faradaic efficiency at −1.8 V *vs.* SCE, −31.8 mA cm^{-2} partial current density, and stable operation for 35 h.

Pan *et al.*[264] further optimized the active center through boron coordination, developing a TiN-supported Ru SAC (RuB_xN_{4-x}@TiN) for CO_2 reduction to CH_4 as another efficient solution. Among them, *o*-RuB_2N_2@TiN, *p*-Ru B_2N_2@TiN and Ru B_3N_1@TiN in Fig. 12c exhibited the best performance. Their formation energies were negative and the structure was stable at 500 K (the fluctuation of Ru–B bond length was only 0.02 Å). The B atom acted as a Lewis acid site, reducing the CO_2 adsorption energy to −1.57 eV, extending the C–O bond to 1.3 Å, and the charge transfer amount was 0.52–0.64e^-, achieving complete activation of CO_2. Moreover, the rate-determining step energy barrier for CH_4 generation was <0.7 eV, and the limiting potential was as low as 0.59–0.68 V, which was significantly superior to RuN_4@TiN (1.28 V) and pure TiN (1.72 V).

The excellent activity and selectivity were demonstrated by the synergistic effect of the coordination environment and the carrier, which showed a key reference for the structural design and path optimization of SACs in multi-electron transfer CO_2 reduction reactions.

3.3.2. Performance and mechanisms on DACs/TACs. In addition to SACs, bimetallic and metal cluster catalysts, through the cooperative effect between metal sites, also exhibit excellent performance in the multi-electron transfer reaction of CO_2 reduction to CH_4, providing a new direction for catalyst system design. Lu *et al.*[265] reported a bimetallic catalyst (M_2-NC) loaded on nitrogen-doped graphene. Among them, Ru_2-NC exhibited the most outstandingly performance, as shown in Fig. 13a. It followed the eight-electron transfer pathway, with the rate-determining step (PDS) being *CO → *CHO, and the free energy barrier was only 0.28 eV, much lower than Fe_2-NC (0.82 eV) and CO_2-NC (1.00 eV). During the reaction process, the energy barrier for *CO to be stably adsorbed at the Ru_2 bimetallic site and then protonation to form *CHO was as low as 0.55 eV. Subsequent steps of *CHOH dihydroxylation to form *CH and gradual hydrogenation to *CH_4 were exothermic reactions (ΔG ranging from −0.06 to −0.58 eV), with the desorption free energy of *CH_4 reaching −0.22 eV, exhibiting excellent thermodynamic feasibility. The limit potential for CH_4 generation was as low as −0.28 V, and the difference between its limit potential and the limit potential of the HER was positive, effectively inhibiting competing reactions. At an applied potential of −0.4 V, the reaction free energy barrier was reduced to a negative value, achieving efficient CH_4 generation. The bimetallic cooperative effect of Ru_2-NC was precisely the core reason for optimizing the adsorption strength of intermediates and reducing the energy barriers of key steps.

The Fe_2Ir@NG bimetallic catalyst developed by Han *et al.*[266] exhibits distinct reaction pathway characteristics. Fig. 13b comprehensively depicts the key process of CO_2 conversion to CH_4 on its surface. As can be seen from the figure, after CO_2 adsorption, a proton-electron pair transfer occurs to generate the CO + OH intermediate, which lowers the free energy by 0.74 eV. This step is a spontaneous reaction and does not require overcoming an energy barrier. Subsequently, CO gradually undergoes hydrogenation to form intermediates such as CHO (ΔG = 0.36 eV) and CHOH (ΔG = 0.49 eV), with the rate-determining step being CHO → CHOH. The corresponding limiting potential is only 0.49 V, significantly lower than that of the similar Fe_3@NG catalyst (0.79 V). Comparing the free energy data of the CH_3OH and CO generation pathways in the figure, the free energies of all intermediates in the CH_4 generation pathway are at a lower level, and there are no high-energy barrier bottlenecks throughout the process. The thermodynamic advantage is significant, which is attributed to the synergistic effect of Fe and Ir atoms, optimizing the adsorption strength of key intermediates such as CO and *CHO, enabling the CH_4 generation process to have a low limiting potential and high spontaneity characteristics.

The Ti_3@NG catalyst studied by the Wang team[267] exhibits extremely high structural stability, providing a stable active environment for catalytic reactions. The adsorption process of CO_2 on its surface occurs spontaneously (with an adsorption free energy of negative value), and Ti_3@NG transfers 1.69*e* of charge to the CO_2 molecule, causing a significant reduction in the O–C–O bond angle and achieving efficient activation of the CO_2 molecule. The reaction path calculation in Fig. 13c indicates that the Ti_3@NG catalyst for CO_2 reduction follows the optimal path of CO_2* → COOH* → CO* → CHO* → HCHO* → H_3CO* → CH_4, with the rate-determining step being the process of combining CHO with proton-electron pairs to form HCHO. The corresponding limiting potential is only −0.53 V, which is superior to most reported catalysts for CH_4 generation. The volcano curve analysis further reveals that the adsorption intensity of Ti_3@NG for the key intermediate CO is moderate, precisely located at the summit active region of the CH_4 generation reaction, avoiding the retention of intermediates due to excessive adsorption or the inhibition of protonation due to insufficient adsorption. At the same time, its adsorption free energy for CO_2 is more negative than that of the H atom, and the limiting potential of the CO_2RR is lower than that of the HER, effectively inhibiting the competition of side reactions.

The above study achieved efficient CO_2 reduction to CH_4 by designing dual-atom (Ru_2-NC, Fe_2Ir@NG) and metal cluster

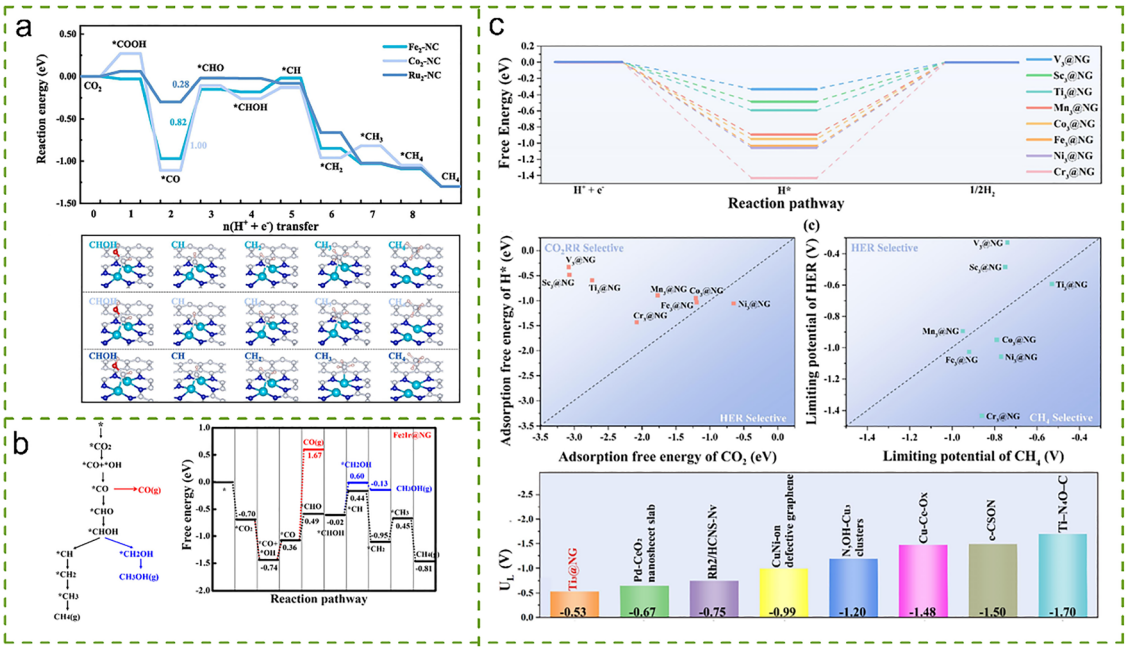

Fig. 13 (a) Free energy profiles of the CO_2RR to CH_4 and corresponding adsorption configurations. Reproduced with permission from ref. 265, Copyright 2024 by Elsevier. (b) Possible C1 pathways of CO_2 reduction on the Fe_2Ir@NG, and the corresponding free energy diagrams. Data denote the ΔG of each elementary step. Reproduced with permission from ref. 266, Copyright 2022 by American Chemical Society. (c) Competition between the CO_2RR and HER. Reproduced with permission from ref. 267, Copyright 2025 by Elsevier.

(Ti_3@NG) catalysts, and optimizing the adsorption of intermediates and reaction pathways through the synergistic effect of metal sites. The core performance advantages were confirmed through free energy calculations, structural stability characterization, and selectivity analysis, providing important references for the design and application of multi-atom cooperative catalytic systems in multi-electron transfer CO_2 reduction reactions.

3.3.3. Performance and mechanisms on metal clusters. In the catalytic system for CO_2 reduction to CH_4, atomic-level doping control and nanostructure engineering are the core strategies for improving performance. Different research teams have achieved optimization of the reaction pathway and breakthroughs in catalytic performance by precisely designing the composition and structure of the catalysts. Shi *et al.*[268] constructed single/multi-atomic alloy catalysts with transition metals (Fe, Co, Ni) doped into Cu13/Cu55 clusters. Through atomic-level local environment regulation, they achieved efficient conversion, as shown in Fig. 14a. The optimal configuration Co666 follows the reaction path of CO_2 → HCOO* → *OCH_2O → *OCH_2OH → CH_2O* → CH_3O* → CH_4. The continuous hydrogenation at the C site is the core mechanism. The rate-determining step (PDS) is *OH* → H_2O*, with a free energy barrier of only 0.33 eV, which is significantly better than the Cu(211) surface (0.74 eV). This performance is closely related to the coordination number of 6 (CN = 6). The CN = 6 sites can weaken the adsorption strength of HCOO* by filling the anti-bonding orbitals (the -ICOHP of Co666 is 1.30, lower than the value of 1.56 for Co565), while maintaining a moderate binding of H_2COO* to lower the energy barrier. Bader charge analysis indicates that after CO_2 adsorption, the C site gains more electrons, preferentially forming the HCOO* intermediate (rather than *COOH), effectively inhibiting the HER. Additionally, a small amount of doped Cu55-based catalyst (such as CO2Cu53) maintains a stable structure without collapse within 5 ps in the 300 K AIMD simulation, balancing activity and stability. The Fe666 and Ni666 configurations also exhibit excellent activity, with free energy barriers of 0.51 eV and superior to the corresponding CN = 5 configurations, providing key support for atomic-level precise design.

Similarly, the atomic-level cerium-doped copper oxide catalyst (Ce/CuO_x-NPs) reported by Chen's team[269] achieved efficient conversion by regulating the electronic structure and the adsorption behavior of intermediates, as shown in Fig. 14b. It followed the reaction path of CO_2 → *CO → *CHO → *CH_2O → *CH_3O → CH_4. *In situ* ATR-SEIRAS characterization detected key intermediate signals of *CHO and *CH_3O at 1490 cm^{-1} and 1397 cm^{-1}, without the appearance of C_2 product signals such as *OCCOH (1190 cm^{-1}). This demonstrated high selectivity. DFT calculations indicated that cerium doping reduced the energy barrier of the rapid step *CO → *CHO to 0.33 eV, which was much lower than that of pure Cu (0.82 eV) and CuO_x (1.10 eV), and simultaneously promoted the breakage of the C–O bond in *CH_3O. Projection density of states (PDOS) analysis showed that the overlap degree of the d orbitals of Cu in Ce/CuO_3 with the p orbitals of C in *CHO was significantly higher than that of pure Cu and CuO_3, strengthening the electron interaction. In electrochemical tests, the catalyst achieved a CH_4 faradaic efficiency (FE_{CH_4}) of 67.4% at −1.6 V (*vs.* RHE), with a partial current density of 293 mA cm^{-2}. The

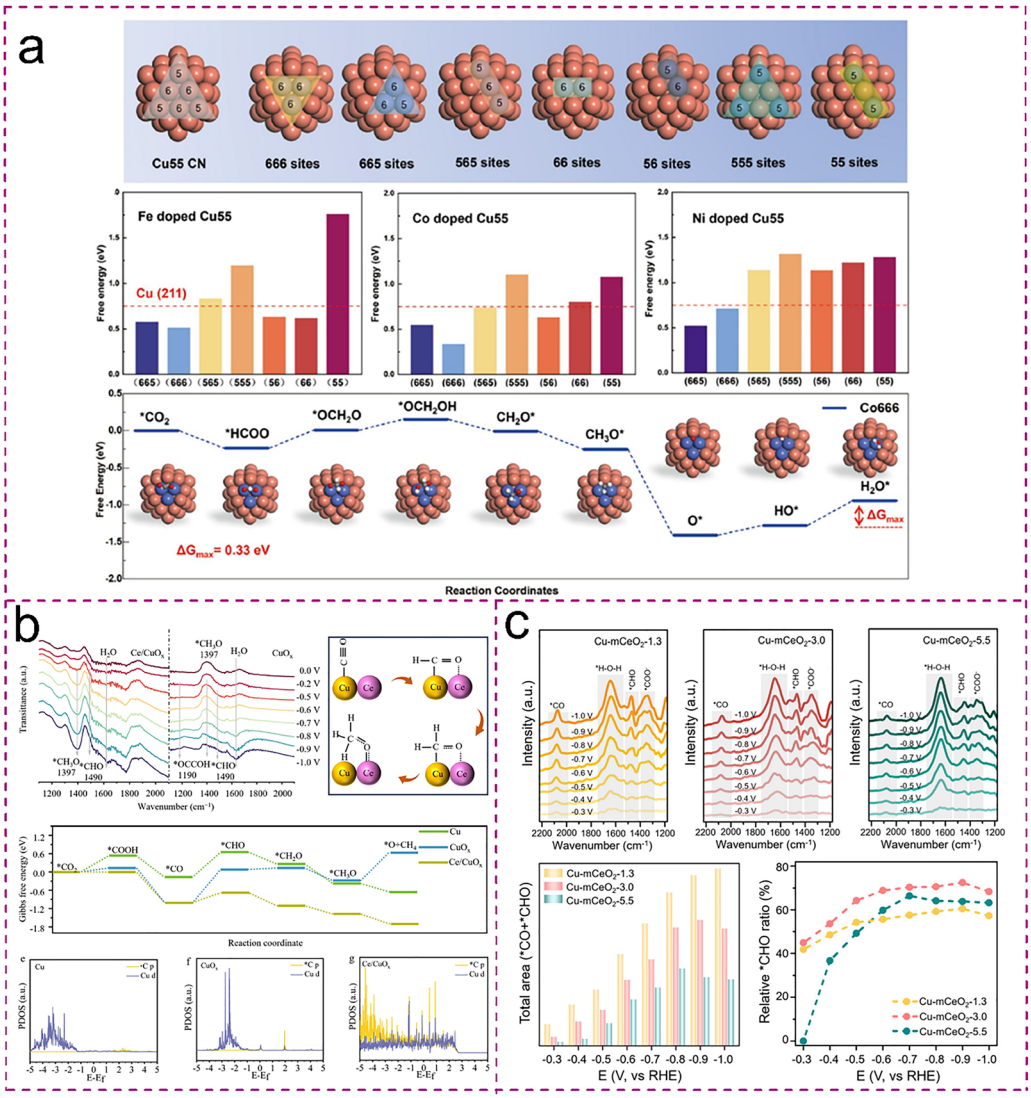

Fig. 14 (a) Coordination environment modulation strategies for CO_2 reduction and theoretical limiting potentials of CO_2-to-CH_4 conversion on Fe, Co, and Ni doped Cu_{55} clusters, along with the free energy diagram and optimized intermediate structures for CH_4 formation on a Co666 cluster. Reproduced with permission from ref. 268, Copyright 2024 by Elsevier. (b) *In situ* ATR-SEIRAS spectra of Ce/CuO_x-NPs and CuO_x-NPs catalysts under varying potentials, proposed reaction pathways for electrochemical CO_2 reduction to CH_4, calculated Gibbs free energy diagrams, and projected density of states analyses for *CHO intermediate adsorption. Reproduced with permission from ref. 269, Copyright 2025 by Elsevier. (c) *In situ* ATR-SEIRAS spectra of Cu-CeO_2 catalysts with varying compositions (Cu-CeO_2-1.3, -3.0, -5.5), total peak area analysis of *CO and *CHO adsorbates, and the relative proportion of *CHO within their combined signal. Reproduced with permission from ref. 270, Copyright 2025 by American Chemical Society.

FE_CH_4 remained above 62% within the voltage window of −1.4 to −1.75 V, and the 10-hour stability test showed no significant degradation in structure and performance, providing solid experimental and theoretical support.

In addition to atomic-level doping, the regulation of nanostructures has also achieved remarkable results. Xiong *et al.*[270] developed mesoporous Cu-CeO_2 nanospherical catalysts, which achieved nano-confined effect regulation through pore size engineering, providing a new path for reaction optimization. As shown in Fig. 14c, *in situ* ATR-SEIRAS characterization revealed that the intensity of the *CO and *CHO characteristic peaks at 2190–2110 cm^{-1} and 1480–1430 cm^{-1} increased with the reduction of pore size, confirming that small-sized pores can enhance the activation of CO_2 and the accumulation of intermediates. Among them, Cu-mCeO_2-3.0 with a pore size of 3.0 nm performed the best, and the peak area ratio of *CHO to *CO was the highest, indicating that the rate of *CO hydrogenation to *CHO (the rapid step of CH_4 formation) was the fastest. This catalyst achieved a CH_4 selectivity of 66.1 ± 2.9% at −1.4 V (*vs.* RHE), with a partial current density of 237.6 ± 14.5 mA cm^{-2}, and maintained high selectivity within a wide potential window. Comparing Cu-mCeO_2-1.3 with a pore size of 1.3 nm (where *CO and *CHO coverage was too high, resulting in C–C coupling) and Cu-mCeO_2-5.5 with a pore size of 5.5 nm (with a weak confined effect), it was confirmed that CH_4 selectivity has a volcano-like relationship with pore size.

Table 1 CO_2RR reduction pathway

Target product	Catalyst category	Representative catalyst	Key advantages	Critical performance metrics
CO	SACs	FeN_5@graphene, F–Ni–N_4, Fe–N_3P–C	100% atom utilization, high selectivity, tunable structure	$FE_{CO} \leq 98\%$, $\eta \leq 0.34$V, $h = 24$ h
	DACs	FeNi–NSC, PdPt@Cu, Ni–Cu@N–C	Dual-site synergy, optimized *CO desorption, suppressed HER	$FE_{CO} \leq 97.7\%$, TOF 20 695 h^{-1}
	TACs	Zn–Ni_1–Ni_2@C, MnMoFe@graphyne	Multi-atom synergy, breaks scaling relationship	$U_L = 0.34$ V, $FE_{CO} > 90\%$
	Clusters	Fe@meso-C, Fe–In–NC, AuCu alloycluster	Quantum-size effect, rich active sites, hybridized e-states	$FE_{CO} \leq 95\%$, enhanced *CO adsorption, durable
HCOOH	SACs	MoSSe–Cu, Zr_1@C_2N, NiN_2S_2	Pathway-specific, low η, robust structure	$FE_{HCOOH} \leq 96\%$, $E = 0.23$ V
	DACs	NiSb@C, Cr–NiFe@N–C	Charge accumulation, suppresses competing reactions	$\eta \leq 0.08$ V, $FE_{HCOOH} > 90\%$
	TACs	3Ti-C_2N_1, MnMoCu@graphyne	Asymmetric active sites, favorable thermodynamics	$U_L = 0.42$ V, strong HER suppression
	Clusters	Bi–Sn aerogel, In–Cu NP, Cu8 cluster	Prominent interface effect, fast mass transfer, dense sites	$FE_{HCOOH} \leq 98.15\%$, $j = 16.5$ mA cm^{-2}
CH_4	SACs	Ru_1/CeO_2, SA-Zn/MNC, RuB_2N_2@TiN	Single active center, precise intermediate tuning	$FE_{CH_4} \leq 85\%$, $h = 35$ h
	DACs	Ru_2-NC, Fe_2Ir@NG	Bimetallic synergy, lowers multi-e transfer barrier	$U_L = 0.28$ V, $FE_{CH_4} > 82\%$
	TACs	Ti_3@NG, N,OH-Cu_3 cluster	Stable framework, moderate *CO, suppressed C–C coupling	$FE_{CH_4} \leq 74.2\%$, $j = 300$ mA cm^{-2}
	Clusters	Co666@Cu55, Ce/CuO_x NPs, Cu-mCeO_2	Tunable e-structure, nano-confinement, abundant sites	$FE_{CH_4} \leq 67.4\%$, $j = 293$ mA cm^{-2}

The above study optimized the catalytic performance through two strategies, atomic-level doping (doping of transition metals in Cu clusters and Ce in CuO_x) and nano-confined effect (control of mesopore diameters). It focused on three core dimensions: electronic structure, intermediate adsorption, and reaction pathway. All achieved efficient CO_2 reduction to CH_4. The common mechanism lies in precisely regulating the local environment and macroscopic structure of the catalyst, reducing the energy barriers of key steps, strengthening the conversion of target intermediates, and inhibiting side reactions. This provides a comprehensive reference for the multi-dimensional design of highly active and highly selective CO_2-to-CH_4 catalysts.

In summary, the core performance and characteristics of different types of 2D loadable catalysts in the CO_2RR process for the production of C_1 products can be summarized as shown in Table 1.

4. Challenges and outlook

As described in this article, the significant progress of two-dimensional supported atomic-level and cluster-type catalysts in carbon dioxide reforming reactions is accompanied by a series of ongoing challenges that involve both experimental realization and theoretical understanding. Overcoming these bottlenecks is crucial for advancing this field from basic research to practical application.

4.1. Experimental challenges

Despite the remarkable achievements, the practical application of these advanced catalysts still faces numerous severe experimental challenges.[271] Precise and scalable synthesis, precisely synthesizing catalysts with uniform composition, specific atomic arrangement, and high-density structures on two-dimensional carriers remains a huge challenge. Current methods often only yield mixtures of individual atoms, clusters, and nanoparticles, which masks the true structure–activity relationship. Developing scalable and repeatable synthesis methods that can produce these catalysts at the atomic level with precision, and conduct industrial evaluations,[272] is of crucial importance. Operational stability and dynamic evolution, although *in situ* characterization has begun to reveal the dynamic characteristics of active sites under reaction conditions, the long-term structural and chemical stability of these catalysts under industrial-related current densities (*e.g.*, greater than 200 milliamperes per square centimeter) and long-term operation (*e.g.*, over 1000 hours) are still unclear.[273] The main issues include metal atom loss, carrier corrosion/collapse, and irreversible aggregation of atoms/clusters. Designing catalysts with inherent stability or understanding and mitigating degradation pathways through advanced electrolyte engineering and carrier modification is crucial.[274] Beyond model systems, the complexity of the actual electrochemical interface, most high-performance catalysts are evaluated in idealized hydrogen battery units using electrolytes saturated with pure carbon dioxide. Applying this evaluation method to more practical membrane electrode assemblies (MEA) or flow batteries introduces a series of complex and difficult-to-understand factors, such as complex ionic environments (*e.g.*, the presence of impurities, substitution of cations/anions), mass transport limitations under high current densities, and the interaction of local pH values, electric fields, and water management.[275–277] Systematic research is urgently needed to bridge model conditions with equipment conditions.

Advanced associated probe characterization requires the development and application of associated probe spectroscopy

and microscopy techniques, which can simultaneously provide chemical (*e.g.*, XAS, Raman), structural (*e.g.*, transmission electron microscopy at the same location, electrochemical scanning tunneling microscopy) and electronic information for the same catalyst under the same operating conditions. This will make it possible to directly correlate dynamic structural changes with catalytic activity and selectivity.

4.2. Frontiers of theory and calculation

Electronic interactions between catalysts and reactants, manifested through adsorption strength, ultimately dictate reaction pathways. Thus, the core objective of diverse strategies is to achieve optimal adsorption energies aligned with the Sabatier criterion. Yet, adsorption energy alone is unable to visually characterize a catalyst's intrinsic properties or their evolution during the CO_2RR. Therefore, it is necessary to design appropriate descriptors as bridges. Some general catalytic descriptors, such as valence state and d-band center theory, can be used as intrinsic properties of catalysts to qualitatively or semi-quantitatively regulate adsorption capacity and have been successfully applied to the CO_2RR.[173,278] Additionally, CO_2RR-specific descriptors, focusing on bonding along with orbital coupling between catalysts and key reaction intermediates, are actively under development.

Despite progress, challenges remain in elucidating how electronic structure relates to electrochemical performance, critical for enhancing CO_2RR efficiency and advancing practical applications. A primary hurdle is probing the dynamic surface states exhibited by catalysts and intermediates. For instance, while CO_2RR studies often emphasize transitions between intermediates when analyzing energy barrier heights and rate-determining steps, conformational changes of intermediates—critical to overall reaction kinetics—are frequently overlooked. A single intermediate, such as *COOH, can adopt multi-site adsorption configurations involving different atoms, profoundly influencing subsequent pathways and final products.[279–281]

Moreover, intermediate transformations are not mere atomic additions, subtractions, or substitutions but complex dynamic processes involving bond formation/cleavage and interactions with both the catalyst and pre-adsorbed species. Concurrently, catalyst surfaces evolve significantly over reaction time—*e.g.*, alloying in metal heterostructures—raising questions about the true active species and deactivation mechanisms under operational conditions. Understanding the evolution of actual active centers throughout long-term reaction processes is thus essential to ensuring catalyst stability and reliability. Current research largely confines catalyst-adsorbate interactions to single adsorbed molecules, neglecting cumulative effects of multiple intermediates or complex reaction patterns arising from interactions between numerous intermediates and the catalyst—phenomena common in practical scenarios. During prolonged CO_2RR, such clustering becomes more pronounced, with diverse intermediates coexisting on the surface. This oversight also extends to the transformation mode of intermediates. Because when the surface is densely covered, its transformation behavior may be completely different from that of isolated molecules, which highlights the inherent limitations of guiding experiments by simulating single-molecule dynamics.[282–284]

Expanding research to encompass dynamic interactions between catalysts and multiple intermediates is therefore urgent to comprehensively understand the CO_2RR under practical conditions. DFT calculations have successfully guided the screening of atomic catalysts,[278,285–287] but computational cost and time restrict the exploration of coordination environments around central metal atoms, rendering traditional DFT unsuitable for large-scale systems. With advancing computing power, first-principles high-throughput screening is poised to guide the design of superior catalysts, when combined with *in situ* characterization, such methods can also screen reaction intermediate structures, further advancing mechanistic studies of dynamics. However, these calculations typically assume ideal environments, whereas electrocatalytic processes involve highly complex external conditions and internal environments, leading to discrepancies between experimental results and theoretical simulations. Larger models are needed to fully simulate electrocatalytic environments, demanding the timely development of new methodologies.

Artificial intelligence (AI) offers innovative approaches to catalyst design, integrating advanced computing technologies *e.g.*, DFT and machine learning (ML) assisted models.[285,288–292] Operating under a variety of conditions can make predictions more directly relevant to real-world use—traditional high-throughput screening typically operates only under "standard" conditions, but these do not account for temperature, pressure, or pH. Building and supporting data sets and open databases are key to improving the effectiveness of the training sets for AI. Catalyst activity originates from active atoms, support materials, coordination environments, and defect distributions, and establishing multi-factor structure–activity relationships models and multi-scale simulations enables effective integration of structural information to refine comprehension of structure–activity relationships. AI-enabled design is capable of enhancing model precision and the efficiency of experimental verification, which in turn speeds up the conversion of theoretical research into real-world applications.

The future of the CO_2RR lies in the integration of precise experiments with complex theories. By resolving the intertwined experimental and computational challenges mentioned above, this field can progress from accidental discoveries to the rational design of next-generation catalysts. The ultimate goal is to develop reliable, highly selective, and energy-efficient catalytic systems that can be integrated into practical electrolyzers, converting carbon dioxide from waste into sustainable fuel and chemical sources, and making meaningful contributions to the circular carbon economy.

5. Summary

Electrochemical transformation of CO_2 into high-value chemicals or fuels can be achieved by storing sustainable energy

within chemical bonds. SACs have advanced substantially in electrocatalysis, leveraging their unique geometric and electronic structures to emerge as promising alternatives to commercial noble metal-based catalysts. DACs, which exploit intermetallic dimer interactions, have also gained traction, demonstrating exceptional electrocatalytic activity and addressing key limitations of SACs. To better accommodate complex multi-electron reactions, TACs have further expanded the toolkit, offering enhanced flexibility in intermediate adsorption and enabling deeper investigations into structure–electrocatalytic activity relationships.

Among these catalyst systems, metal clusters stand out as a critical architecture for advancing the CO_2RR, especially for complex products requiring multi-step electron transfer and C–C coupling. Composed of several to hundreds of atoms (1–3 nm in size), clusters integrate the advantages of atomic-level precision and nano-scale functionality, exhibiting unique quantum size effects and hybrid electronic structures that bridge molecular-like states and bulk material band structures. Their structural diversity including constituent atom count, elemental proportions, atomic arrangement, and geometric symmetry enables the creation of abundant active sites tailored to adsorb and convert specific reactants and intermediates in the CO_2RR. Unlike isolated SACs/DACs/TACs, clusters provide a synergistic multi-nuclear environment that effectively modulates the adsorption energetics of key intermediates (*e.g.*, *COOH, *OCHO, *CO) and reduces kinetic barriers for rate-determining steps, particularly C–C coupling for C_{2+} products and deep hydrogenation for CH_4.

In the reduction of CO_2 to C_1 products, clusters demonstrate remarkable performance advantages. For CO production, Fe-based clusters anchored on mesoporous carbon, Fe–In–NC clusters, and AuCu alloy clusters leverage quantum-size effects and rich active sites to enhance *CO adsorption and suppress the HER, achieving CO faradaic efficiencies (FE) up to 95% and durable stability. In HCOOH synthesis, Bi–Sn bimetallic aerogels, In–Cu nanoparticles, and double tetrahedral Cu_8 clusters exhibit prominent interface effects and fast mass transfer, with FE_{HCOOH} reaching as high as 98.15% and current densities of 16.5 mA cm^{-2}. For CH_4 generation, Co666@Cu55 clusters, Ce/CuO_x NPs, and mesoporous Cu–CeO_2 nanospheres rely on tunable electronic structures and nano-confinement effects to optimize intermediate adsorption and hydrogenation pathways, achieving FE_{CH_4} up to 74.2% at industrial-grade current densities (300 mA cm^{-2}). Notably, high-entropy alloy clusters (*e.g.*, CoNiCuRh@FeN_4) have emerged as a frontier, with their ultra-high configurational entropy endowing unique electronic structures and structural stability, enabling precise regulation of multiple product pathways.

This review highlights recent progress in classical two-dimensional material catalysts for the CO_2RR and strategies to regulate the selectivity of C_{1+} products. By systematically examining the performance of diverse electrocatalysts, we elucidate reaction mechanisms and design principles at a fundamental level. The pursuit of efficient CO_2RR catalysts reveals a fundamental design principle, in which the number and size of active sites determine the reaction pathway and product selectivity. From SACs to DACs and TACs, and finally to the development of atomic clusters, a clear scale-functional paradigm has been defined. SACs feature uniform and isolated metal centers, which exhibit excellent selectivity for simple two-electron transfer products such as CO while maximizing atomic utilization efficiency. However, their peculiar geometric structures inherently restrict the adsorption configuration of key intermediates, thereby hindering complex multi-step reactions, most crucially, C–C coupling.

To overcome this limitation, DACs and TACs introduced adjacent metal sites, creating a unique coordinated environment and thus achieving a synergy effect. This atomic-level partnership allows for the simultaneous stabilization of multiple intermediates or the cleavage of specific bonds, effectively circumventing the limitations imposed by linear scaling relationships in traditional heterogeneous catalysis. This development has opened up thermodynamic and kinetic pathways for more valuable multi-electron products such as HCOOH, C_2H_4 and CH_4. When the catalytic target further shifts to high-value C_{2+} products, atomic clusters typically composed of several to hundreds of atoms become the preferred architecture. Their multi-nuclear structure provides a set of active sites with hybrid electronic states, which are particularly good at reducing the kinetic barrier of C-C coupling, a step that is often regarded as the bottleneck for the formation of C_{2+}. Therefore, the complexity of the required CO_2RR product combination directly determines the optimal scale of the active site, among which SACs exhibit excellent catalytic performance for the generation of CO. The synthesis of C_{2+} substance requires the synergy of multi-atom sets, although the latter faces greater challenges in terms of precise synthesis and structural stability.

Author contributions

Yimeng Sun: data curation, formal analysis, investigation, methodology, writing – original draft. Lin Tao: methodology, supervision, funding acquisition, conceptualization, writing – review & editing. Yaqiong Su: methodology, formal analysis, writing – review & editing. Davoud Dastan: investigation, formal analysis. Han Zhang: investigation, formal analysis. Hongwei Zhao: investigation, formal analysis. Lixiang Li: methodology, supervision, resources. Baigang An: supervision, formal analysis, resources, writing – review & editing.

Conflicts of interest

The authors declare that they have no known competing financial interests or personal relationships that could have appeared to influence the work reported in this paper.

Data availability

No primary research results, software or code have been included and no new data were generated or analysed as part of this review.

Acknowledgements

The funding from the National Natural Science Foundation of China (Grant No. 52304330 and 52371224), the Natural Science Foundation of Liaoning Province (Grant No. 2024-BS-218), the University of Science and Technology Liaoning Talent Project Grants (Grant No. 6003000317), the Outstanding Youth Fund of University of Science and Technology Liaoning (Grant No. 2023YQ11), and the Youth Fund of the Education Department of Liaoning Province (Grant No. LJKQZ20222324) ais gratefully acknowledged.

References

1 Z. Liu, X. Gao, B. Liu, Q. Ma, T.-S. Zhao and J. Zhang, Recent advances in thermal catalytic CO_2 methanation on hydrotalcite-derived catalysts, *Fuel*, 2022, **321**, 124115.
2 H. Wang, Nanostructure@metal-organic frameworks (MOFs) for catalytic carbon dioxide (CO_2) conversion in photocatalysis, electrocatalysis, and thermal catalysis, *Nano Res.*, 2022, **15**, 2834–2854.
3 S. Feng, F. Jiang, H. Wang, Y. Liu, W. He, H. Wang, Y. Shen, L. Zhang, M. Jia, W. Ju and J. M. Chen, China's Fossil Fuel CO_2 Emissions Estimated Using Surface Observations of Coemitted NO2, *Environ. Sci. Technol.*, 2024, **58**, 8299–8312.
4 P. Gao, S. Yue and H. Chen, Carbon emission efficiency of China's industry sectors: From the perspective of embodied carbon emissions, *J. Cleaner Prod.*, 2021, **283**, 124655.
5 L. Tao, J. Huang, D. Dastan, T. Wang, J. Li, X. Yin and Q. Wang, New insight into absorption characteristics of CO_2 on the surface of calcite, dolomite, and magnesite, *Appl. Surf. Sci.*, 2021, **540**, 148320.
6 C. Halliday and T. A. Hatton, Sorbents for the Capture of CO_2 and Other Acid Gases: A Review, *Ind. Eng. Chem. Res.*, 2021, **60**, 9313–9346.
7 F. M. Baena-Moreno, R.-G. Mónica, V. Fernando, A.-F. Bernabé, L. F. Vilches Arenas and B. Navarrete, Carbon capture and utilization technologies: a literature review and recent advances, *Energy Sources, Part A*, 2019, **41**, 1403–1433.
8 D.-H. Nam, P. De Luna, A. Rosas-Hernández, A. Thevenon, F. Li, T. Agapie, J. C. Peters, O. Shekhah, M. Eddaoudi and E. H. Sargent, Molecular enhancement of heterogeneous CO_2 reduction, *Nat. Mater.*, 2020, **19**, 266–276.
9 G. A. Olah, A. Goeppert and G. K. S. Prakash, Chemical Recycling of Carbon Dioxide to Methanol and Dimethyl Ether: From Greenhouse Gas to Renewable, Environmentally Carbon Neutral Fuels and Synthetic Hydrocarbons, *J. Org. Chem.*, 2009, **74**, 487–498.
10 G. Glockler, Carbon–Oxygen Bond Energies and Bond Distances, *J. Phys. Chem.*, 1958, **62**, 1049–1054.
11 P. Verma, A. Singh, F. A. Rahimi, P. Sarkar, S. Nath, S. K. Pati and T. K. Maji, Charge-transfer regulated visible light driven photocatalytic H_2 production and CO_2 reduction in tetrathiafulvalene based coordination polymer gel, *Nat. Commun.*, 2021, **12**, 7313.
12 Y. Liu, Y. Yang, Q. Sun, Z. Wang, B. Huang, Y. Dai, X. Qin and X. Zhang, Chemical Adsorption Enhanced CO_2 Capture and Photoreduction over a Copper Porphyrin Based Metal Organic Framework, *ACS Appl. Mater. Interfaces*, 2013, **5**, 7654–7658.
13 S. Das, J. Pérez-Ramírez, J. Gong, N. Dewangan, K. Hidajat, B. C. Gates and S. Kawi, Core–shell structured catalysts for thermocatalytic, photocatalytic, and electrocatalytic conversion of CO_2, *Chem. Soc. Rev.*, 2020, **49**, 2937–3004.
14 S. Roy, A. Cherevotan and S. C. Peter, Thermochemical CO_2 Hydrogenation to Single Carbon Products: Scientific and Technological Challenges, *ACS Energy Lett.*, 2018, **3**, 1938–1966.
15 S. N. Habisreutinger, L. Schmidt-Mende and J. K. Stolarczyk, Photocatalytic Reduction of CO_2 on TiO_2 and Other Semiconductors, *Angew. Chem., Int. Ed.*, 2013, **52**, 7372–7408.
16 L. Hou, J. Yan, L. Takele, Y. Wang, X. Yan and Y. Gao, Current progress of metallic and carbon-based nanostructure catalysts towards the electrochemical reduction of CO_2, *Inorg. Chem. Front.*, 2019, **6**, 3363–3380.
17 Z. Fu, C. Fang, S. Liu, A. Cao and J. Yan, Mechanism of Potential-Dependent CO_2 Reduction and H2 Evolution during Electrocatalytic CO_2 Process, *ACS Catal.*, 2025, **15**, 13507–13515.
18 Z. Guo, T. Wang, H. Liu, X. Jia, D. Zhang, L. Wei, J. Xu and H. Li, Electrochemical CO_2 Reduction on SnO: Insights into C1 Product Dynamic Distribution and Reaction Mechanisms, *ACS Catal.*, 2025, **15**, 3173–3183.
19 Y. Xu and B. Xu, Thermodynamics of CO Adsorption on Electrodes and Its Implications for Selectivity Control in Electrochemical CO_2 Reduction, *ACS Catal.*, 2025, **15**, 7934–7943.
20 A. Zamader, A. Singh, B. Giri, M. Caruso, W. R. Osterloh, N. Desbois, C. P. Gros and M. Robert, Electrocatalytic CO_2 to CO and Methanol Conversion Using a Molecular Cobalt Corrole Complex, *ACS Catal.*, 2025, **15**, 11093–11102.
21 Y. Zhang, Q. Yu, Z. Wang, W. Zhang, X. She, Q. Zhang, Y. Liu, H. Li and H. Xu, Boosting the C–C Coupling Efficiency for Diluted CO_2 Electroreduction to Dual Carbon Products, *ACS Catal.*, 2025, **15**, 7352–7360.
22 V. D. Brandão, H. Song, A. Venkataraman, Y. Fishler, S. S. Arora, S. S. Bhargava, C. Villa, A. Holewinski, S. Nair, M. C. Hatzell and C. Sievers, Temperature Effects on the Surface CO Population during CO_2 Electroreduction over Copper, *ACS Catal.*, 2025, **15**, 8979–8990.
23 X. Wang, Y. Wang, H. Xu and D. Cheng, Revisits the Selectivity toward C2+ Products for CO_2 Electroreduction over Subnano-Copper Clusters Based on Structural Descriptors, *ACS Catal.*, 2025, **15**, 7390–7402.
24 X. Zhao and Y. Liu, Unveiling the Active Structure of Single Nickel Atom Catalysis: Critical Roles of Charge Capacity and Hydrogen Bonding, *J. Am. Chem. Soc.*, 2020, **142**, 5773–5777.

25 L. Tao, D. Dastan, W. Wang, P. Poldorn, X. Meng, M. Wu, H. Zhao, H. Zhang, L. Li and B. An, Metal-Decorated InN Monolayer Senses N_2 against CO_2, *ACS Appl. Mater. Interfaces*, 2023, **15**, 12534–12544.
26 X. Yu, P. Han, Z. Wei, L. Huang, Z. Gu, S. Peng, J. Ma and G. Zheng, Boron-Doped Graphene for Electrocatalytic N_2 Reduction, *Joule*, 2018, **2**, 1610–1622.
27 Z. Wei, Y. Zhang, S. Wang, C. Wang and J. Ma, Fe-doped phosphorene for the nitrogen reduction reaction, *J. Mater. Chem. A*, 2018, **6**, 13790–13796.
28 C. Song, L. Tao, J. Dang, D. Dastan, W. Wang, X. Zhang, L. Li and B. An, Tuning NO_2 selectivity in $MoSe_2$ sensors via metal modification: Fermi-level electronic state control, *Comput. Theor. Chem.*, 2025, **1250**, 115296.
29 L. Mei, Z. Cao, T. Ying, R. Yang, H. Peng, G. Wang, L. Zheng, Y. Chen, C. Y. Tang, D. Voiry, H. Wang, A. B. Farimani and Z. Zeng, Simultaneous Electrochemical Exfoliation and Covalent Functionalization of MoS2 Membrane for Ion Sieving, *Adv. Mater.*, 2022, **34**, 2201416.
30 W. Fu, Y. Chen, J. Lin, X. Wang, Q. Zeng, J. Zhou, L. Zheng, H. Wang, Y. He, H. He, Q. Fu, K. Suenaga, T. Yu and Z. Liu, Controlled Synthesis of Atomically Thin 1T-TaS2 for Tunable Charge Density Wave Phase Transitions, *Chem. Mater.*, 2016, **28**, 7613–7618.
31 Y. Wang, N. Ma, Y. Zhang, B. Liang and J. Fan, $Cu_4@C_2N$ for effective electrochemical CO_2 reduction and intermediates dependent adsorption behaviours: A computational study, *ApSS*, 2023, **626**, 157126.
32 M. Mon, M. A. Rivero-Crespo, J. Ferrando-Soria, A. Vidal-Moya, M. Boronat, A. Leyva-Pérez, A. Corma, J. C. Hernández-Garrido, M. López-Haro, J. J. Calvino, G. Ragazzon, A. Credi, D. Armentano and E. Pardo, Synthesis of Densely Packaged, Ultrasmall Pt02 Clusters within a Thioether-Functionalized MOF: Catalytic Activity in Industrial Reactions at Low Temperature, *Angew. Chem., Int. Ed.*, 2018, **57**, 6186–6191.
33 D.-C. Zhong, W.-X. Zhang, F.-L. Cao, L. Jiang and T.-B. Lu, A three-dimensional microporous metal–organic framework with large hydrogen sorption hysteresis, *ChCom*, 2011, **47**, 1204–1206.
34 W. Chen, J. Pei, C.-T. He, J. Wan, H. Ren, Y. Wang, J. Dong, K. Wu, W.-C. Cheong, J. Mao, X. Zheng, W. Yan, Z. Zhuang, C. Chen, Q. Peng, D. Wang and Y. Li, Single Tungsten Atoms Supported on MOF-Derived N-Doped Carbon for Robust Electrochemical Hydrogen Evolution, *Adv. Mater.*, 2018, **30**, 1800396.
35 Y. Zheng, N. Martín, M. Boronat, J. Ferrando-Soria, M. Mon, D. Armentano, E. Pardo and A. Leyva-Pérez, $Ag_2(0)$ dimers within a thioether-functionalized MOF catalyze the CO_2 to CH_4 hydrogenation reaction, *Sci. Rep.*, 2023, **13**, 10376.
36 J. Jiang, P. Jiang, D. Wang and Y. Li, The synthetic strategies for single atomic site catalysts based on metal–organic frameworks, *Nanoscale*, 2020, **12**, 20580–20589.
37 K. S. Novoselov, A. K. Geim, S. V. Morozov, D. Jiang, Y. Zhang, S. V. Dubonos, I. V. Grigorieva and A. A. Firsov, Electric field in atomically thin carbon films, *Science*, 2004, **306**, 666–669.
38 C. Berger, Z. Song, T. Li, X. Li, A. Y. Ogbazghi, R. Feng, Z. Dai, A. N. Marchenkov, E. H. Conrad, P. N. First and W. A. de Heer, Ultrathin Epitaxial Graphite: 2D Electron Gas Properties and a Route toward Graphene-based Nanoelectronics, *J. Phys. Chem. B*, 2004, **108**, 19912–19916.
39 T. H. Choudhury, X. Zhang, Z. Y. Al Balushi, M. Chubarov and J. M. Redwing, Epitaxial Growth of Two-Dimensional Layered Transition Metal Dichalcogenides, *Annu. Rev. Mater. Res.*, 2020, **50**, 155–177.
40 M. J. Allen, V. C. Tung and R. B. Kaner, Honeycomb Carbon: A Review of Graphene, *Chem. Rev.*, 2010, **110**, 132–145.
41 C. Soldano, A. Mahmood and E. Dujardin, Production, properties and potential of graphene, *Carbon*, 2010, **48**, 2127–2150.
42 S. Bae, H. Kim, Y. Lee, X. Xu, J.-S. Park, Y. Zheng, J. Balakrishnan, T. Lei, H. Ri Kim, Y. I. Song, Y.-J. Kim, K. S. Kim, B. Özyilmaz, J.-H. Ahn, B. H. Hong and S. Iijima, Roll-to-roll production of 30-inch graphene films for transparent electrodes, *Nat. Nanotechnol.*, 2010, **5**, 574–578.
43 F. Xia, D. B. Farmer, Y.-m. Lin and P. Avouris, Graphene Field-Effect Transistors with High On/Off Current Ratio and Large Transport Band Gap at Room Temperature, *Nano Lett.*, 2010, **10**, 715–718.
44 J.-W. Jiang, Graphene versus MoS_2: A short review, *Front. Phys.*, 2015, **10**, 287–302.
45 S. Liu, Z. Chen, M. Wang, S. Cao, Y. Yin, H. Zhang, Z. Wang, S. Wei, W. Lyu and X. Lu, Revealing the Joint Contribution of Potential and Water Molecules to the High CO_2RR Activity of a Single Nickel Atom Catalyst, *ACS Appl. Nano Mater.*, 2025, **8**, 11484–11494.
46 F. Xia, D. B. Farmer, Y.-M. Lin and P. Avouris, Graphene Field-Effect Transistors with High On/Off Current Ratio and Large Transport Band Gap at Room Temperature, *Nano Lett.*, 2010, **10**, 715–718.
47 J.-W. Jiang, Graphene versus MoS_2: A short review, *Front. Phys.*, 2015, **10**, 287–302.
48 S. Liu, Z. Chen, M. Wang, S. Cao, Y. Yin, H. Zhang, Z. Wang, S. Wei, W. Lyu and X. Lu, Revealing the Joint Contribution of Potential and Water Molecules to the High CO_2RR Activity of a Single Nickel Atom Catalyst, *ACS Appl. Nano Mater.*, 2025, **8**, 11484–11494.
49 D. Zaoralová, R. Langer and M. Otyepka, Iron Single-Atom Catalysts Anchored on Defect-Engineered N-Doped Graphene Reveal an Interplay between CO_2 Reduction Activity and Stability, *ACS Sustainable Chem. Eng.*, 2025, **13**, 8319–8330.
50 M. Urso, X. Ju, R. Nittoor-Veedu, H. Lee, D. Zaoralová, M. Otyepka and M. Pumera, Single Atom Engineering for Electrocatalysis: Fundamentals and Applications, *ACS Catal.*, 2025, **15**, 11617–11663.
51 M. Bilgili, X. Wang and J. Young, Computational Evaluation of N8 Polynitrogen-Stabilized Single-Atom Catalysts for CO_2 Reduction, *Energy Fuels*, 2025, **39**, 10562–10571.

52 Y. Du and C. Chen, CO_2 Reduction Mechanism Based on a Partially Reduced Cu Single-Atom Catalyst: A First-Principles Study, *J. Phys. Chem. C*, 2025, **129**, 6211–6224.
53 M. A. Akhound, M. Soleimani and M. Pourfath, Tunable N2 Fixation Enabled by Ferroelectric Switching in Doped Graphene/In_2Se_3 Dual-Atom Catalysts, *ACS Appl. Mater. Interfaces*, 2025, **17**, 15385–15397.
54 J. Ma, W. Lee, J. H. Kim, J. Jeong, K.-M. Jo, S.-Y. Choi, S. Back and S. Y. Kim, Leveraging the Intermetal Distance in Dual-Atom Catalysts: Revealing Optimized Synergistic Interactions for CO_2 Electroreduction, *ACS Nano*, 2025, **19**, 18698–18707.
55 T. Xu, Z. Wang, T. Liu, F. Wang and Y. Jing, Mechanistic Insights into Methylamine Electrosynthesis from CO_2 and NO on Co-Based Dual-Atom Catalysts, *J. Am. Chem. Soc.*, 2025, **147**, 26969–26979.
56 J. Zhu, M. Xiao, D. Ren, R. Gao, X. Liu, Z. Zhang, D. Luo, W. Xing, D. Su, A. Yu and Z. Chen, Quasi-Covalently Coupled Ni–Cu Atomic Pair for Synergistic Electroreduction of CO_2, *J. Am. Chem. Soc.*, 2022, **144**, 9661–9671.
57 X. Wei, S. Cao, S. Wei, S. Liu, Z. Wang, F. Dai and X. Lu, Theoretical investigation on electrocatalytic reduction of CO_2 to methanol and methane by bimetallic atoms TM1/TM2-N@Gra (TM = Fe, Co, Ni, Cu), *ApSS*, 2022, **593**, 153377.
58 S. Li, L. Tong, Z. Peng, B. Zhang and X. Fu, Efficient CO_2 reduction for CO production using triatomic catalyst screening: A DFT study, *ApSS*, 2024, **644**, 158804.
59 F. Pan, L. Fang, B. Li, X. Yang, T. O'Carroll, H. Li, T. Li, G. Wang, K. J. Chen and G. Wu, N and OH-Immobilized Cu(3) Clusters In Situ Reconstructed from Single-Metal Sites for Efficient CO(2) Electromethanation in Bicontinuous Mesochannels, *J. Am. Chem. Soc.*, 2024, **146**, 1423–1434.
60 S. Zhou, S. Cao, S. Wei, Z. Wang, H. Chen, X. Lin, X. Chen, S. Liu and X. Lu, Triple-atom catalysts 3TM-GYs (TM = Cu, Fe, and Co; GY = graphyne) for high-performance CO_2 reduction reaction to C1 products, *Appl. Mater. Today*, 2021, **25**, 101245.
61 J. Zhang, Y. Wang and Y. Li, Not One, Not Two, But at Least Three: Activity Origin of Copper Single-Atom Catalysts toward CO_2/CO Electroreduction to C2+ Products, *J. Am. Chem. Soc.*, 2024, **146**, 14954–14958.
62 X. Zheng, Y. Liu and Y. Yao, Trimetallic single-cluster catalysts for electrochemical nitrogen reduction reaction: Activity prediction, mechanism, and electronic descriptor, *Chem. Eng. J.*, 2021, **426**, 130745.
63 T. Tsukamoto, T. Kambe, T. Imaoka and K. Yamamoto, Modern cluster design based on experiment and theory, *Nat. Rev. Chem.*, 2021, **5**, 338–347.
64 X. Zhang, C. Liu, Y. Zhao, L. Li, Y. Chen, F. Raziq, L. Qiao, S.-X. Guo, C. Wang, G. G. Wallace, A. M. Bond and J. Zhang, Atomic nickel cluster decorated defect-rich copper for enhanced C2 product selectivity in electrocatalytic CO_2 reduction, *Appl. Catal., B*, 2021, **291**, 120030.
65 Q. Hu, Z. Han, X. Wang, G. Li, Z. Wang, X. Huang, H. Yang, X. Ren, Q. Zhang, J. Liu and C. He, Facile Synthesis of Sub-Nanometric Copper Clusters by Double Confinement Enables Selective Reduction of Carbon Dioxide to Methane, *Angew. Chem., Int. Ed.*, 2020, **59**, 19054–19059.
66 J.-W. Liu, D. Peng, S.-J. Liu, H.-R. Wen, Z.-H. Zhu, J. Zhao and J.-L. Chen, New Insight into the Conjugation Effect of Tetranuclear Copper(I) Cluster Catalysts for Efficient Electrocatalytic Reduction of CO_2 into CH_4, *ACS Sustainable Chem. Eng.*, 2025, **13**, 2564–2573.
67 S. Wang, C. Han, X. Chen, Y. Xiang, Q. Li, J. Chai, S. Yang, Y. Du, Q. Luo and M. Zhu, Constructing Atomic-Level Defect as the Catalytic Site by Removing a Single Metal Atom from the Nanoclusters, *ACS Nano*, 2025, **19**, 25334–25341.
68 A. Vidal-López, J. Gassó-Capdevila, M. Solà, A. Poater and S. Posada-Pérez, Hydrogen Evolution and Carbon Dioxide Reduction Pathways on Graphitic Carbon Nitride Decorated by Single Atoms of Transition Metals, *J. Phys. Chem. C*, 2025, **129**(17), 8075–8085.
69 L. M. Azofra, D. R. MacFarlane and C. Sun, A DFT study of planar *vs.* corrugated graphene-like carbon nitride (g-C_3N_4) and its role in the catalytic performance of CO_2 conversion, *Phys. Chem. Chem. Phys.*, 2016, **18**, 18507–18514.
70 M. Gu, L. Tao, D. Dastan, J. Dang, T. Fang and B. An, Metal-Modified C_3N_1 Monolayer Sensors for Battery Instability Monitoring, *J. Mater. Chem. A*, 2024, **12**, 15254–15264.
71 C. Hu, Y. Mu, S. Bai, J. Yang, L. Gao, S.-D. Cheng, S.-B. Mi and J. Qiu, Polyvinyl pyrrolidone mediated fabrication of Fe, N-codoped porous carbon sheets for efficient electrocatalytic CO_2 reduction, *Carbon*, 2019, **153**, 609–616.
72 H. Dong, M. Lu, Y. Wang, H.-L. Tang, D. Wu, X. Sun and F.-M. Zhang, Covalently anchoring covalent organic framework on carbon nanotubes for highly efficient electrocatalytic CO_2 reduction, *Appl. Catal., B*, 2022, **303**, 120897.
73 Z.-Y. Song, Y.-Y. Li, W. Duan, X.-Y. Xiao, Z.-W. Gao, Y.-H. Zhao, B. Liang, S.-H. Chen, P.-H. Li, M. Yang and X.-J. Huang, Decisive role of electronic structure in electroanalysis for sensing materials: Insights from density functional theory, *TrAC, Trends Anal. Chem.*, 2023, **160**, 116977.
74 Z. Zhang, L. Tao, X. Quan, M. Gu, H. Zhang, B. An and L. Li, Regulating the H_2 selectivity of MoS_2 sensors through synergistic metal–non-metal co-doping, *Mater. Sci. Semicond. Process.*, 2025, **206**, 110460.
75 A. Fedotov, A. Vakhrushev, O. Severyukhina, A. S. Sidorenko, Y. B. Savva, N. V. Klenov and I. Soloviev, Theoretical Basis of Quantum-Mechanical Modeling of Functional Nanostructures, *Symmetry*, 2021, **13**, 883.
76 S. Fan, X. Lu, H. Li, X. Du, X. Huang, Y. Ma, J. Wang, X. Tao, Z. Dang and G. Lu, Efficient removal of organophosphate esters by ligand functionalized MIL-101 (Fe): Modulated adsorption and DFT calculations, *Chemosphere*, 2022, **302**, 134881.
77 B. Delley, From molecules to solids with the DMol3 approach, The, *J. Chem. Phys.*, 2000, **113**, 7756–7764.
78 S. Zhuo, Y. Huang, J. Hu, H. Liu, Y. Hu and J. Jiang, Computer Simulation for Adsorption of CO_2, N_2 and Flue Gas in a Mimetic MCM-41, *J. Phys. Chem. C*, 2008, **112**, 11295–11300.

79 B. Wulan, X. Cao, D. Tan, J. Ma and J. Zhang, To Stabilize Oxygen on In/In_2O_3 Heterostructure via Joule Heating for Efficient Electrocatalytic CO_2 Reduction, *Adv. Funct. Mater.*, 2023, **33**(1), 2209114.
80 K. Liu, J. Wang, M. Shi, J. Yan and Q. Jiang, Simultaneous Achieving of High faradaic Efficiency and CO Partial Current Density for CO_2 Reduction via Robust, Noble-Metal-Free Zn Nanosheets with Favorable Adsorption Energy, *Adv. Energy Mater.*, 2019, **9**(21), 1900276.
81 X.-L. Lu, X. Rong, C. Zhang and T.-B. Lu, Carbon-based single-atom catalysts for CO_2 electroreduction: progress and optimization strategies, *J. Mater. Chem. A*, 2020, **8**, 10695–10708.
82 S. Wang, L. Wang, D. Wang and Y. Li, Recent advances of single-atom catalysts in CO_2 conversion, *Energy Environ. Sci.*, 2023, **16**, 2759–2803.
83 C. Chen, J. Li, X. Tan, Y. Zhang, Y. Li, C. He, Z. Xu, C. Zhang and C. Chen, Harnessing single-atom catalysts for CO_2 electroreduction: a review of recent advances, *EES Catal.*, 2024, **2**, 71–93.
84 X. Zheng, P. Li, S. Dou, W. Sun, H. Pan, D. Wang and Y. Li, Non-carbon-supported single-atom site catalysts for electrocatalysis, *Energy Environ. Sci.*, 2021, **14**, 2809–2858.
85 Y. Luo, X. Wang, F. Gao, L. Jiang, D. Wang and H. Pan, From Single Atom Photocatalysts to Synergistic Photocatalysts: Design Principles and Applications, *Adv. Funct. Mater.*, 2025, **35**, 2418427.
86 B. Wang, S. Chen, Z. Zhang and D. Wang, Low-dimensional material supported single-atom catalysts for electrochemical CO_2 reduction, *SmartMat*, 2022, **3**, 84–110.
87 D. Gao, T. Liu, G. Wang and X. Bao, Structure Sensitivity in Single-Atom Catalysis toward CO_2 Electroreduction, *ACS Energy Lett.*, 2021, **6**, 713–727.
88 N. Fu, X. Liang, Z. Li and Y. Li, Single-atom site catalysts based on high specific surface area supports, *Phys. Chem. Chem. Phys.*, 2022, **24**, 17417–17438.
89 Z. Chen, R. Shen, C. Chen, J. Li and Y. Li, Synergistic effect of bimetallic PdAu nanocrystals on oxidative alkyne homocoupling, *ChCom*, 2018, **54**, 13155–13158.
90 Y. Wang, J. Mao, X. Meng, L. Yu, D. Deng and X. Bao, Catalysis with Two-Dimensional Materials Confining Single Atoms: Concept, Design, and Applications, *Chem. Rev.*, 2019, **119**, 1806–1854.
91 T. Cui, L. Li, C. Ye, X. Li, C. Liu, S. Zhu, W. Chen and D. Wang, Heterogeneous Single Atom Environmental Catalysis: Fundamentals, Applications, and Opportunities, *Adv. Funct. Mater.*, 2022, **32**, 2108381.
92 J. Yang, W. Li, D. Wang and Y. Li, Electronic Metal–Support Interaction of Single-Atom Catalysts and Applications in Electrocatalysis, *Adv. Mater.*, 2020, **32**, 2003300.
93 T. Liu, G. Wang and X. Bao, Electrochemical CO_2 Reduction Reaction on 3d Transition Metal Single-Atom Catalysts Supported on Graphdiyne: A DFT Study, *J. Phys. Chem. C*, 2021, **125**, 26013–26020.
94 H. Wang, X. Li, Y. Deng, J. Jiang, H. Ma and J. Zou, Advances in MXene-based single-atom catalysts for electrocatalytic applications, *Coord. Chem. Rev.*, 2025, **529**, 216462.
95 G. Chen, C. Lin, F. Han, H. Zhang, S. Zhou, F. Yang, Y. Kong and E. H. Ang, Recent advances in photocatalytic H_2O_2 production: modification strategies of 2D materials and in situ application of H2O2, *Mater. Horiz.*, 2025, **12**, 5492–5512.
96 H. Lu, J. Li, R. Zhang, K. Nie, Q. Li, Ya Chen and F. Pan, Advances and perspectives of two-dimensional materials MXenes: Efficient catalysts for magnesium hydride, *Renewable Sustainable Energy Rev.*, 2025, **217**, 115759.
97 S. Wang, J. Xia, X. Yang, Q. Xie, Z. Zhuang, H. Feng, H. Xiang, Z. Chen, H. Li, L. Zhang, Y. Li, B. Yu and T. Ma, Two-dimensional materials for NOx reduction to ammonia: From electrocatalyst to system, *Coord. Chem. Rev.*, 2025, **535**, 216610.
98 X. Wang, Z. Chen, X. Zhao, T. Yao, W. Chen, R. You, C. Zhao, G. Wu, J. Wang, W. Huang, J. Yang, X. Hong, S. Wei, Y. Wu and Y. Li, Regulation of Coordination Number over Single Co Sites: Triggering the Efficient Electroreduction of CO_2, *Angew. Chem., Int. Ed.*, 2018, **57**, 1944–1948.
99 H. Zhang, J. Li, S. Xi, Y. Du, X. Hai, J. Wang, H. Xu, G. Wu, J. Zhang, J. Lu, J. Wang and A. Graphene-Supported Single-Atom FeN5, Catalytic Site for Efficient Electrochemical CO_2 Reduction, *Angew. Chem., Int. Ed.*, 2019, **58**, 14871–14876.
100 Z. Li, R. Wu, S. Xiao, Y. Yang, L. Lai, J. S. Chen and Y. Chen, Axial chlorine coordinated iron-nitrogen-carbon single-atom catalysts for efficient electrochemical CO_2 reduction, *Chem. Eng. J.*, 2022, **430**, 132882.
101 Y. J. Sa, H. Jung, D. Shin, H. Y. Jeong, S. Ringe, H. Kim, Y. J. Hwang and S. H. Joo, Thermal Transformation of Molecular Ni2+–N4 Sites for Enhanced CO_2 Electroreduction Activity, *ACS Catal.*, 2020, **10**, 10920–10931.
102 W. Ren, X. Tan, W. Yang, C. Jia, S. Xu, K. Wang, S. C. Smith and C. Zhao, Isolated Diatomic Ni-Fe Metal–Nitrogen Sites for Synergistic Electroreduction of CO_2, *Angew. Chem., Int. Ed.*, 2019, **58**, 6972–6976.
103 J.-d Yi, X. Gao, H. Zhou, W. Chen and Y. Wu, Design of Co-Cu Diatomic Site Catalysts for High-efficiency Synergistic CO_2 Electroreduction at Industrial-level Current Density, *Angew. Chem., Int. Ed.*, 2022, **61**, e202212329.
104 Y. Zhu, W. Sun, W. Chen, T. Cao, Y. Xiong, J. Luo, J. Dong, L. Zheng, J. Zhang, X. Wang, C. Chen, Q. Peng, D. Wang and Y. Li, Scale-Up Biomass Pathway to Cobalt Single-Site Catalysts Anchored on N-Doped Porous Carbon Nanobelt with Ultrahigh Surface Area, *Adv. Funct. Mater.*, 2018, **28**, 1802167.
105 X. Li, Y. Zeng, C.-W. Tung, Y.-R. Lu, S. Baskaran, S.-F. Hung, S. Wang, C.-Q. Xu, J. Wang, T.-S. Chan, H. M. Chen, J. Jiang, Q. Yu, Y. Huang, J. Li, T. Zhang and B. Liu, Unveiling the In Situ Generation of a Monovalent Fe(I) Site in the Single-Fe-Atom Catalyst for Electrochemical CO_2 Reduction, *ACS Catal.*, 2021, **11**, 7292–7301.
106 Q. Zhang, Z. Song, X. Sun, Y. Liu, J. Wan, S. B. Betzler, Q. Zheng, J. Shangguan, K. C. Bustillo, P. Ercius, P. Narang,

Y. Huang and H. Zheng, Atomic dynamics of electrified solid–liquid interfaces in liquid-cell TEM, *Nature*, 2024, **630**, 643–647.

107 B. Qiao, A. Wang, X. Yang, L. F. Allard, Z. Jiang, Y. Cui, J. Liu, J. Li and T. Zhang, Single-atom catalysis of CO oxidation using Pt1/FeO_x, *Nat. Chem.*, 2011, **3**, 634–641.

108 A. Wang, J. Li and T. Zhang, Heterogeneous single-atom catalysis, *Nat. Rev. Chem.*, 2018, **2**, 65–81.

109 M. K. Samantaray, V. D'Elia, E. Pump, L. Falivene, M. Harb, S. Ould Chikh, L. Cavallo and J.-M. Basset, The Comparison between Single Atom Catalysis and Surface Organometallic Catalysis, *Chem. Rev.*, 2020, **120**, 734–813.

110 Y. Yang, J. Li, C. Zhang, Z. Yang, P. Sun, S. Liu and Q. Cao, Theoretical Insights into Nitrogen-Doped Graphene-Supported Fe, Co, and Ni as Single-Atom Catalysts for CO_2 Reduction Reaction, *J. Phys. Chem. C*, 2022, **126**, 4338–4346.

111 Y. Bao, M. Zha, P. Sun, G. Hu and L. Feng, PdNi/N-doped graphene aerogel with over wide potential activity for formic acid electrooxidation, *J. Energy Chem.*, 2021, **59**, 748–754.

112 Y. Zhang, H. Jang, X. Ge, W. Zhang, Z. Li, L. Hou, L. Zhai, X. Wei, Z. Wang, M. G. Kim, S. Liu, Q. Qin, X. Liu and J. Cho, Single-Atom Sn on Tensile-Strained ZnO Nanosheets for Highly Efficient Conversion of CO_2 into Formate, *Adv. Energy Mater.*, 2022, **12**(45), 2202695.

113 S. Ji, Y. Qu, T. Wang, Y. Chen, G. Wang, X. Li, J. Dong, Q. Chen, W. Zhang, Z. Zhang, S. Liang, R. Yu, Y. Wang, D. Wang and Y. Li, Rare-Earth Single Erbium Atoms for Enhanced Photocatalytic CO_2 Reduction, *Angew. Chem., Int. Ed.*, 2020, **59**, 10651–10657.

114 Y. Wang, Y. Liu, W. Liu, J. Wu, Q. Li, Q. Feng, Z. Chen, X. Xiong, D. Wang and Y. Lei, Regulating the coordination structure of metal single atoms for efficient electrocatalytic CO_2 reduction, *Energy Environ. Sci.*, 2020, **13**, 4609–4624.

115 W. Zhang, Q. Fu, Q. Luo, L. Sheng and J. Yang, Understanding Single-Atom Catalysis in View of Theory, *JACS Au*, 2021, **1**, 2130–2145.

116 R. Lang, X. Du, Y. Huang, X. Jiang, Q. Zhang, Y. Guo, K. Liu, B. Qiao, A. Wang and T. Zhang, Single-Atom Catalysts Based on the Metal–Oxide Interaction, *Chem. Rev.*, 2020, **120**, 11986–12043.

117 C. Schilling, M. Ziemba, C. Hess and M. V. Ganduglia-Pirovano, Identification of single-atom active sites in CO oxidation over oxide-supported Au catalysts, *JCat*, 2020, **383**, 264–272.

118 S. Zhang, P. Kang, S. Ubnoske, M. K. Brennaman, N. Song, R. L. House, J. T. Glass and T. J. Meyer, Polyethylenimine-Enhanced Electrocatalytic Reduction of CO_2 to Formate at Nitrogen-Doped Carbon Nanomaterials, *J. Am. Chem. Soc.*, 2014, **136**, 7845–7848.

119 B. Kumar, M. Asadi, D. Pisasale, S. Sinha-Ray, B. A. Rosen, R. Haasch, J. Abiade, A. L. Yarin and A. Salehi-Khojin, Renewable and metal-free carbon nanofibre catalysts for carbon dioxide reduction, *Nat. Commun.*, 2013, **4**, 2819.

120 A. S. Varela, N. Ranjbar Sahraie, J. Steinberg, W. Ju, H.-S. Oh and P. Strasser, Metal-Doped Nitrogenated Carbon as an Efficient Catalyst for Direct CO_2 Electroreduction to CO and Hydrocarbons, *Angew. Chem., Int. Ed.*, 2015, **54**, 10758–10762.

121 A. S. Varela, W. Ju, A. Bagger, P. Franco, J. Rossmeisl and P. Strasser, Electrochemical Reduction of CO_2 on Metal-Nitrogen-Doped Carbon Catalysts, *ACS Catal.*, 2019, **9**, 7270–7284.

122 Y. Peng, B. Lu and S. Chen, Carbon-Supported Single Atom Catalysts for Electrochemical Energy Conversion and Storage, *Adv. Mater.*, 2018, **30**, 1801995.

123 Q. Lu, K. Eid, W. Li, A. M. Abdullah, G. Xu and R. S. Varma, Engineering graphitic carbon nitride (g-C3N4) for catalytic reduction of CO_2 to fuels and chemicals: strategy and mechanism, *Green Chem.*, 2021, **23**, 5394–5428.

124 J. Zhu, P. Xiao, H. Li and S. A. C. Carabineiro, Graphitic Carbon Nitride: Synthesis, Properties, and Applications in Catalysis, *ACS Appl. Mater. Interfaces*, 2014, **6**, 16449–16465.

125 C. Cometto, A. Ugolotti, E. Grazietti, A. Moretto, G. Bottaro, L. Armelao, C. Di Valentin, L. Calvillo and G. Granozzi, Copper single-atoms embedded in 2D graphitic carbon nitride for the CO_2 reduction, *npj 2D Mater. Appl.*, 2021, **5**, 63.

126 X. Zhang, L. Tao, D. Dastan, H. Zhang and B. Gao, Tuning the electrochemical stability of carbon based single-atom structures via doping: trade-off between electrosorption/leaching behavior, *J. Mater. Chem. A*, 2025, **13**, 23715–23723.

127 S. Li, X. Jiang, Z. Wang, S. Song, Z. Cai, K. C. F. Leung and T. Zeng, Free-Standing Janus Nanosheets: Ultrafast Self-Assembly and Versatile Biphase-Application, *Adv. Funct. Mater.*, 2024, **34**(26), 2309966.

128 X. Li, Z. Su, Z. Zhao, Q. Cai, Y. Li and J. Zhao, Single Ir atom anchored in pyrrolic-N4 doped graphene as a promising bifunctional electrocatalyst for the ORR/OER: a computational study, *J. Colloid Interface Sci.*, 2022, **607**, 1005–1013.

129 L. Ju, X. Tang, Y. Zhang, X. Li, X. Cui and G. Yang, Single Selenium Atomic Vacancy Enabled Efficient Visible-Light-Response Photocatalytic NO Reduction to NH3 on Janus WSSe Monolayer, *Molecules*, 2023, **28**, 2959.

130 X. Zhang, Z. Luo, Z. Zhou, Y. Wang, Z. Cui, Z. Gao, J. Shi, T. Cao and X. Fan, Transition metal atom anchored by defective WSSe monolayer as bifunctional single atom catalyst for ORR and OER, *J. Electroanal. Chem.*, 2022, **922**, 116731.

131 J.-X. Guo, S.-Y. Wu, S.-Y. Zhong, G.-J. Zhang, G.-Q. Shen and X.-Y. Yu, Janus WSSe monolayer adsorbed with transition-metal atoms (Fe, Co and Ni): excellent performance for gas sensing and CO catalytic oxidation, *ApSS*, 2021, **565**, 150558.

132 X. Li, Z. Li and J. Yang, Proposed Photosynthesis Method for Producing Hydrogen from Dissociated Water Molecules Using Incident Near-Infrared Light, *Phys. Rev. Lett.*, 2014, **112**, 018301.

133 X. W. Zhao, B. Qiu, G. C. Hu, W. W. Yue, J. F. Ren and X. B. Yuan, Transition-metal doping/adsorption induced valley polarization in Janus WSSe: First-principles calculations, *ApSS*, 2019, **490**, 172–177.

134 J. Ye, D. Rao and X. Yan, Regulating the electronic properties of MoSe2 to improve its CO_2 electrocatalytic reduction performance via atomic doping, *NJCh*, 2021, **45**, 5350–5356.

135 Y. Qin, M. Sayyad, A. R. P. Montblanch, M. S. G. Feuer, D. Dey, M. Blei, R. Sailus, D. M. Kara, Y. Shen, S. Yang, A. S. Botana, M. Atature and S. Tongay, Reaching the Excitonic Limit in 2D Janus Monolayers by In Situ Deterministic Growth, *Adv. Mater.*, 2022, **34**(6), 2106222.

136 X. Chen, Y. Huang, J. Niu, H. Lin, X. Wei and F. Ma, Efficient screening and influencing effect of superior catalysts among TM@Janus WSSe for CO_2RR to various C1 products, *Surf. Interfaces*, 2025, **63**, 106291.

137 Y. Tan, Y. Niu, X. Ji, X. Cui, H. Duan and Q. Jing, Single-Atom-Embedded Nitrogen-Doped Graphene as Efficient Electrocatalysts for the CO_2 Reduction Reaction, *Langmuir*, 2025, **41**, 7912–7921.

138 Q. Sun, C. Jia, Y. Zhao and C. Zhao, Single atom-based catalysts for electrochemical CO_2 reduction, *Chin. J. Catal.*, 2022, **43**, 1547–1597.

139 W. Dong, N. Zhang, S. Li, S. Min, J. Peng, W. Liu, D. Zhan and H. Bai, A Mn single atom catalyst with Mn–N2O2 sites integrated into carbon nanosheets for efficient electrocatalytic CO_2 reduction, *J. Mater. Chem. A*, 2022, **10**, 10892–10901.

140 J. Wang, Y. Song, C. Chen, X. Zhao and W. Fan, Trade-Off between the Coordination Environment and Active-Site Density on Fe–N_xC_y–C Catalysts for Enhanced Electrochemical CO_2 Reduction to CO, *ACS Catal.*, 2023, 15794–15810.

141 Y. Duan, Y. Wang, W. Zhang, J. Zhang, C. Ban, D. Yu, K. Zhou, J. Tang, X. Zhang, X. Han, L. Gan, X. Tao and X. Zhou, Simultaneous CO_2 and H_2O Activation via Integrated Cu Single Atom and N Vacancy Dual-Site for Enhanced CO Photo-Production, *Adv. Funct. Mater.*, 2023, **33**(28), 2301729.

142 H. Wang, X. Wang, J. Pan, L. Zhang, M. Zhao, J. Xu, B. Liu, W. Shi, S. Song and H. Zhang, Ball-Milling Induced Debonding of Surface Atoms from Metal Bulk for Construing High-Performance Dual-Site Single-Atom Catalysts, *Angew. Chem., Int. Ed.*, 2021, **60**, 23154–23158.

143 D.-C. Zhong, Y.-N. Gong, C. Zhang and T.-B. Lu, Dinuclear metal synergistic catalysis for energy conversion, *Chem. Soc. Rev.*, 2023, **52**, 3170–3214.

144 S. Zhang, L. Tao, H. Zhang, H. Zhao, L. Di, L. Li and B. An, Theoretical study of metal-doped WSe_2 sensors for NO detection in human exhalation, *Surf. Interfaces*, 2025, **73**, 107553.

145 X. Wang, Z. Chen, Z. Han, H. Gai, J. Zhou, Y. Wang, P. Cui, J. Ge, W. Xing, X. Zheng, M. Huang and H. Jiang, Manipulation of New Married Edge-Adjacent Fe_2N_5 Catalysts and Identification of Active Species for Oxygen Reduction in Wide pH Range, *Adv. Funct. Mater.*, 2022, **32**, 2111835.

146 M. Xiao, H. Zhang, Y. Chen, J. Zhu, L. Gao, Z. Jin, J. Ge, Z. Jiang, S. Chen, C. Liu and W. Xing, Identification of binuclear CO_2N_5 active sites for oxygen reduction reaction with more than one magnitude higher activity than single atom CoN_4 site, *Nano Energy*, 2018, **46**, 396–403.

147 Q. Hao, H.-X. Zhong, J.-Z. Wang, K.-H. Liu, J.-M. Yan, Z.-H. Ren, N. Zhou, X. Zhao, H. Zhang, D.-X. Liu, X. Liu, L.-W. Chen, J. Luo and X.-B. Zhang, Nickel dual-atom sites for electrochemical carbon dioxide reduction, *Nat. Synth.*, 2022, **1**, 719–728.

148 M. Xiao, Y. Chen, J. Zhu, H. Zhang, X. Zhao, L. Gao, X. Wang, J. Zhao, J. Ge, Z. Jiang, S. Chen, C. Liu and W. Xing, Climbing the Apex of the ORR Volcano Plot via Binuclear Site Construction: Electronic and Geometric Engineering, *J. Am. Chem. Soc.*, 2019, **141**, 17763–17770.

149 G. Yang, J. Zhu, P. Yuan, Y. Hu, G. Qu, B.-A. Lu, X. Xue, H. Yin, W. Cheng, J. Cheng, W. Xu, J. Li, J. Hu, S. Mu and J.-N. Zhang, Regulating Fe-spin state by atomically dispersed Mn-N in Fe-N-C catalysts with high oxygen reduction activity, *Nat. Commun.*, 2021, **12**, 1734.

150 X. Zheng, J. Yang, Z. Xu, Q. Wang, J. Wu, E. Zhang, S. Dou, W. Sun, D. Wang and Y. Li, Ru–Co Pair Sites Catalyst Boosts the Energetics for the Oxygen Evolution Reaction, *Angew. Chem., Int. Ed.*, 2022, **61**, e202205946.

151 P.-Y. Shi, Y. Yan, S.-Y. Yang, J.-J. Hao, M. Wang and T.-B. Lu, Dual-metal synergistic catalysis for promoting electrocatalytic CO_2 reduction, *Chem. Sci.*, 2025, **16**, 11711–11739.

152 Z. Liu, Y. Wen, Z. Wang, L. Guo, R. Chen, A. Zhang and B. Shan, Synergistic Dual-Atom Catalysts on Ceria for Enhanced CO Preferential Oxidation: Insights from High-Throughput First-Principles Microkinetics, *ACS Catal.*, 2025, **15**, 664–675.

153 K. Huang, R. Li, H. Qi, S. Yang, S. An, C. Lian, Q. Xu, H. Liu and J. Hu, Regulating Adsorption of Intermediates via the Sulfur Modulating Dual-Atomic Sites for Boosting CO_2RR, *ACS Catal.*, 2024, **14**, 8889–8898.

154 H. T. D. Bui, V. Q. Bui, S. G. Kim, Y. Kawazoe and H. Lee, Revealing well-defined cluster-supported bi-atom catalysts for enhanced CO_2 electroreduction: a theoretical investigation, *Phys. Chem. Chem. Phys.*, 2021, **23**, 25143–25151.

155 D. Chen, Z. Chen, Z. Lu, J. Tang, X. Zhang and C. V. Singh, Computational screening of homo and hetero transition metal dimer catalysts for reduction of CO_2 to C_2 products with high activity and low limiting potential, *J. Mater. Chem. A*, 2020, **8**, 21241–21254.

156 M. Zhou, W. Kong, M. Xue, H. Li, M. A. Khan, B. Liu, F. Lu and X. Zeng, Recent progress of dual-site catalysts in emerging electrocatalysis: a review, *Catal. Sci. Technol.*, 2023, **13**, 4615–4634.

157 S. Guan, L. Tao, P. Tang, R. Fang, H. Wu, N. Piao, H. Yang, G. Hu, X. Geng, L. Li, B. An and F. Li, Regulating interfacial chemistry and kinetic behaviors of F/Mo co-doping Ni-rich layered oxide cathode for long-cycling lithium-ion batteries over −20 °C–60 °C, *J. Energy Chem.*, 2024, **94**, 449–457.

158 P. V. Bakharev, M. Huang, M. Saxena, S. W. Lee, S. H. Joo, S. O. Park, J. Dong, D. C. Camacho-Mojica, S. Jin, Y. Kwon, M. Biswal, F. Ding, S. K. Kwak, Z. Lee and R. S. Ruoff, Chemically induced transformation of chemical vapour deposition grown bilayer graphene into fluorinated single-layer diamond, *Nat. Nanotechnol.*, 2019, **15**, 59–66.

159 K. Yao, J. Li, A. Ozden, H. Wang, N. Sun, P. Liu, W. Zhong, W. Zhou, J. Zhou, X. Wang, H. Liu, Y. Liu, S. Chen, Y. Hu, Z. Wang, D. Sinton and H. Liang, In situ copper faceting enables efficient CO(2)/CO electrolysis, *Nat. Commun.*, 2024, **15**, 1749.

160 Y. Wang, J. Zhang, J. Zhao, Y. Wei, S. Chen, H. Zhao, Y. Su, S. Ding and C. Xiao, Strong Hydrogen-Bonded Interfacial Water Inhibiting Hydrogen Evolution Kinetics to Promote Electrochemical CO_2 Reduction to C2+, *ACS Catal.*, 2024, **14**, 3457–3465.

161 S. Li, M. Shi, C. Wu, K. Nie, Z. Wei, X. Jiang, X. Liu, H. Chen, X. Tian, D. Wu and Y. Li, Surface addition of Ag on PbO_2 to enable efficient oxygen evolution reaction in pH-neutral media, *Chem. Eng. J.*, 2024, **485**, 150043.

162 T. Pu, J. Ding, X. Tang, K. Yang, K. Wang, B. Huang, S. Dai, Y. He, Y. Shi and P. Xie, Rational Design of Precious-Metal Single-Atom Catalysts for Methane Combustion, *ACS Appl. Mater. Interfaces*, 2022, **14**, 43141–43150.

163 S. Jia, Q. Zhu, H. Wu, S. Han, M. Chu, J. Zhai, X. Xing, W. Xia, M. He and B. Han, Preparation of trimetallic electrocatalysts by one-step co-electrodeposition and efficient CO_2 reduction to ethylene, *Chem. Sci.*, 2022, **13**, 7509–7515.

164 S. Kim, A. Ruiz Puigdollers, P. Gamallo, F. Viñes and J. Y. Lee, Functionalization of γ-graphyne by transition metal adatoms, *Carbon*, 2017, **120**, 63–70.

165 S. Siahrostami, S. J. Villegas, A. H. Bagherzadeh Mostaghimi, S. Back, A. B. Farimani, H. Wang, K. A. Persson and J. Montoya, A Review on Challenges and Successes in Atomic-Scale Design of Catalysts for Electrochemical Synthesis of Hydrogen Peroxide, *ACS Catal.*, 2020, **10**, 7495–7511.

166 X. Lei, Q. Tang, Y. Zheng, P. Kidkhunthod, X. Zhou, B. Ji and Y. Tang, High-entropy single-atom activated carbon catalysts for sustainable oxygen electrocatalysis, *Nat. Sustainable*, 2023, **6**, 816–826.

167 X. Lin, Q. Li, Y. Hu, Z. Jin, K. M. Reddy, K. Li, X. Lin, L. Ci and H.-J. Qiu, Revealing Atomic Configuration and Synergistic Interaction of Single-Atom-Based Zn-Co-Fe Trimetallic Sites for Enhancing Oxygen Reduction and Evolution Reactions, *Small*, 2023, **19**, 2300612.

168 Z. W. Chen, L. X. Chen, C. C. Yang and Q. Jiang, Atomic (single, double, and triple atoms) catalysis: frontiers, opportunities, and challenges, *J. Mater. Chem. A*, 2019, **7**, 3492–3515.

169 H.-B. He, X.-L. Ding, Y.-Y. Wang, Y. Chen, M.-M. Wang, J.-J. Chen and W. Li, Catalysts with Trimetallic Sites on Graphene-like C2N for Electrocatalytic Nitrogen Reduction Reaction: A Theoretical Investigation, *Chem. Phys. Chem.*, 2024, **25**, e202400143.

170 J. Liu, H. Xu, J. Zhu and D. Cheng, Understanding the Pathway Switch of the Oxygen Reduction Reaction from Single- to Double-/Triple-Atom Catalysts: A Dual Channel for Electron Acceptance–Backdonation, *JACS Au*, 2023, **3**, 3031–3044.

171 W. Yang, Z. Jia, B. Zhou, L. Chen, X. Ding, L. Jiao, H. Zheng, Z. Gao, Q. Wang and H. Li, Why Is C–C Coupling in CO_2 Reduction Still Difficult on Dual-Atom Electrocatalysts?, *ACS Catal.*, 2023, **13**, 9695–9705.

172 J. Xiao, Z. Liu, X. Wang, F. Li and Z. Zhao, Homonuclear multi-atom catalysts for CO_2 electroreduction: a comparison density functional theory study with their single-atom counterparts, *J. Mater. Chem. A*, 2023, **11**, 25662–25670.

173 Y. Sun, L. Tao, M. Wu, D. Dastan, J. Rehman, L. Li and B. An, Multi-atomic loaded C_2N_1 catalysts for CO_2 reduction to CO or formic acid, *Nanoscale*, 2024, **16**, 9791–9801.

174 S. S. Deshpande, M. D. Deshpande, T. Hussain and R. Ahuja, Investigating CO_2 storage properties of C_2N monolayer functionalized with small metal clusters, *J. CO2 Util*, 2020, **35**, 1–13.

175 W. Liu, J. Liu, Y. Yang, B. Xiong and H. Bai, Tunable trimetallic TM-NiFe catalysts for enhancing the products selectivity of CO_2 electroreduction, *Fuel*, 2023, **335**, 127026.

176 F. Pan, L. Fang, B. Li, X. Yang, T. O'Carroll, H. Li, T. Li, G. Wang, K.-J. Chen and G. Wu, N and OH-Immobilized Cu3 Clusters In Situ Reconstructed from Single-Metal Sites for Efficient CO_2 Electromethanation in Bicontinuous Mesochannels, *J. Am. Chem. Soc.*, 2024, **146**, 1423–1434.

177 T. Tsukamoto, Recent advances in atomic cluster synthesis: a perspective from chemical elements, *Nanoscale*, 2024, **16**, 10533–10550.

178 Index, in *Nanoparticle Technology Handbook*, ed. M. Naito, T. Yokoyama, K. Hosokawa and K. Nogi, Elsevier, 3rd edn, 2018, pp. 845–877.

179 C. Burda, X. Chen, R. Narayanan and M. A. El-Sayed, Chemistry and Properties of Nanocrystals of Different Shapes, *Chem. Rev.*, 2005, **105**, 1025–1102.

180 K. D. Gilroy, A. Ruditskiy, H.-C. Peng, D. Qin and Y. Xia, Bimetallic Nanocrystals: Syntheses, Properties, and Applications, *Chem. Rev.*, 2016, **116**, 10414–10472.

181 M. Arndt, O. Nairz, J. Vos-Andreae, C. Keller, G. van der Zouw and A. Zeilinger, Wave–particle duality of C_{60} molecules, *Nature*, 1999, **401**, 680–682.

182 M. Haruta, When Gold Is Not Noble: Catalysis by Nanoparticles, *Chem. Rec.*, 2003, **3**, 75–87.

183 T. Tsukamoto, N. Haruta, T. Kambe, A. Kuzume and K. Yamamoto, Periodicity of molecular clusters based on symmetry-adapted orbital model, *Nat. Commun.*, 2019, **10**, 3727.

184 N. Haruta, T. Tsukamoto, A. Kuzume, T. Kambe and K. Yamamoto, Nanomaterials design for super-degenerate electronic state beyond the limit of geometrical symmetry, *Nat. Commun.*, 2018, **9**, 3758.

185 M. Sun, T. Wu, A. W. Dougherty, M. Lam, B. Huang, Y. Li and C.-H. Yan, Self-Validated Machine Learning Study of

Graphdiyne-Based Dual Atomic Catalyst, *Adv. Energy Mater.*, 2021, **11**, 2003796.

186 D. Wu, X. Wang, L. Shi, K. Jiang, M. Wang, C. Lu, Z. Chen, P. Liu, J. Zhang, D. Tranca, Y. Hou, Y. Chen and X. Zhuang, Iron clusters boosted performance in electrocatalytic carbon dioxide conversion, *J. Mater. Chem. A*, 2020, **8**, 21661–21667.

187 S. Xue, X. Liang, Q. Zhang, X. Ren, L. Gao, T. Ma and A. Liu, Density Functional Theory Study of CuAg Bimetal Electrocatalyst for CO_2RR to Produce CH_3OH, *Catalysts*, 2023, **14**, 7.

188 M. Tamtaji, M. Kazemeini and J. Abdi, Ab initio calculations of high-entropy clusters for oxygen reduction and evolution as well as CO_2 reduction reactions, *ApSS*, 2025, **681**, 161555.

189 N. Sakamoto, K. Sekizawa, S. Shirai, T. Nonaka, T. Arai, S. Sato and T. Morikawa, Dinuclear Cu(I) molecular electrocatalyst for CO_2-to-C_3 product conversion, *Nat. Catal.*, 2024, **7**, 574–584.

190 X. Liang, X. Ren, M. Guo, Y. Li, W. Xiong, W. Guan, L. Gao and A. Liu, CO_2 electroreduction by AuCu bimetallic clusters: A first principles study, *IJER*, 2021, **45**, 18684–18694.

191 R. An, X. Chen, Q. Fang, Y. Meng, X. Li and Y. Cao, Structure–activity relationship of Cu-based catalysts for the highly efficient CO_2 electrochemical reduction reaction, *Front. Chem.*, 2023, **11**, 1141453.

192 Q. Zhang, Y. Li, H. Zhu and B. Suo, High-Performance of Electrocatalytic CO_2 Reduction on Defective Graphene-Supported Cu_4S_2 Cluster, *Catalysts*, 2022, **12**, 454.

193 D. Y. Jo, H. C. Ham and K.-Y. Lee, Facet-dependent electrocatalysis in the HCOOH synthesis from CO_2 reduction on Cu catalyst: a density functional theory study, *ApSS*, 2020, **527**, 146857.

194 Z. Xu, T. Wu, Y. Cao, C. Chen, X. Zeng, P. Lin and W.-W. Zhao, Dynamic restructuring induced Cu nanoparticles with ideal nanostructure for selective multicarbon compounds production via carbon dioxide electroreduction, *JCat*, 2020, **383**, 42–50.

195 X. Deng, D. Alfonso, T.-D. Nguyen-Phan and D. R. Kauffman, Breaking the Limit of Size-Dependent CO_2RR Selectivity in Silver Nanoparticle Electrocatalysts through Electronic Metal–Carbon Interactions, *ACS Catal.*, 2023, **13**, 15301–15309.

196 H. Yang, W. Zou, C. Zhang and A. Du, Ab Initio Studies of Electrocatalytic CO_2 Reduction for Small Cu Cluster Supported on Polar Substrates, *ACS Appl. Mater. Interfaces*, 2024, **16**, 33688–33695.

197 Z. Zhang, G. Wen, D. Luo, B. Ren, Y. Zhu, R. Gao, H. Dou, G. Sun, M. Feng, Z. Bai, A. Yu and Z. Chen, ''Two Ships in a Bottle'' Design for Zn–Ag–O Catalyst Enabling Selective and Long-Lasting CO_2 Electroreduction, *J. Am. Chem. Soc.*, 2021, **143**, 6855–6864.

198 Y. Gang, J. Pellessier, Z. Du, S. Fang, L. Fang, F. Pan, M. Suarez, K. Hambleton, F. Chen, H.-C. Zhou, T. Li, Y. H. Hu and Y. Li, Facile and Scalable Synthesis of Metal- and Nitrogen-Doped Carbon Nanotubes for Efficient Electrochemical CO_2 Reduction, *ACS Sustainable Chem. Eng.*, 2023, **11**, 7231–7243.

199 O. Wang, H. Wang, Y. Tang, Z. Ma, B.-L. An, Y. Zhao, X. Wang and J. Xu, Anchoring Sn-Containing High-Entropy Alloy PtFeCoNiCuSn on SnO2 for Improving Acetone Detection Ability, *ACS Nano*, 2025, **19**, 42466–42479.

200 L. Li, Y. Lv, H. Sheng, Y. Du, H. Li, Y. Yun, Z. Zhang, H. Yu and M. Zhu, A low-nuclear Ag_4 nanocluster as a customized catalyst for the cyclization of propargylamine with CO_2, *Nat. Commun.*, 2023, **14**, 6989.

201 Z. Sun, T. Ma, H. Tao, Q. Fan and B. Han, Fundamentals and Challenges of Electrochemical CO_2 Reduction Using Two-Dimensional Materials, *Chem*, 2017, **3**, 560–587.

202 S. Jin, Z. Hao, K. Zhang, Z. Yan and J. Chen, Advances and Challenges for the Electrochemical Reduction of CO_2 to CO: From Fundamentals to Industrialization, *Angew. Chem., Int. Ed.*, 2021, **60**, 20627–20648.

203 X. Wang, Z. Wang, F. P. García de Arquer, C.-T. Dinh, A. Ozden, Y. C. Li, D.-H. Nam, J. Li, Y.-S. Liu, J. Wicks, Z. Chen, M. Chi, B. Chen, Y. Wang, J. Tam, J. Y. Howe, A. Proppe, P. Todorović, F. Li, T.-T. Zhuang, C. M. Gabardo, A. R. Kirmani, C. McCallum, S.-F. Hung, Y. Lum, M. Luo, Y. Min, A. Xu, C. P. O'Brien, B. Stephen, B. Sun, A. H. Ip, L. J. Richter, S. O. Kelley, D. Sinton and E. H. Sargent, Efficient electrically powered CO_2-to-ethanol via suppression of deoxygenation, Nature, *Energy*, 2020, **5**, 478–486.

204 J. Li and W. Shen, Guest Editorial Special Section on 2019 IEEE International Conference on Automation Science and Engineering, *IEEE Trans. Autom. Sci. Eng.*, 2021, **18**, 216–217.

205 Y. Guo, S. Yao, Y. Xue, X. Hu, H. Cui and Z. Zhou, Nickel single-atom catalysts intrinsically promoted by fast pyrolysis for selective electroreduction of CO_2 into CO, *Appl. Catal., B*, 2022, **304**, 120997.

206 M.-J. Cheng, E. L. Clark, H. H. Pham, A. T. Bell and M. Head-Gordon, Quantum Mechanical Screening of Single-Atom Bimetallic Alloys for the Selective Reduction of CO_2 to C1 Hydrocarbons, *ACS Catal.*, 2016, **6**, 7769–7777.

207 S.-G. Han, D.-D. Ma, S.-H. Zhou, K. Zhang, W.-B. Wei, Y. Du, X.-T. Wu, Q. Xu, R. Zou and Q.-L. Zhu, Fluorine-tuned single-atom catalysts with dense surface Ni-N_4 sites on ultrathin carbon nanosheets for efficient CO_2 electroreduction, *Appl. Catal., B*, 2021, **283**, 119591.

208 Y. Cao, Y. Meng, Y. Wu, Z. Shen, Q. Xia, H. Huang, J.-P. Lang, H. Gu, Y. Wang and X. Li, Regulation of the Coordination Structures of Transition Metals on Nitrogen-Doped Carbon Nanotubes for Electrochemical CO_2 Reduction, *Inorg. Chem.*, 2022, **61**, 18957–18969.

209 K. Li, S. Zhang, X. Zhang, S. Liu, H. Jiang, T. Jiang, C. Shen, Y. Yu and W. Chen, Atomic Tuning of Single-Atom Fe–N–C Catalysts with Phosphorus for Robust Electrochemical CO_2 Reduction, *Nano Lett.*, 2022, **22**, 1557–1565.

210 Z. Wei, Y. Liu, J. Ding, Q. He, Q. Zhang and Y. Zhai, Promoting Electrocatalytic CO_2 Reduction to CO via

Sulfur-Doped Co-N-C Single-Atom Catalyst, *Chin. J. Chem.*, 2023, **41**, 3553–3559.

211 Q. Wang, M. Dai, H. Li, Y.-R. Lu, T.-S. Chan, C. Ma, K. Liu, J. Fu, W. Liao, S. Chen, E. Pensa, Y. Wang, S. Zhang, Y. Sun, E. Cortés and M. Liu, Asymmetric Coordination Induces Electron Localization at Ca Sites for Robust CO_2 Electroreduction to CO, *Adv. Mater.*, 2023, **35**, 2300695.

212 Z. Wang, C. Wang, Y. Hu, S. Yang, J. Yang, W. Chen, H. Zhou, F. Zhou, L. Wang, J. Du, Y. Li and Y. Wu, Simultaneous diffusion of cation and anion to access N, S co-coordinated Bi-sites for enhanced CO_2 electroreduction, *Nano Res.*, 2021, **14**, 2790–2796.

213 C. Hepburn, E. Adlen, J. Beddington, E. A. Carter, S. Fuss, N. Mac Dowell, J. C. Minx, P. Smith and C. K. Williams, The technological and economic prospects for CO_2 utilization and removal, *Nature*, 2019, **575**, 87–97.

214 S. Li, S. Zhao, X. Lu, M. Ceccato, X.-M. Hu, A. Roldan, J. Catalano, M. Liu, T. Skrydstrup and K. Daasbjerg, Low-Valence $Zn^{\delta+}$ $(0 < \delta < 2)$ Single-Atom Material as Highly Efficient Electrocatalyst for CO_2 Reduction, *Angew. Chem., Int. Ed.*, 2021, **60**, 22826–22832.

215 J. Song, X. Lei, J. Mu, J. Li, X. Song, L. Yan and Y. Ding, Boron-Doped Nickel–Nitrogen–Carbon Single-Atom Catalyst for Boosting Electrochemical CO_2 Reduction, *Small*, 2023, **19**, 2305666.

216 J. Guo, W. Zhang, L.-H. Zhang, D. Chen, J. Zhan, X. Wang, N. R. Shiju and F. Yu, Control over Electrochemical CO_2 Reduction Selectivity by Coordination Engineering of Tin Single-Atom Catalysts, *Adv. Sci.*, 2021, **8**, 2102884.

217 N. Chaipraditgul, T. Numpilai, C. Kui Cheng, N. Siri-Nguan, T. Sornchamni, C. Wattanakit, J. Limtrakul and T. Witoon, Tuning interaction of surface-adsorbed species over Fe/K-Al_2O_3 modified with transition metals (Cu, Mn, V, Zn or Co) on light olefins production from CO_2 hydrogenation, *Fuel*, 2021, **283**, 119248.

218 J. Jiao, R. Lin, S. Liu, W.-C. Cheong, C. Zhang, Z. Chen, Y. Pan, J. Tang, K. Wu, S.-F. Hung, H. M. Chen, L. Zheng, Q. Lu, X. Yang, B. Xu, H. Xiao, J. Li, D. Wang, Q. Peng, C. Chen and Y. Li, Copper atom-pair catalyst anchored on alloy nanowires for selective and efficient electrochemical reduction of CO_2, *Nat. Chem.*, 2019, **11**, 222–228.

219 C. Hu, Y. Wang, J. Chen, H.-F. Wang, K. Shen, K. Tang, L. Chen and Y. Li, Main-Group Metal Single-Atomic Regulators in Dual-Metal Catalysts for Enhanced Electrochemical CO_2 Reduction, *Small*, 2022, **18**, 2201391.

220 L. Zhang, J. Feng, S. Liu, X. Tan, L. Wu, S. Jia, L. Xu, X. Ma, X. Song, J. Ma, X. Sun and B. Han, Atomically Dispersed Ni–Cu Catalysts for pH-Universal CO_2 Electroreduction, *Adv. Mater.*, 2023, **35**, 2209590.

221 J. Sun, Z. Liu, H. Zhou, M. Cao, W. Cai, C. Xu, J. Xu and Z. Huang, Ionic Liquids Modulating Local Microenvironment of Ni–Fe Binary Single Atom Catalyst for Efficient Electrochemical CO_2 Reduction, *Small*, 2024, **20**, 2308522.

222 M. Huang, S.-H. Zhou, C.-J. Yang, C.-L. Dong, Y. He, W. Wei, X. Li, Q.-L. Zhu and Z. Huang, Selenic Acid Etching Assisted Atomic Engineering for Designing Metal-Semimetal Dual Single-Atom Catalysts for Enhanced CO_2 Electroreduction, *ACS Nano*, 2024, **18**, 33210–33219.

223 H. Han, S. Lee, J. Im, M. Lee, T. Lee, S. T. Hyun, J. Hong, T. Seok and D. Choo, Large-scale CO_2-to-CO electroconversion on highly efficient diatomic catalysts, *Chem. Eng. J.*, 2024, **479**, 147603.

224 B. Xiong, J. Liu, Y. Yang, W. Liu, M. Chen and H. Bai, Machine Learning-Assisted Screening of Cu-Based Trimetallic Catalysts for Electrochemical Conversion of CO_2 to CO, *Energy Fuels*, 2024, **38**, 2074–2083.

225 Z. Min, C. Shao, B. Chang, N. Wang, Y. Zhao, S. Gao, X.-G. Zhang, M. Fan, S. Zhang and J. Wang, Constructing Triple-Atom sites for H_2O Participated Electrocatalytic CO_2 Reduction, *Chem. Eng. J.*, 2024, **502**, 157813.

226 C. Cai, B. Liu, K. Liu, P. Li, J. Fu, Y. Wang, W. Li, C. Tian, Y. Kang, A. Stefancu, H. Li, C.-W. Kao, T.-S. Chan, Z. Lin, L. Chai, E. Cortés and M. Liu, Heteroatoms Induce Localization of the Electric Field and Promote a Wide Potential-Window Selectivity Towards CO in the CO_2 Electroreduction, *Angew. Chem., Int. Ed.*, 2022, **61**, e202212640.

227 Y. Xu, J. Long, L. Tu, W. Dai, L. Yang, J. Zou, X. Luo and S. Luo, CoO engineered Co_9S_8 catalyst for CO_2 photoreduction with accelerated electron transfer endowed by the built-in electric field, *Chem. Eng. J.*, 2021, **426**, 131849.

228 X. Li, Z. Yang, L. Zhang, Z. He, R. Fang, Z. Wang, Y. Yan and J. Ran, Effect of Pd doping in (Fe/Ni)/CeO_2 catalyst for the reaction path in CO_2 oxidative ethane dehydrogenation/reforming, *Energy*, 2021, **234**, 121261.

229 Y. Wang, H. Arandiyan, J. Scott, K.-F. Aguey-Zinsou and R. Amal, Single Atom and Nanoclustered Pt Catalysts for Selective CO_2 Reduction, *ACS Appl. Energy Mater.*, 2018, **1**, 6781–6789.

230 V. V. Galvita, H. Poelman, C. Detavernier and G. B. Marin, Catalyst-assisted chemical looping for CO_2 conversion to CO, *Appl. Catal., B*, 2015, **164**, 184–191.

231 A. Zhanaidarova, S. C. Jones, E. Despagnet-Ayoub, B. R. Pimentel and C. P. Kubiak, Re(*t*Bu-bpy)$(CO)_3$Cl Supported on Multi-Walled Carbon Nanotubes Selectively Reduces CO_2 in Water, *J. Am. Chem. Soc.*, 2019, **141**, 17270–17277.

232 S. Huo, Z. Weng, Z. Wu, Y. Zhong, Y. Wu, J. Fang and H. Wang, Coupled Metal/Oxide Catalysts with Tunable Product Selectivity for Electrocatalytic CO_2 Reduction, *ACS Appl. Mater. Interfaces*, 2017, **9**, 28519–28526.

233 E. B. Nursanto, H. S. Jeon, C. Kim, M. S. Jee, J. H. Koh, Y. J. Hwang and B. K. Min, Gold catalyst reactivity for CO_2 electro-reduction: From nano particle to layer, *Catal. Today*, 2016, **260**, 107–111.

234 D. R. Alfonso, D. Kauffman and C. Matranga, Active sites of ligand-protected Au25 nanoparticle catalysts for CO_2 electroreduction to CO, *J. Chem. Phys.*, 2016, **144**, 184705.

235 Z. Wu, D.-e Jiang, A. K. P. Mann, D. R. Mullins, Z.-A. Qiao, L. F. Allard, C. Zeng, R. Jin and S. H. Overbury, Thiolate Ligands as a Double-Edged Sword for CO Oxidation on CeO2 Supported Au25(SCH2CH2Ph)18 Nanoclusters, *J. Am. Chem. Soc.*, 2014, **136**, 6111–6122.

236 Y. Xiao, F. Xie, H.-T. Zhang and M.-T. Zhang, Bioinspired Binickel Catalyst for Carbon Dioxide Reduction: The Importance of Metal–ligand Cooperation, *JACS Au*, 2024, **4**, 1207–1218.

237 Y. Han, Y. Sun and Q. Sun, Regulating Adsorption of Intermediates via d–p Orbital Electron Coupling for Boosting CO_2RR, *ACS Appl. Energy Mater.*, 2025, **8**, 6400–6406.

238 Y. Fang, X. Liu, Z. Liu, L. Han, J. Ai, G. Zhao, O. Terasaki, C. Cui, J. Yang, C. Liu, Z. Zhou, L. Chen and S. Che, Synthesis of amino acids by electrocatalytic reduction of CO_2 on chiral Cu surfaces, *Chem*, 2023, **9**, 460–471.

239 N. Zhang, D. Li, X. Wang, R. Cai, C.-L. Dong, T. Thi Thuy Nga, L. Zhang and D. Yang, Charge-acquired Pb^{2+} boosts actively and selectively electrochemical carbon dioxide reduction reaction to formate, *Appl. Catal., B*, 2023, **326**, 122404.

240 M. Fan, R. K. Miao, P. Ou, Y. Xu, Z. Y. Lin, T. J. Lee, S. F. Hung, K. Xie, J. E. Huang, W. Ni, J. Li, Y. Zhao, A. Ozden, C. P. O'Brien, Y. Chen, Y. C. Xiao, S. Liu, J. Wicks, X. Wang, J. Abed, E. Shirzadi, E. H. Sargent and D. Sinton, Single-site decorated copper enables energy- and carbon-efficient CO_2 methanation in acidic conditions, *Nat. Commun.*, 2023, **14**, 3314.

241 Z. Li, B. Sun, D. Xiao, Z. Wang, Y. Liu, Z. Zheng, P. Wang, Y. Dai, H. Cheng and B. Huang, Electron-Rich Bi Nanosheets Promote CO_2 − Formation for High-Performance and pH-Universal Electrocatalytic CO_2 Reduction, *Angew. Chem., Int. Ed.*, 2023, **62**(11), e202217569.

242 T. Zheng, C. Liu, C. Guo, M. Zhang, X. Li, Q. Jiang, W. Xue, H. Li, A. Li, C.-W. Pao, J. Xiao, C. Xia and J. Zeng, Copper-catalysed exclusive CO_2 to pure formic acid conversion via single-atom alloying, *Nat. Nanotechnol.*, 2021, **16**, 1386–1393.

243 J. Zhang, T. Xu, D. Yuan, J. Tian and D. Ma, CO_2 electro-reduction by transition metal-embedded two-dimensional C3N: A theoretical study, *J. CO2 Util.*, 2021, **43**, 101367.

244 S. Lu, H. L. Huynh, F. Lou, M. Guo and Z. Yu, Electrochemical reduction of CO_2 to CH_4 over transition metal atom embedded antimonene: First-principles study, *J. CO2 Util.*, 2021, **51**, 101645.

245 Y.-P. He, S.-Y. Wu, J.-X. Guo, T.-H. Guo and X.-Y. Li, A study on the single atom Cu adsorbed Janus MoSSe monolayer as the catalyst for reduction of CO_2 to HCOOH, *Mol. Catal.*, 2023, **549**, 113511.

246 Z. Chen, S. Cao, J. Li, C. Yang, S. Wei, S. Liu, Z. Wang and X. Lu, N,S coordination in Ni single-atom catalyst promoting CO(2)RR towards HCOOH, *Phys. Chem. Chem. Phys.*, 2023, **25**, 29951–29959.

247 X. Zeng, C. Xiao, L. Liao, Z. Tu, Z. Lai, K. Xiong and Y. Wen, Two-Dimensional (2D) TM-Tetrahydroxyquinone Metal–Organic Framework for Selective CO_2 Electrocatalysis: A DFT Investigation, *Nanomaterials*, 2022.

248 L. Qian, K.-Y. Ma, Z.-J. Zhou and F. Ma, Design of a catalyst through Fe doping of the boron cage $B_{10}H_{14}$ for CO_2 hydrogenation and investigation of the catalytic character of iron hydride (Fe–H), *Phys. Chem. Chem. Phys.*, 2017, **19**, 32723–32732.

249 X. Li, B. Zhao, R. Wan, J. Wang and Z. Li, Single-Atom Transition Metals Anchored NbS2: Electrocatalytic Reduction of CO_2 to HCOOH, *J. Phys. Chem. C*, 2025, **129**, 20931–20937.

250 B. Kumar, V. Atla, J. P. Brian, S. Kumari, T. Q. Nguyen, M. Sunkara and J. M. Spurgeon, Reduced SnO2 Porous Nanowires with a High Density of Grain Boundaries as Catalysts for Efficient Electrochemical CO_2-into-HCOOH Conversion, *Angew. Chem., Int. Ed.*, 2017, **56**, 3645–3649.

251 T. Liu, Z. Yang, Z. Wang, T. Xu, T. Li and Y. Jing, Dynamic CO_2 Adsorption Reconfiguration Directs Product Branching on Heterogeneous Dual-Atom Catalysts, *ACS Catal.*, 2025, **15**, 8479–8488.

252 Y. Yang, J. Liu, D. Wu, J. Ding and B. Xiong, Two-dimensional pyrite supported transition metal for highly-efficient electrochemical CO_2 reduction: A theoretical screening study, *Chem. Eng. J.*, 2021, **424**, 130541.

253 Y.-w Sun and J.-y Liu, CO_2 electroreduction performance of PtS2 supported single transition metal atoms: a theoretical study, *Phys. Chem. Chem. Phys.*, 2023, **25**, 4773–4779.

254 Z. Wu, H. Wu, W. Cai, Z. Wen, B. Jia, L. Wang, W. Jin and T. Ma, Engineering Bismuth–Tin Interface in Bimetallic Aerogel with a 3D Porous Structure for Highly Selective Electrocatalytic CO_2 Reduction to HCOOH, *Angew. Chem., Int. Ed.*, 2021, **60**, 12554–12559.

255 B. Wei, Y. Xiong, Z. Zhang, J. Hao, L. Li and W. Shi, Efficient electrocatalytic reduction of CO_2 to HCOOH by bimetallic In-Cu nanoparticles with controlled growth facet, *Appl. Catal., B*, 2021, **283**, 119646.

256 B. Jiang, X.-G. Zhang, K. Jiang, D.-Y. Wu and W.-B. Cai, Boosting Formate Production in Electrocatalytic CO_2 Reduction over Wide Potential Window on Pd Surfaces, *J. Am. Chem. Soc.*, 2018, **140**, 2880–2889.

257 Q. Tang, Y. Lee, D.-Y. Li, W. Choi, C. W. Liu, D. Lee and D.-E. Jiang, Lattice-Hydride Mechanism in Electrocatalytic CO_2 Reduction by Structurally Precise Copper-Hydride Nanoclusters, *J. Am. Chem. Soc.*, 2017, **139**, 9728–9736.

258 G. Wang, J. Chen, Y. Ding, P. Cai, L. Yi, Y. Li, C. Tu, Y. Hou, Z. Wen and L. Dai, Electrocatalysis for CO_2 conversion: from fundamentals to value-added products, *Chem. Soc. Rev.*, 2021, **50**, 4993–5061.

259 W. Zhang, Y. Hu, L. Ma, G. Zhu, P. Zhao, X. Xue, R. Chen, S. Yang, J. Ma, J. Liu and Z. Jin, Liquid-phase exfoliated ultrathin Bi nanosheets: Uncovering the origins of enhanced electrocatalytic CO_2 reduction on two-dimensional metal nanostructure, *Nano Energy*, 2018, **53**, 808–816.

260 L.-J. Liu, Z.-Y. Wang, Z.-Y. Wang, R. Wang, S.-Q. Zang and T. C. W. Mak, Mediating CO_2 Electroreduction Activity and Selectivity over Atomically Precise Copper Clusters, *Angew. Chem., Int. Ed.*, 2022, **61**, e202205626.

261 X. Wang, X.-L. Wang, J. Lv, Z. Wu, J. Zhang, D. Hu, C. Xue, D. Li, X. Zhu and T. Wu, 0D/1D heterostructure for efficient electrocatalytic CO_2-to-C1 conversion by ultra-

small cluster-based multi-metallic sulfide nanoparticles and MWCNTs, *Chem. Eng. J.*, 2021, **422**, 130045.

262 Q.-f Zhang, Z.-K. Yu, Z.-Q. Wang, L. Wang, X.-Q. Gong and Y. Guo, Hydride-species-induced enhancement of CO_2 hydrogenation selectivity on Ru-atom-modified CeO2 catalysts, *Catal. Sci. Technol.*, 2025, **15**, 2564–2570.

263 L. Han, S. Song, M. Liu, S. Yao, Z. Liang, H. Cheng, Z. Ren, W. Liu, R. Lin, G. Qi, X. Liu, Q. Wu, J. Luo and H. L. Xin, Stable and Efficient Single-Atom Zn Catalyst for CO_2 Reduction to CH_4, *J. Am. Chem. Soc.*, 2020, **142**, 12563–12567.

264 J. Pan, Y. Kong, Y. Li, Y. Zhang and W. Lin, Coordination-tuned Ru single-atom catalyst for efficient catalysis of CO_2 to CH4 on RuB_xN_{4-x}@TiN (x = 0–4), *J. CO2 Util.*, 2024, **84**, 102849.

265 X. Lu, C. Yang, S. Cao, H. Chen, J. Li, Z. Chen, S. Wei, S. Liu and Z. Wang, Tackling the activity and selectivity challenges of electrocatalysts towards CO_2 reduction reaction via atomically dispersed dual atom catalysts, *ApSS*, 2024, **655**, 159687.

266 B. Han, H. Meng and F. Li, Supported Bimetallic Trimers Fe_2M@NG: Triple-Atom Catalysts for CO_2 Electroreduction, *ACS Omega*, 2022, **7**, 16080–16086.

267 H. Wang, R. Hu, R. Zhu, X. Yang, S. Yang, Y. Nie, J. Yu and X. Jiang, Rational design of trimetallic single-cluster catalysts for efficient electrocatalytic reduction of CO_2, *ApSS*, 2025, **692**, 162672.

268 L. Shi, H. Wu, W. Xu, W. Fu, X. Wang, Z. Gu, X. Zhang, J. Chen, Y. Ma and J. Zhao, Electrocatalytic conversion of CO_2 to CH_4 over Cu-based cluster *via* atomically precise local environment modulation, *Sci. China Mater.*, 2024, **67**, 3602–3608.

269 X. Chen, A. Xu, D. Wei, F. Huang, J. Ma, H. He and J. Xu, Atomic cerium-doped CuO_x catalysts for efficient electrocatalytic CO_2 reduction to CH4, *Chin. Chem. Lett.*, 2025, **36**, 110175.

270 L. Xiong, X. Fu, W. Fan, J. Zhang, Z. Zheng, S. Lu, D. Wang, M. Hao and Q. Yue, Unveiling the Nanoconfinement Effect in CO_2 Electroreduction to CH4 over Mesoporous Cu-CeO_2 Nanospheres, *ACS Cent. Sci.*, 2025, **11**, 1902–1910.

271 R. Rajaram, S. Karuppusamy, T. Christopher Jeyakumar and V. Maruthapandian, Recent advances in the development of various electrocatalysts for CO_2 reduction reactions: A review, *JAllC*, 2025, **1038**, 182601.

272 S. Banerjee, C. S. Gerke and V. S. Thoi, Guiding CO_2RR Selectivity by Compositional Tuning in the Electrochemical Double Layer, *Acc. Chem. Res.*, 2022, **55**, 504–515.

273 S. Ren, E. W. Lees, C. Hunt, A. Jewlal, Y. Kim, Z. Zhang, B. A. W. Mowbray, A. G. Fink, L. Melo, E. R. Grant and C. P. Berlinguette, Catalyst Aggregation Matters for Immobilized Molecular CO_2RR Electrocatalysts, *J. Am. Chem. Soc.*, 2023, **145**, 4414–4420.

274 J. Jiang, B. Huang, R. Daiyan, B. Subhash, C. Tsounis, Z. Ma, C. Han, Y. Zhao, L. H. Effendi, L. C. Gallington, J. N. Hart, J. A. Scott and N. M. Bedford, Defective Sn-Zn perovskites through bio-directed routes for modulating CO_2RR, *Nano Energy*, 2022, **101**, 107593.

275 P. S. Mantovi, J. C. da Cruz, L. D. De Angelis, M. L. Souza, L. M. Rossi, S. I. Córdoba de Torresi, F. H. B. Lima and R. M. Torresi, Tuning CO_2RR Pathways through Water Control in Ionic Liquids, *ACS Catal.*, 2025, **15**, 18261–18269.

276 Z. Xu, J. Mao, B. Mei, S. Gu, J. Ma, F. Sun, J. Li, L. Wang, W. Chen, F. Song and Z. Jiang, Quantitatively unveiling the effect of mass transfer on CO_2RR through operando EXAFS and HERFD-XAFS, *Sci. China: Chem.*, 2025, **68**, 2044–2050.

277 Q. Chang, G. Zhang, J. Chen, X. Du, C. Wang, Y. Cai, Y. Du, P. Zhang, T. Wang and J. Gong, Construction of efficient electrodes for CO_2RR through microenvironment regulation of hydrophobic ionomer, *J. Energy Chem.*, 2025, **108**, 373–380.

278 S. Nie, L. Tao, H. Yu, D. Dastan, W. Wang, L. Hong, L. Li, B. An and Y. Su, Theoretical and machine learning exploration of electronic factors governing Ni-centered CO_2 reduction catalysts, *Phys. Chem. Chem. Phys.*, 2025, **27**, 21810–21823.

279 Z. Xu, J. Mao, B. Mei, S. Gu, J. Ma, S. Fanfei, J. Li, L. Wang, W. Chen, F. Song and Z. Jiang, Quantitatively unveiling the effect of mass transfer on CO_2RR through operando EXAFS and HERFD-XAFS, *Sci. China: Chem.*, 2025, **68**, 2044–2050.

280 Y. Gong and T. He, Gaining Deep Understanding of Electrochemical CO_2RR with In Situ/Operando Techniques, Small, *Methods*, 2023, **7**, 2300702.

281 S. Li, J. Yu, S. Zhang, W. Qiu, X. Tang, Z. Lin, R. Cai, Y. Fang, S. Yang and X. Cai, Operando Reconstruction of Porous Carbon Supported Copper Selenide Promotes the C2 Production from CO_2RR, *Adv. Funct. Mater.*, 2024, **34**, 2311989.

282 A. Soni, X. Lu, C. Zhou, S. Singh and C. P. Berlinguette, Thermoelectric CO_2RR electrolysis, *Device*, 2024, **2**, 100603.

283 D. Chen, Y. Wei, Z. Sun, X. Zhao, X. Tang, X. Zhu, G. Li, L. Yao, S. Chen, R. Lin, J. Wang, Q. Li, X. Fan, T. Qiu and Q. Hao, Unveiling the Cation Effects on Electrocatalytic CO_2 Reduction via Operando Surface-enhanced Raman Spectroscopy, *Small*, 2025, **21**, 2409569.

284 T. Zhang, Y. Jin, S. N. Lou, T. Yan, T. Xiao, Z. Liu, J. Lin, S. Kuang, S. Zhang and X. Ma, Fine-tuning copper dispersion in Cu/SiO_2 core-shell particles regulates electrochemical CO_2 reduction product selectivity, *Appl. Catal., B*, 2024, **353**, 124065.

285 P. Pu, H. Feng, X. Song, S. Wang, J. J. Bao and X. Zhang, Transforming Catalysis with Machine Learning: Emerging Tools and Next-Gen Strategies, *ACS Appl. Mater. Interfaces*, 2025, **17**(31), 44073–44100.

286 M. Gu, L. Tao, D. Dastan, J. Dang, X. Zhang, L. Li and B. An, Metal-enhanced carbon-nitrogen material for selective detection of hazardous gases: Insights from interface electronic states, *Surf. Interfaces*, 2024, **53**, 105097.

287 M. Lu, L. Tao, Y. Su, Y. Sun, D. Dastan, J. Rehman, H. Zhang, H. Zhao, L. Li and B. An, First-Principles Study of Bonding-Driven Selectivity in CO_2 Electroreduction on

Metal–Nitrogen–Carbon Catalysts, *J. Phys. Chem. C*, 2025, **130**, 326–335.

288 C. Martínez-Alonso, V. Vassilev-Galindo, B. M. Comer, F. Abild-Pedersen, K. T. Winther and J. Llorca, Application of machine learning to discover new intermetallic catalysts for the hydrogen evolution and the oxygen reduction reactions, *Catal. Sci. Technol.*, 2024, **14**, 3784–3799.

289 G. Lin, T. Guo, W. Lin, H. Fan, L. Guo, Z. Zhang, B. Li, J. Wang, H. Ji, W. Song and J. Fu, Machine Learning Accelerated Screening Advanced Single-Atom Anchored MXenes Electrocatalyst for Nitrogen Fixation, *ACS Catal.*, 2025, **15**, 13534–13548.

290 L.-H. Mou, J. Du, Y. Li, J. Jiang and L. Chen, Effective Screening Descriptors of Metal–Organic Framework-Supported Single-Atom Catalysts for Electrochemical CO_2 Reduction Reactions: A Computational Study, *ACS Catal.*, 2024, **14**, 12947–12955.

291 H. Sun and J.-y Liu, Advancing CO_2RR with O-Coordinated Single-Atom Nanozymes: A DFT and Machine Learning Exploration, *ACS Catal.*, 2024, **14**, 14021–14030.

292 J. Chen, Y. Gu, Q. Zhu, Y. Gu, X. Liang and J. Ma, Automated Machine Learning of Interfacial Interaction Descriptors and Energies in Metal-Catalyzed N_2 and CO_2 Reduction Reactions, *Langmuir*, 2025, **41**, 3490–3502.